Dottorato di Ricerca in Fisica
XXXII Ciclo

The Structure of Compact Stars

Spring 2017

Omar Benhar

Contents

Introduction

Compact stars, i.e. white dwarfs, neutron stars and black holes, are believed to be the final stage of stellar evolution. They are different from normal stars, the stability of which against gravitational collapse is due to thermal pressure. In compact stars, the nuclear fuel necessary to ignite fusion reactions leading to heat production is no longer available, and the pressure needed for hydrostatic equilibrium is produced by different mechanisms, driven by quantum effects and interactions between the constituents of matter in the star interior.

Compacts stars provide a unique laboratory to study the structure of matter under extreme conditions, in which all known forces - gravitation, electromagnetism, weak and strong interactions - play a role. Hence, understanding their properties is of paramount importance for both astrophysics and fundamental physics.

In 1844, the german astronomer Friedrich Bessel deduced that the star called Sirius had an unseen companion, which was first observed two decades later by Alvan Graham Clark and named Sirius B. The mass of Sirius B was determined by applying Kepler's third law to the orbit of the binary system, while its radius was obtained in the 1920s from the equation describing blackbody emission, using the measured spectrum and luminosity. The resulting values, $M \sim 0.75-0.95\ M_\odot$ ($M_\odot = 1.989 \times 10^{33}$ g denotes the mass of the sun) and $R \sim 18800$ Km, comparable to the radius of a planet [1], revealed that Sirius B was a very compact object, of density reaching millions of g/cm^3. In his book *The Internal Constitution of the Stars*, published in 1926, Sir Arthur Eddington wrote: "we have a star of mass about equal to the sun and radius much less than Uranus". Sirius B is now known to belong to the class of stellar objects called white dwarfs.

The observation of the first white dwarf triggered the early efforts aimed at understanding the properties of matter at densities exceeding by many orders of magnitude the typical density of terrestrial macroscopic objects ($\rho \sim 20$ g/cm^3), the structure of which is mainly determined by electromagnetic interactions. In contrast, at very large density the role of electromagnetic interactions becomes negligible and the structure of matter is determined by quantum statistics and nuclear interactions.

The discovery, made by Chandrasekhar in 1931, of an upper bound to the mass of white dwarfs, started the speculations on the fate of stars of mass exceeding the limiting value. Neutron stars, whose existence is said to have been first discussed by Bohr, Landau and Rosenfeld right after the discovery of the neutron, were predicted to occur in the aftermath of a supernova explosion by Baade and Zwicky in 1934 [1] . Due to the large densities involved, up to $\sim 10^{15}$ g/cm^3, the theoretical description of neutron star matter must take into account the full complexity of the dynamcs of strong interactions, including the forces acting at nuclear and hadronic level, as well as the possible occurrence of

[1] Note that this is about four times bigger than the value resulting from more recent measurements

a core of deconfined quark matter. In addition, the effects predicted by Einstein's theory of general relativity, that play a negligible role in white dwarfs, in neutron stars become large.

These notes provide an introduction to the structure of matter at densities $10^4 \lesssim \rho \lesssim 10^{15}$ g/cm^3, typical of white dwarfs and neutron stars. The focus will mainly be on the density region $\rho > \rho_0$, where $\rho_0 = 2.67 \times 10^{14}$ g/cm^3 is the the central density of atomic nuclei, i.e. the largest density observed on earth under ordinary conditions. Describing this region necessarily requires a significant amount of extrapolation of the available empirical data on the properties of strongly interacting matter. In addition, as the density exceeds $\sim 2\rho_0$, new form of matter, whose occurrence is predicted by the fundamental theories of weak and strong interactions, may appear.

The classic references on the Physics of compact stars are the books of Shapiro and Teukolskii [2], Glendenning [3] and Weber [4]. A number of aspects of the structure of matter at high density have been also discussed in a somewhat more concise fashion by Leung [5].

These notes have been written using a system of units in which $\hbar = h/2\pi = c = K_B = 1$, where h, c and K_B denote Plank's constant, the speed of light and Boltzmann's constant, respectively.

Chapter 1

The structure of white dwarfs

The formation of a star is believed to be triggered by the contraction of a self-gravitating hydrogen cloud. As the density increases, the cloud becomes more and more opaque, and the energy released cannot be efficiently radiated away. As a consequence, the temperature also increases, and eventually becomes high enough ($\sim 6 \times 10^7$ K)to ignite the nuclear reactions turning hydrogen into helium:

$$\begin{aligned} p + p &\rightarrow {}^2\mathrm{H} + e^+ + \nu + 0.4\ \mathrm{MeV}\,, \\ e^+ + e^- &\rightarrow \gamma + 1.0\ \mathrm{MeV}\,, \\ {}^2\mathrm{H} + p &\rightarrow {}^3\mathrm{He} + \gamma + 5.5\ \mathrm{MeV}\,, \\ {}^3\mathrm{He} + {}^3\mathrm{He} &\rightarrow {}^4\mathrm{He} + 2p + 26.7\ \mathrm{MeV}\,. \end{aligned}$$

Note that the above reactions are all exothermic, and energy is released in form of kinetic energy of the produced particles (1 MeV = 1.6021917×10^{-6} erg). Equilibrium is reached as soon as gravitational attraction is balanced by matter pressure.

When the nuclear fuel is exhausted the core stops producing heat, the internal pressure cannot be sustained and the contraction produced by gravitational attraction resumes. If the mass of the helium core is large enough, its contraction, associated with a further increase of the temperature, can then lead to the ignition of new fusion reactions, resulting in the appearance of heavier nuclei: carbon and oxygen. Depending on the mass of the star, this process can take place several times, the final result being the formation of a core made of the most stable nuclear species, nickel and iron, at density $\sim 10^{14}$ g/cm^3 (note that the central density of atomic nuclei, the highest density observable on earth, is $\rho_0 \approx 2 \times 10^{14}$ g/cm^3). Even larger densities are believed to occur in the interior of neutron stars, astrophisical objects resulting from the contraction of the iron core in very massive stars (M > 4 $\mathrm{M}_\odot$).

If the star is sufficiently small, so that the gravitational contraction of the core does not produce a temperature high enough to ignite the burning of heavy nuclei, it will eventually turn into a white dwarf, i.e. a star consisting mainly of helium, carbon and oxygen.

The over 2000 observed white dwarfs have luminosity L $\sim 10^{-2}$ $\mathrm{L}_\odot$ ($\mathrm{L}_\odot = 4 \times 10^{33}$ erg s^{-1} is the luninosity of the sun) and surface temperature $T_s \sim 10^4$ K. The radius of many white dwarfs has been determined from their measured flux, defined as

$$F(D) = \frac{L}{4\pi D^2}\,, \tag{1.1}$$

Nuclear fuel	Main products	Temperature [K]	Density [g/cm^3]	Duration [yrs]
H	He	6×10^7	5	7×10^6
He	C, O	2×10^8	700	5×10^5
C	O, Ne, Mg	9×10^8	2×10^5	600
Ne	O, Mg, Si	1.7×10^9	4×10^5	1
O	Si, S	2.3×10^9	10^7	0.5
Si	Fe	4×10^9	3×10^7	0.0025

Table 1.1: Stages of nucleosynthesis for a star of mass $\sim 25\ M_\odot$

where D is the distance from the earth, obtained using the parallax method. Combining the above equation to the equation describing black body emission

$$L = 4\pi\sigma R^2 T_s^4\ , \tag{1.2}$$

one obtains

$$R = \sqrt{\frac{FD^2}{\sigma T_s^4}}\ . \tag{1.3}$$

The measured values of mass and radius of three white dwarfs are given in Table 1.2. The corresponding average densities are $\sim\ 10^7$ g/cm^3, to be compared to the typical density of terrestrial macroscopic objects, not exceeding ~ 20 g/cm^3.

	Mass $[M_\odot]$	Radius $[R_\odot]$
Sirius B	1.000 ± 0.016	0.0084 ± 0.0002
Procyon B	0.604 ± 0.018	0.0096 ± 0.0004
40 Eri B	0.501 ± 0.011	0.0136 ± 0.0002

Table 1.2: Measured mass and radius of three white dwarfs

The pressure required to ensure the stability of white dwarfs against gravitational collapse is provided by a gas of noninteracting electrons at very low temperature. The properties of this systems will

be discussed in the following Sections,

1.1 Energy-density and pressure of the degenerate Fermi gas

Let us consider a system of noninteracting electrons uniformly distributed in a cubic box of volume $V = \mathrm{L}^3$. If the temperature is sufficiently low, so that thermal energies can be neglected, the lowest quantum levels are occupied by two electrons, one for each spin state. Both electrons have the same energy, i.e. they are *degenerate*. This configuration corresponds to the ground state of the system. A gas of noninteracting electrons in its ground state is said to be *fully degenerate*. At higher temperature, the thermal energy can excite electrons to higher energy states, leaving some of the lower lying levels not fully degenerate.

As the electrons are uniformly distributed, their wave functions must exhibit translational invariance. They can be written in the form

$$\psi_{\mathbf{p}s}(\mathbf{r}) = \phi_{\mathbf{p}}(\mathbf{r})\chi_s \,, \tag{1.4}$$

where χ_s is a Pauli spinor specifying the spin projection and

$$\phi_{\mathbf{p}}(\mathbf{r}) = \sqrt{\frac{1}{V}}\, \mathrm{e}^{i\mathbf{p}\cdot\mathbf{r}} \,, \tag{1.5}$$

is an eigenfunctions of the the momentum, the generator of spacial translation, satisfying the periodic boundary conditions (x, y and z denote the components of the vector $\mathbf{r}$, specifying the electron position)

$$\phi_{\mathbf{p}}(x,y,z) = \phi_{\mathbf{p}}(x + n_x L, y + n_y L, z + n_z L) \,, \tag{1.6}$$

where $n_x, n_y, n_z = 0, \pm 1, \pm 2, \ldots$. The above equation obviously implies the relations ($\mathbf{p} \equiv (p_x, p_y, p_z)$)

$$p_x = \frac{2\pi n_x}{L}, \;\; p_y = \frac{2\pi n_y}{L}, \;\; p_z = \frac{2\pi n_z}{L} \,, \tag{1.7}$$

which in turn determine the momentum eigenvalues.

Each quantum state is associated with an eigenvalue of the momentum $\mathbf{p}$, i.e. with a specific triplet of integers (n_x, n_y, n_z). The corresponding energy eigenvalue is ($p^2 = |\mathbf{p}|^2 = p_x^2 + p_y^2 + p_z^2$)

$$\epsilon_p = \frac{p^2}{2m_e} = \left(\frac{2\pi}{L}\right)^2 \frac{1}{2m_e}\,(n_x^2 + n_y^2 + n_z^2) \,, \tag{1.8}$$

m_e being the electron mass ($m_e = 9.11 \times 10^{-28}$ g, or 0.511 MeV). The highest energy reached, called the Fermi Energy of the system, is denoted by ϵ_F, and the associated momentum, the Fermi momentum, is $p_F = \sqrt{2m_e\epsilon_F}$.

The number of quantum states with energy less or equal to ϵ_F can be easily calculated. Since each triplet (n_x, n_y, n_z) corresponds to a point in a cubic lattice with unit lattice spacing, the number of momentum eigenstates is equal to the number of lattice points within a sphere of radius $R = p_F L/(2\pi)$. The number of electrons in the system can then be obtained from (note: the factor 2 takes into account spin degeneracy, i.e. the fact that there are two electrons with opposite spin projections sitting in each momentum eigenstate)

$$N = 2\,\frac{4\pi}{3}\,R^3 = V\,\frac{p_F^3}{3\pi^2} \,, \tag{1.9}$$

and the electron number density, i.e. the number of electrons per unit volume, is given by

$$n_e = \frac{N}{V} = \frac{p_F^3}{3\pi^2} \,. \tag{1.10}$$

The total ground state energy can be easily evaluated from

$$E = 2 \sum_{p<p_F} \frac{p^2}{2m_e} \tag{1.11}$$

replacing (use (1.7) again and take the limit of large L, corresponding to vanishingly small level spacing)

$$\sum_{p<p_F} \to \frac{V}{(2\pi)^3} \int_{p<p_F} d^3p \tag{1.12}$$

to obtain

$$E = 2\,\frac{V}{(2\pi)^3}\,4\pi \int_0^{p_F} p^2 dp\,\frac{p^2}{2m_e} = N\,\frac{3}{5}\,\frac{p_F^2}{2m_e} \,. \tag{1.13}$$

The resulting energy density is

$$\epsilon = \frac{E}{V} = \frac{1}{(2\pi)^3}\,4\pi\,\frac{p_F^5}{5m_e} \,. \tag{1.14}$$

From Eq.(1.10) it follows that the Fermi energy can be written in terms of the number density according to

$$\epsilon_F = \frac{p_F^2}{2m_e} = \frac{1}{2m_e}\,\left(3\pi^2 n_e\right)^{2/3} \,. \tag{1.15}$$

The above equation can be used to define a density n_0 such that for $n_e \gg n_0$ the electron gas at given temperature T is fully degenerate. Full degeneracy is realized when the thermal energy $K_B T$ (K_B is the Boltzman constant: $K_B = 1.38 \times 10^{-16}$ erg/K) is much smaller than the Fermi energy ϵ_F, i.e. when

$$n_e \gg n_0 = \frac{1}{3\pi^2}\,(2m_e\,K_B T)^{3/2} \,. \tag{1.16}$$

For an ordinary star at the stage of hydrogen burning, like the Sun, the interior temperature is $\sim 10^7$ K, and the corresponding value of n_0 is $\sim 10^{26}$ cm^{-3}. If we assume that the electrons come from a fully ionized hydrogen gas, the *matter* density of the proton-electron plasma is

$$\rho = (m_p + m_e)\,n_0 \sim 200\ \mathrm{g/cm^3} \,, \tag{1.17}$$

m_p being the proton mass ($m_p = 1.67 \times 10^{-24}$ g). This density is high for most stars in the early stage of hydrogen burning, while for ageing stars that have developed a substantial helium core the density (m_n denotes the neutron mass: $m_n \approx m_p$).

$$\rho = (m_p + m_n + m_e)\,n_0 \sim 400\ \mathrm{g/cm^3} \tag{1.18}$$

can be largely exceeded within the core. For example, white dwarfs have core densities of the order of 10^7 g/cm^3. As a consequence, in the study of their structure thermal energies can be safely neglected, the primary role being played by the degeneracy energy $p^2/2m_e$.

The pressure P of the electron gas, i.e. the force per unit area on the walls of the box, is defined in kinetic theory as the rate of momentum transferred by the electrons colliding on a surface of unit area. Consider first one dimensional motion along the x-axis. The momentum transfer associated with the reflection of electrons carrying momentum p_x off the box wall during a time dt is

$$\frac{dp_x}{dt} = \frac{1}{2} \times (2p_x) \times (n_e v_x L^2) \,. \tag{1.19}$$

In the above equation, the second factor is the momentum transfer associated with a single electron, while the third factor is the electron flux, i.e. the number of electrons hitting the wall during the time dt. The factor $1/2$ accounts for the fact that half of the electrons go the wrong way and do not collide with the box wall. The resulting pressure is

$$P(p_x) = \frac{1}{L^2}\frac{dp_x}{dt} = n_e p_x v_x = \frac{n_e p_x^2}{m_e} \,. \tag{1.20}$$

In the three dimensional case the electron carries momentum $p = \sqrt{p_x^2 + p_y^2 + p_z^2}$ and we have to repeat the calculation carried out for the x-projection of the momentum transfer. As the system is isotropic

$$\frac{p_x^2}{m_e} = p_x v_x = \frac{1}{3}\,(p_x v_x + p_y v_y + p_z v_z) = \frac{1}{3}\,(\mathbf{p}\cdot\mathbf{v}) = \frac{1}{3}\,\frac{p^2}{m_e} \,, \tag{1.21}$$

and Eq.(1.20) becomes

$$P(p) = \frac{1}{3}\,n_e(pv) == \frac{1}{3}\frac{N}{V}\frac{p^2}{m_e} \,. \tag{1.22}$$

The pressure can therefore be obtained averaging over all momenta. We find (as usual, the factor 2 accounts for the two possible spin projections)

$$P = \frac{1}{N}\,2\sum_{p\le p_F} P(p) = \frac{2}{3}\,\frac{1}{(2\pi)^3}\,4\pi\int_0^{p_F} p^2 dp\,(pv) \;= \frac{p_F^5}{15\pi^2 m_e} \,. \tag{1.23}$$

Note that the above result can also be obtained from the standard thermodynamical definition of pressure

$$P = -\left(\frac{\partial E}{\partial V}\right)_N \,, \tag{1.24}$$

using E given by Eq.(1.13) and $(\partial p_F/\partial V)_N = -p_F/(3V)$.

Eq.(1.23) shows that the pressure of a degenerate Fermi gas decreases linearly as the mass of the constituent particle increases. For example, the pressure of an electron gas at number density n_e is ~ 2000 times larger than the pressure of a gas of nucleons, neutrons and protons, at the same number density.

So far, we have been assuming the electrons in the degenerate gas to be nonrelativistic. However, the properties of the system depend primarily on the distribution of quantum states, which is dictated by translation invariance only, and is not affected by this assumption. Releasing the nonrelativivstic approximation simply amounts to replace the nonrelativistic energy with its relativistic counterpart:

$$\frac{p^2}{2m_e} \to \sqrt{p^2 + m_e^2} - m_e \,. \tag{1.25}$$

The transition from the nonrelativistic regime to the relativistic one occurs when the electron energy becomes comparable to the energy assciated with the electron rest mass, m_e. It is therefore possible to define a density n_c such that at $n_e \ll n_c$ the system is nonrelativistic, while $n_e \gg n_c$ corresponds to the relativistic regime. The value of n_c can be found requiring that the Fermi energy at $n_e = n_c$ be equal to m_e. The resulting expression is

$$n_c = \frac{2^{3/2}}{3\pi^2}\, m_e^3 \sim 1.6 \times 10^{30} \mathrm{cm}^{-3} \,. \tag{1.26}$$

The energy density of a fully degenerate gas of relativistic electrons can be obtained from (compare to Eqs.(1.13) and (1.14))

$$\epsilon = 2\,\frac{1}{(2\pi^3)}\,4\pi \int_0^{p_F} p^2 dp \left[\sqrt{p^2 + m_e^2} - m_e\right] . \tag{1.27}$$

while the equation for the pressure reads (compare to Eq.(1.23) and use again $v = \partial\epsilon_p/\partial p$ with relativistic ϵ_p)

$$P = \frac{2}{3}\,\frac{1}{(2\pi)^3}\,4\pi \int_0^{p_F} p^2 dp \left(p\frac{\partial \epsilon_p}{\partial p}\right) . \tag{1.28}$$

Carrying out the integrations involved in Eqs.(1.27) and (1.28) we find:

$$\epsilon = \frac{\pi m_e}{\lambda_e^3}\left[t\left(2t^2+1\right)\sqrt{t^2+1} - \ln\left(t+\sqrt{t^2+1}\right) - \frac{8t^3}{3}\right] , \tag{1.29}$$

and

$$P = \frac{\pi m_e}{\lambda_e^3}\left[\frac{1}{3}\,t\left(2t^2-3\right)\sqrt{t^2+1} + \ln\left(t+\sqrt{t^2+1}\right)\right] , \tag{1.30}$$

where $\lambda_e = 2\pi/m_e c$ is the electron Compton wavelength and (see Eq.(1.15))

$$t = \frac{p_F}{m_e} = \frac{1}{m_e}\left(3\pi^2 n_e\right)^{1/3} . \tag{1.31}$$

Eqs.(1.29) and (1.30) give the energy density and pressure of a fully degenerate electron gas as a function of the variable t, which can in turn be written in terms of the number density n_e according to Eq.(1.31).

As a final remark, we briefly discuss the possible relevance of electrostatic interactions. In a fully ionized plasma their effect can be estimated noting that the corresponding energy is

$$E_c = Z\,\frac{e^2}{\langle r\rangle} \propto Z\,e^2\,n_e^{1/3} , \tag{1.32}$$

where Ze is the electric charge of the ions and $\langle r\rangle \propto n_e^{1/3}$ is the typical electron-ion separation distance. It follows that the ratio between E_c and the Fermi energy is given by

$$\frac{E_c}{\epsilon_F} \propto \frac{1}{n_e^{1/3}} . \tag{1.33}$$

The above equation shoes that, for sufficiently high density, the contribution of electrostatic interactions becomes negligibly small. As this condition is largely satisfied at the densities typical of white dwarfs, electrons can be safely described as a fully degenerate Fermi gas.

1.2 Dynamical content of the equation of state

The equation of state (EOS) is a nontrivial relation linking the thermodynamic variables specifying the state of a physical system. The best known example of EOS is Boyle's *ideal gas law*, stating that the pressure of a collection of N noninteracting, pointlike classical particles, enclosed in a volume V, grows linearly with the temperature T and the average particle density $n = N/V$.

The ideal gas law provides a good description of very dilute systems. In general, the EOS can be written as an expansion of the pressure, P, in powers of the density (from now on we use units such that Boltzmann's constant is $K_B = 1$):

$$P = nT\left[1 + nB(T) + n^2C(T) + \ldots\right] . \tag{1.34}$$

The coefficients appearing in the above series, that goes under the name of *virial expansion*, are functions of temperature only. They describe the deviations from the ideal gas law and can be calculated in terms of the underlying elementary interaction. Therefore, the EOS carries a great deal of dynamical information, and its knowledge makes it possible to establish a link between measurable *macroscopic* quantities, such as pressure or temperature, and the forces acting between the constituents of the system at *microscopic* level.

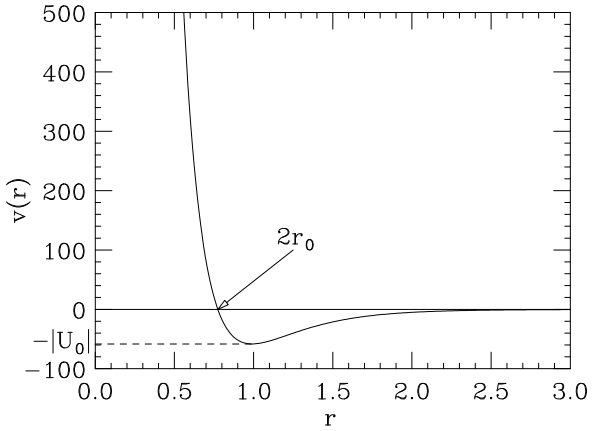

Figure 1.1: Behavior of the potential describing the interactions between constituents of a van der Waals fluid (the interparticle distance r and $v(r)$ are both given in arbitrary units).

This point is best illustrated by the van der Waals EOS, which describes a collection of particles interacting through a potential featuring a strong repulsive core followed by a weaker attactive tail (see Fig.1.1). At $|U_0|/T << 1$, U_0 being the strength of the attractive part of the potential, the van der Waals EOS takes the simple form

$$P = \frac{nT}{1-nb} - an^2 , \tag{1.35}$$

and the two quantities a and b, taking into account interaction effects, can be directly related to the potential $v(r)$ through [6]

$$a = \pi \int_{2r_0}^{\infty} |v(r)|\, r^2 dr \quad , \quad b = \frac{16}{3}\pi r_0^3 , \tag{1.36}$$

where $2r_0$ denotes the radius of the repulsive core (see Fig.1.1).

In spite of its simplicity, the van der Waals EOS describes most of the features of both the gas and liquid phases of the system, as well as the nature of the phase transition.

1.3 Equation of state of the degenerate Fermi gas

Equation (1.30) is the EOS of the degenerate electron gas, providing a link between its pressure P and the matter density ρ, which is in turn related to the electron number density n_e through

$$\rho = \frac{m_p}{Y_e}\, n_e\,, \tag{1.37}$$

where Y_e is the number of electrons per nucleon in the system. For example, for a fully ionized helium plasma $Y_e = 0.5$, whereas for a plasma of iron nuclei $Y_e = Z/A = 26/56 = 0.464$ (Z and A denote the nuclear charge and mass number, respectively).

The EOS of the fully degenerate electron gas takes a particularly simple form in the nonrelativistic limit (corresponding to $t \ll 1$), as well as in the extreme relativistic limit (corresponding to $t \gg 1$). From Eq.(1.30) we find

$$P = \frac{8}{15}\,\frac{\pi m_e}{\lambda_e^3}\left(\frac{3\pi^2 Y_e}{m_p}\right)^{5/3}\rho^{5/3}\,. \tag{1.38}$$

for $e_F \ll m_e$ and

$$P = \frac{2}{3}\,\frac{\pi m_e}{\lambda_e^3}\left(\frac{3\pi^2 Y_e}{m_p}\right)^{4/3}\rho^{4/3}\,. \tag{1.39}$$

for $e_F \gg m_e$.

A EOS that can be written in the form

$$P \propto \rho^{\Gamma}\,, \tag{1.40}$$

is said to be *polytropic*. The exponent Γ is called *adiabatic index*, whereas the quantity n, defined through

$$\Gamma = 1 + \frac{1}{n}\,, \tag{1.41}$$

goes under the name of *polytropic index*.

The adiabatic index, whose definition for a generic equation of state reads

$$\Gamma = \frac{d\,(lnP)}{d\,(ln\rho)}\,. \tag{1.42}$$

is related to the compressibility χ, characterizing the change of pressure with volume according to

$$\frac{1}{\chi} = -V\left(\frac{\partial P}{\partial V}\right)_N = \rho\left(\frac{\partial P}{\partial \rho}\right)_N\,. \tag{1.43}$$

through

$$\Gamma = \frac{1}{\chi P}\,. \tag{1.44}$$

The compressibility is also simply related to speed of sound in matter, c_s, defined as

$$c_s = \left(\frac{\partial P}{\partial \rho}\right)^{1/2} = \frac{1}{\chi \rho} \,. \tag{1.45}$$

The magnitude of the adiabatic index reflects the so called *stiffnes* of the equation of state. Larger stiffness corresponds to more incompressible matter. As we will see in the following lectures, stiffness turns out to be critical in determining a number of stellar properties.

1.4 Hydrostatic equilibrium and structure of white dwarfs

Let us assume that white dwarfs consist of a plasma of fully ionized helium at zero temperature. The pressure of the system, P, is provided by the electrons, the contribution of the helium nuclei being negligible due to their large mass. For any given value of the matter density ρ, P can be computed from Eqs.(1.30) and (1.31) (in this case $Y_e = 0.5$, implying $n_e = \rho/2m_p$). The results of this calculation are shown by the diamonds in fig. 1.2. For comparison, the nonrelativistic (Eq.(1.38)) and extreme relativistic (Eq.(1.39)) limits are also shown by the solid and dashed line, respectively. Note that the value of matter density corresponding to n_c defined in Eq.(1.26) is $\rho \sim 6.3\ \ 10^6$ g/cm^3.

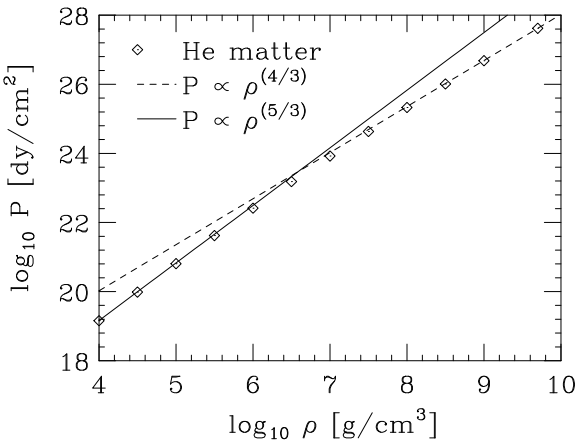

Figure 1.2: Equation of state of a fully ionized helium plasma at zero temperature (diamonds). The solid and dashed line correspond to the nonrelativistic and extreme relativistic limits, respectively.

In order to show the sensitivity of the EOS to the value of Y_e, in Fig. 1.3 the EOS of the fully ionized helium plasma ($Y_e = 0.5$) is compared to that of a hydrogen plasma ($Y_e = 1$).

The surface gravity of white dwarfs, GM/R (G is the gravitational constant), is small, of order $\sim 10^{-4}$. Hence, their structure can be studied assuming that they consist of a spherically symmetric fluid in hydrostatic equilibrium and neglecting relativistic effects.

Consider a perfect fluid in thermodynamic equilibrium, subject to gravity only. The Euler equation can be written in the form

$$\frac{\partial \mathbf{v}}{\partial t} + (\mathbf{v}\cdot\boldsymbol{\nabla})\mathbf{v} = -\frac{1}{\rho}\boldsymbol{\nabla} P - \boldsymbol{\nabla}\phi \,, \tag{1.46}$$

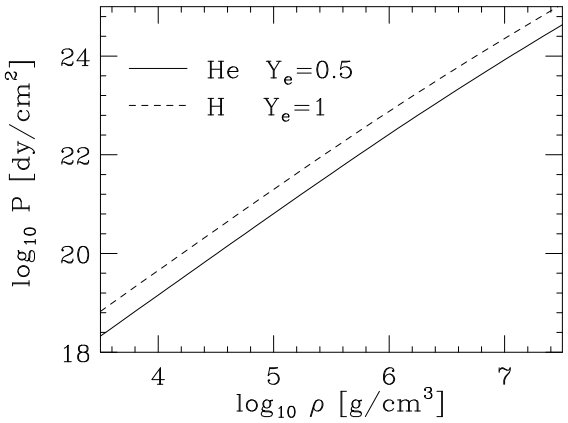

Figure 1.3: Comparison between the EOS of a fully ionized plasma of helium (solid line) and hydrogen (dashed line).

where ρ is the density and ϕ is the gravitational potential, satisfying Poisson's equation

$$\nabla^2\phi = 4\pi G\rho \,. \tag{1.47}$$

Eq.(1.46) describes the motion of a fluid in which processes leading to energy dissipation, occurring due to viscosity (i.e. internal friction) and heat exchange between different regions, can be neglected. For a fluid at rest (i.e. for $\mathbf{v} = 0$), it reduces to

$$\boldsymbol{\nabla} P = -\rho\,(\boldsymbol{\nabla}\phi) \,. \tag{1.48}$$

For a spherically symmetric fluid, Eqs. (1.47) and (1.48) become

$$\frac{dP}{dr} = -\rho\frac{d\phi}{dr} \,, \tag{1.49}$$

and

$$\frac{1}{r^2}\frac{d}{dr}\left(r^2\,\frac{d\phi}{dr}\right) = 4\pi G\rho \,. \tag{1.50}$$

Substitution of Eq. (1.49) in Eq. (1.50) yields

$$\frac{1}{r^2}\frac{d}{dr}\left(\frac{r^2}{\rho}\,\frac{dP}{dr}\right) = -4\pi G\rho \,, \tag{1.51}$$

implying

$$\frac{dP}{dr} = -\rho(r)\,\frac{GM(r)}{r^2} \,, \tag{1.52}$$

with $M(r)$ given by

$$M(r) = 4\pi\int_0^r \rho(r')r'^2 dr' \,. \tag{1.53}$$

The above result simply state that, at equilibrium, the gravitational force acting on an volume element at distance r from the center of the star is balanced by the force produced by the spacial variation of the pressure.

Given a EOS, Eq.(1.52) can be integrated numerically for any value of the central density ρ_c to obtain the radius of the star, i.e. the value of r corresponding to vanishingly small density. The mass can then be obtained from Eq.(1.53).

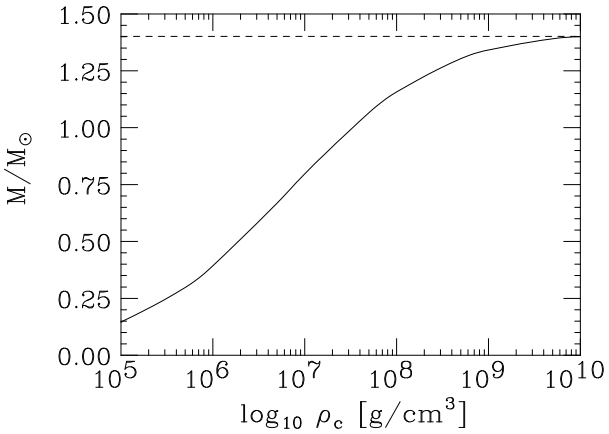

Figure 1.4: Dependence of the mass of a white dwarf upon its central density, obtained from the integration of Eq.(1.52) using the equation of state of a fully ionized helium plasma.

For polytropic EOS Eqs.(1.52) and (1.53) reduce to the Lane-Emden equation, whose integration with the polytropic index $n = 3/2$, corresponding to the non relativistic regime, yields the relation

$$M = \frac{2.79}{Y_e^2}\left(\frac{\rho_c}{\overline{\rho}}\right)^{1/2} M_\odot \,, \tag{1.54}$$

where $\overline{\rho}$ denotes the matter density corresponding to the electron number density of Eq.(1.26). The resulting values of M agree with the results of astronomical observations of white dwarfs. However, it is very important to realize that Lane-Emden equation predicts the existence of equilibrium configurations for any values of the star mass.

In 1931 Chandrasekhar pointed out that, due to the large Fermi enegies, the non relativistic treatment of the electron gas was not justified [7]. Replacing the EOS of Eq.(1.38) with its relativistic counterpart, Eq.(1.39), he predicted the existence of a maximum mass for white dwarfs. If the mass exceeds this limiting value gravitational attraction prevails on the pressure gradient, and the star becomes unstable against gravitational collapse.

The dependence of the mass of a white dwarf upon its central density, obtained from integration of Eq.(1.52) using the equation of state of a fully ionized helium plasma, is illustrated in Fig.1.4. The figure shows that the mass increases as the central density increases, until a value $M \sim 1.44\ M_\odot$ is reached at $\rho_0 \sim 10^{10}$ g/cm^3. This value is close to the one found by Chandrasekhar. However, as we will see in Chapter 2, at $\rho \sim 10^8$ g/cm^3 the *neutronization* process sets in, and the validity of the description in terms of a helium plasma breaks down. At $\rho \geq 10^8$ g/cm^3, matter does not support

pressure as effectively as predicted by the equation of state of the helium plasma. As a consequence, a more realistic estimate of the limiting mass, generally referred to as the *Chandrasekhar mass*, is given by the mass corresponding to a central density of 10^8 g/cm^3, i.e. $\sim 1.2\,M_\odot$.

1.5 Equilibrium equation in general relativity

The Newtonian equilibrium equation employed in the case of white dwarfs represents a good approximation when the matter density does not produce an appreciable space-time curvature, in which case the metric is simply given by

$$ds^2 = \eta_{\mu\nu} dx^\mu dx^\nu \,, \tag{1.55}$$

with

$$\eta = \begin{pmatrix} -1 & 0 & 0 & 0 \\ 0 & 1 & 0 & 0 \\ 0 & 0 & 1 & 0 \\ 0 & 0 & 0 & 1 \end{pmatrix} . \tag{1.56}$$

In Einstein's theory of general relativity, Eq.(1.55) is repalced by

$$ds^2 = g_{\mu\nu} dx^\mu dx^\nu \,, \tag{1.57}$$

where the metric tensor $g_{\mu\nu}$ is a function of space-time coordinates.

The effects of space-time distortion are negligible when the surface gravitational potential fulfills the requirement $GM/R \ll 1$. This condition is satisfied by white dwarfs, having $GM/R \sim 10^{-4}$, but not by neutron stars, to be discussed in the following Chapters, whose larger density leads to much higher values of GM/R, typically $\sim 10^{-1}$.

Relativistic corrections to the hydrostatic equilibrium equations (1.52) and (1.53) are obtained solving Einstein's field equations

$$G_{\mu\nu} = 8\pi G T_{\mu\nu} \,, \tag{1.58}$$

where $T_{\mu\nu}$ is the energy-momentum tensor and the Einstein's tensor $G_{\mu\nu}$ is defined in terms of the metric tensor $g_{\mu\nu}$ describing space-time geometry. Equations (1.58) state the relation between the distribution of matter, described by $T_{\mu\nu}$, and space-time curvature, described by $g_{\mu\nu}$.

Consider a star consisting of a static and spherically simmetric distribution of matter in chemical, hydrostatic and thermodynamic equilibrium. The metric of the corresponding gravitational field can be written in the form ($x^0 = t, x^1 = r, x^2 = \theta, x^3 = \varphi$)

$$ds^2 = g_{\mu\nu} dx^\mu dx^\nu = e^{2\nu(r)} dt^2 - e^{2\lambda(r)} dr^2 - r^2 (d\theta^2 + \sin^2\theta\, d\varphi^2) \,, \tag{1.59}$$

implying

$$g = \begin{pmatrix} e^{2\nu(r)} & 0 & 0 & 0 \\ 0 & -e^{2\lambda(r)} & 0 & 0 \\ 0 & 0 & -r^2 & 0 \\ 0 & 0 & 0 & -r^2 \sin^2\theta \end{pmatrix} , \tag{1.60}$$

$\nu(r)$ e $\lambda(r)$ being functions to be determined solving Einstein's equations

Under the standard assumption that matter in the star interior behave as an ideal fluid, the energy-momentum tensor can be written in the form

$$T_{\mu\nu} = (\epsilon + P)u_\mu u_\nu - P g_{\mu\nu} \,, \tag{1.61}$$

where ϵ and P denote energy density and pressure, respectively, while

$$u_\mu = \frac{dx_\mu}{d\tau} \equiv (\mathrm{e}^{-\nu(r)}, 0, 0, 0) \,, \tag{1.62}$$

is the local four-velocity.

The Einstein tensor $G_{\mu\nu}$, given by

$$G_{\mu\nu} = R_{\mu\nu} - \frac{1}{2} g_{\mu\nu} R \,, \tag{1.63}$$

with

$$R = g^{\mu\nu} R_{\mu\nu} \,, \tag{1.64}$$

depends on $g_{\mu\nu}$ through the Christoffel symbols

$$\Gamma^{\lambda}{}_{\mu\nu} = \frac{1}{2} g^{\alpha\lambda} (g_{\alpha\mu,\nu} + g_{\alpha\nu,\mu} + g_{\mu\nu,\alpha}) \,, \tag{1.65}$$

appearing in the definition of the Ricci tensor $R_{\mu\nu}$

$$R_{\mu\nu} = \Gamma^{\alpha}_{\mu\alpha,\nu} - \Gamma^{\alpha}_{\mu\nu,\alpha} - \Gamma^{\alpha}_{\mu\nu}\Gamma^{\beta}_{\alpha\beta} + \Gamma^{\alpha}_{\mu\beta}\Gamma^{\beta}_{\nu\alpha} \,. \tag{1.66}$$

From Eqs.(1.66) and (1.59) it follows that the nonvanishing elements of $R_{\mu\nu}$ are

$$\begin{aligned}
R_{00} &= \left[-\nu'' + \lambda'\nu' - (\nu')^2 - \frac{2\nu'}{r} \right] \mathrm{e}^{2(\nu-\lambda)} \,, \\
R_{11} &= \nu'' - \lambda'\nu' + (\nu')^2 - \frac{2\lambda'}{r} \,, \\
R_{22} &= \left(1 + r\nu' - r\lambda'\right) \mathrm{e}^{-2\lambda} - 1 \,, \\
R_{33} &= R_{22} \sin^2\theta \,,
\end{aligned} \tag{1.67}$$

implying

$$R = \left[-2\nu'' + 2\lambda'\nu' - 2(\nu')^2 - \frac{2}{r^2} + \frac{4\lambda'}{r} - \frac{4\nu'}{r} \right] \mathrm{e}^{-2\lambda} + \frac{2}{r^2} \,. \tag{1.68}$$

Substitution of Eqs.(1.61),(1.67) and (1.68) into Eqs.(1.58) leads to the system of differential equations

$$\begin{aligned}
\left(\frac{1}{r^2} - \frac{2\lambda'}{r} \right) \mathrm{e}^{-2\lambda} - \frac{1}{r^2} &= 8\pi G\epsilon(r) \,, \\
\left(\frac{1}{r^2} + \frac{2\nu'}{r} \right) \mathrm{e}^{-2\lambda} - \frac{1}{r^2} &= -8\pi G P(r) \,, \\
\left[\nu'' + (\nu')^2 - \lambda'\nu' + \frac{\nu' - \lambda'}{r} \right] \mathrm{e}^{-2\lambda} &= -8\pi G P(r) \,,
\end{aligned}$$

where $\epsilon(r)$ and $P(r)$ denote the space distribution of energy density and pressure, respectively.

The above equation can be cast in the form originally derived by Tolman, Oppenheimer and Volfoff (TOV) [8, 9]

$$\frac{dP(r)}{dr} = -\epsilon(r)\frac{GM(r)}{r^2}\left[1+\frac{P(r)}{\epsilon(r)}\right]\left[1+\frac{4\pi r^3 P(r)}{M(r)}\right], \left[1-\frac{2GM(r)}{r}\right]^{-1} \tag{1.69}$$

with

$$\frac{dM(r)}{dr} = 4\pi r^2 \epsilon(r)\,. \tag{1.70}$$

The first term in the right hand side of Eq.(1.69) is the newtonian gravitational force. It is the same as the one appearing in Eq.(1.52), but with matter density replaced by energy density. The first two additional factors take into account relativistic corrections, that become vanishingly small in the limit $p_F/m \to 0$, m and p_F being the mass and Fermi momentum of the star constituents, respectively. Finally, the third factor describes the effect of space-time curvature. Obviously, in the nonrelativistic limit Eq.(1.69) reduces to the classical equilibrium equation (1.52).

Chapter 2

Introduction to neutron stars

The temperatures attained in stars with initial mass larger than $\sim M_\odot$ are high enough to bring nucleosynthesis to its final stage (see Table 1.1), i.e. to the formation of a core of ^{56}Fe. If the mass of the core exceeds the Chandrasekhar mass, electron pressure is no longer sufficient to balance gravitational contraction and the star evolves towards the formation of a neutron star or a black hole.

The formation of the core in massive stars is characterized by the appearance of neutrinos, produced in the process

$$^{56}Ni \rightarrow {}^{56}Fe + 2e^{+} + 2\nu_e \,. \tag{2.1}$$

Neutrinos do not have appreciable interactions with the surrounding matter and leave the core region carrying away energy. Thus, neutrino emission contributes to the collapse of the core. Other processes leading to a decrease of the pressure are electron capture

$$e^{-} + p \rightarrow n + \nu_e \,, \tag{2.2}$$

the main effect of which is the disappearance of electrons carrying large kinetic energies, and iron photodisintegration

$$\gamma + {}^{56}Fe \rightarrow 13^{4}He + 4n \,, \tag{2.3}$$

which is an endothermic reaction.

Due to the combined effect of the above mechanisms, when the mass exceeds the Chandrasekhar limit the core collapses within fractions of a second to reach densities $\sim 10^{14}$ g/cm^3, comparable with the central density of atomic nuclei.

At this stage the core behaves as a giant nucleus, made mostly of neutrons, and reacts elestically to further compression producing a strong shock wave which trows away a significant fraction of matter in the outher layers of the star. Nucleosynthesis of elements heavier than Iron is believed to take place during this explosive phase.

The above sequence of events leads to the appearance of a *supernova*, a star the luminosity of which first grows fast, until it reaches a value exceeding sun luminosity by a factor $\sim 10^9$, and then descreases by a factor $\sim 10^2$ within few months. The final result of the explosion of the formation of a *nebula*, the center of which is occupied by the remnant of the core, i.e. a neutron star.

The existence of compact astrophysical objects made of neutrons was predicted by Bohr, Landau and Rosenfeld shortly after the discovery of the neutron, back in 1932. In 1934, Baade and Zwicky

first suggested that a neutron star may be formed in the aftermath of a supernova explosion. Finally, in 1968 the newly observed pulsars, radio sources blinking on and off at a constant frequency, were identified with rotating neutron stars.

The results of a pioneering study, carried out in 1939 by Oppenheimer and Volkoff within the framework of general relativity (i.e. using the equilibrium equations discussed in Section 1.5), show that the mass of a star consisting of noninteracting neutrons cannot exceed $\sim 0.8\ M_\odot$. The fact that this maximum mass, the analogue of the Chandrasekhar mass of white dwarfs, turns out to be much smaller that the observed neutron star masses (typically $\sim 1.4\ M_\odot$) clearly shows that neutron star equilibrium requires a pressure other than the degeneracy pressure, the origin of which has to be ascribed to hadronic interactions.

Unfortunately, the need of including dynamical effects in the EOS is confronted with the complexity of the fundamental theory of strong interactions. As a consequence, all available description of the EOS of neutron star matter are obtained within models, based on the theoretical knowledge of the underlying dynamics and constrained, as much as possible, by empirical data.

The internal structure of a neutron star, schematically illustrated in Fig. 2.1, is believed to feature a sequence of layers of different composition and density.

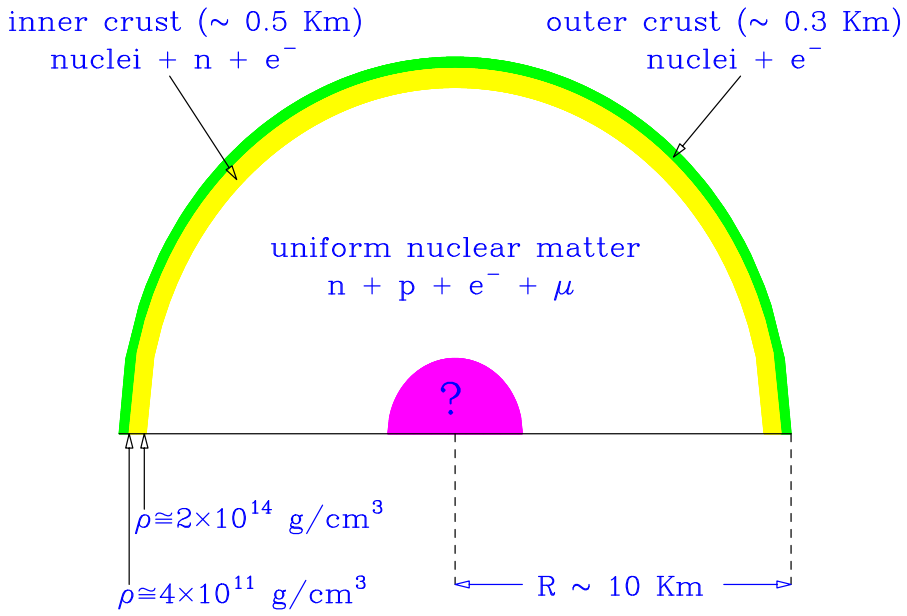

Figure 2.1: Schematic illustration of a neutron star cross section. Note that the equilibrium density of uniform nuclear matter corresponds to $\sim 2\times 10^{14}$g/cm^3.

The properties of matter in the outer crust, corresponding to densities ranging from $\sim 10^7$ g/cm^3 to the *neutron drip* density $\rho_d = 4\times 10^{11}$ g/cm^3, can be obtained directly from nuclear data. On the other hand, models of the EOS at $4\times 10^{11} < \rho < 2\times 10^{14}$ g/cm^3 are somewhat based on extrapolations

of the available empirical information, as the extremely neutron rich nuclei appearing in this density regime are not observed on earth.

The density of the neutron star core ranges between $\sim \rho_0$ ($= 2.67 \times 10^{14}$ g/cm^3) at the boundary with the inner crust, and a central value that can be as large as $1 \div 4 \times 10^{15}$ g/cm^3. All models of EOS based on hadronic degrees of freedom predict that in the density range $\rho_0 \lesssim \rho \lesssim 2\rho_0$ neutron star matter consists mainly of neutrons, with the admixture of a small number of protons, electrons and muons. At any given density the fraction of protons and leptons is determined by the requirements of equilibrium with respect to β-decay and charge neutrality.

This picture may change significantly at larger density with the appearance of heavy strange baryons produced in weak interaction processes. For example, although the mass of the Σ^- exceeds the neutron mass by more than 250 MeV, the reaction $n + e^- \rightarrow \Sigma^- + \nu_e$ is energetically allowed as soon as the sum of the neutron and electron chemical potentials becomes equal to the Σ^- chemical potential.

Finally, as nucleons are known to be composite objects of size $\sim 0.5 - 1.0$ fm, corresponding to a density $\sim 10^{15}$ g/cm^3, it is expected that if the density in the neutron star core reaches this value matter undergoes a transition to a new phase, in which quarks are no longer clustered into nucleons or hadrons.

The theoretical description of matter in the outer and inner neutron star crust will be outlined in the following Sections, whereas the region corresponding to supranuclear density will be described in Chapter 3.

2.1 Outer crust

A solid is expected to form when the ratio of Coulomb energy to thermal energy becomes large, i.e. when

$$\Gamma = \frac{Z^2 e^2}{T r_L} \gg 1 \,, \tag{2.4}$$

with r_L defined through

$$n_I \frac{4\pi r_L^3}{3} = 1 \,, \tag{2.5}$$

n_I being the number density of ions. If the condition (2.4) is fulfilled Coulomb forces are weakly screened and become dominant, while the fluctuation of the ions is small compared to average ion spacing r_L. From (2.4) it follows that a solid is expected to form at temperature

$$T < T_m = \frac{Z^2 e^2}{r_L} \propto Z^2 e^2 n_I^{1/3} \,. \tag{2.6}$$

For example, in the case of ^{56}Fe at densities $\sim 10^7$ g/cm^3 solidification occurs at temperatures below 10^8 °K and Coulomb energy is minimized by a Body Centered Cubic (BCC) lattice. As the density further increases, r_L decreases, so that the condition for solidification continues to be fulfilled. However, as matter density advances into the density domain, 10^7 - 10^{11} g/cm^3, the large kinetic energy of the relativistic electrons shifts the energy balance, favouring inverse β-decay (i.e. electron capture) that leads to the appearance of new nuclear species through sequences like

$$Fe \rightarrow Ni \rightarrow Se \rightarrow Ge \,. \tag{2.7}$$

This process is called neutronization, because the resulting nuclide is always richer in neutron content than that initial one.

Before going on with the analysis of the neutronization process in the neutron star crust, we will duscuss a simple but instructive example, that will allows us to introduce some concepts and procedures to be used in the following Sections.

2.1.1 Inverse β-decay

Consider a gas of noninteracting protons and electrons at $T = 0$. The neutronization process is due to the occurrence of weak interactions turning protons into neutrons through

$$p + e^- \rightarrow n + \nu_e \,. \tag{2.8}$$

Assuming neutrinos to be massless and non interacting, the above process is energetically favorable as soon as the electron energy becomes equal to the neutron-proton mass difference

$$\Delta m = m_n - m_p = 939.565 - 938.272 = 1.293 \text{ MeV} \,. \tag{2.9}$$

As a consequence, the value of n_e at which inverse β-decay sets in can be estimated from

$$\sqrt{p_{F_e}^2 + m_e^2} = \Delta m \,, \tag{2.10}$$

where (see Section 1.1)

$$p_{F_e} = (3\pi^2 n_e)^{1/3} \,, \tag{2.11}$$

leading to

$$n_e = \frac{1}{3\pi^2}\left(\Delta m^2 - m_e^2\right)^{3/2} \approx 7 \times 10^{30} \text{cm}^{-3} \,. \tag{2.12}$$

The corresponding mass density for a system having $Y_e \sim 0.5$, is $\rho \approx 2.4 \times 10^7$ g/cm^3.

Now we want to address the problem of determining the ground state of the system consisting of protons, electrons and neutrons, once equilibrium with respect to the inverse β-decay of Eq. (2.8) has been reached. All interactions, except the weak interaction, will be neglected. Note that process (2.8) conserves baryon number N_B (i.e. the baryon number density n_B) and electric charge.

For any given value of n_B, the ground state is found by minimization of the total energy density of the systems, $\epsilon(n_p, n_n, n_e)$, n_p and n_n being the proton and neutron density, respectively, with the constraints $n_B = n_p + n_n$ (conservation of baryon number) and $n_p = n_e$ (charge neutrality).

Let us define the function

$$F(n_p, n_n, n_e) = \epsilon(n_p, n_n, n_e) + \lambda_B\left(n_B - n_p - n_n\right) + \lambda_Q\left(n_p - n_e\right) \,, \tag{2.13}$$

where ϵ is the energy density, while λ_B and λ_Q are Lagrange multipliers.

The minimum of F corrisponds to the values of n_p, n_n and n_e satisfying the conditions

$$\frac{\partial F}{\partial n_p} = \frac{\partial F}{\partial n_n} = 0 \quad , \quad \frac{\partial F}{\partial n_e} = 0 \tag{2.14}$$

as well as the aditional costraints

$$\frac{\partial F}{\partial \lambda_B} = \frac{\partial F}{\partial \lambda_Q} = 0 \,. \tag{2.15}$$

From the definition of chemical potential of the particles of species i ($i = p, n, e$)

$$\mu_i = \left(\frac{\partial E}{\partial N_i}\right)_V = \left(\frac{\partial \epsilon}{\partial n_i}\right)_V \tag{2.16}$$

it follows that Eqs. (2.14) imply

$$\mu_p - \lambda_B + \lambda_Q = 0 \;\;,\;\; \mu_n - \lambda_B = 0 \;\;,\;\; \mu_e - \lambda_Q = 0 \,, \tag{2.17}$$

leading to the condition of chemical equilibrium

$$\mu_n - \mu_p = \mu_e \,, \tag{2.18}$$

where, in the case of noninteracting particles at $T = 0$,

$$\begin{aligned} \mu_i &= \frac{\partial \epsilon}{\partial n_i} = \frac{2}{(2\pi)^3}\left(\frac{\partial p_{F_i}}{\partial n_i}\right)\frac{\partial}{\partial p_{F_i}} 4\pi \int_0^{p_{F_i}} p^2\, dp\, \sqrt{p^2 + m_i^2} \\ &= \frac{8\pi}{(2\pi)^3}\left(\frac{\partial n_i}{\partial p_{F_i}}\right)^{-1} p_{F_i}^2 \sqrt{p_{F_i}^2 + m_i^2} = \sqrt{p_{F_i}^2 + m_i^2} \,. \end{aligned} \tag{2.19}$$

Defining now the proton and neutron fraction of the system as

$$x_p = \frac{n_p}{n_B} = \frac{n_p}{n_p + n_n} \;\;,\;\; x_n = \frac{n_n}{n_B} = 1 - x_p \tag{2.20}$$

we can rewrite

$$p_{F_p} = p_{F_e} = \left(3\pi^2 x_p n_B\right)^{1/3} \;\;,\;\; p_{F_n} = \left[3\pi^2 \left(1 - x_p\right) n_B\right]^{1/3} \,. \tag{2.21}$$

For fixed baryon density, use of the above definitions in Eq. (2.19) and substitution of the resulting chemical potentials into Eq. (2.18) leads to an equation in the single variable x_p. Hence, for any given n_B the requirements of chemical equilibrium and charge neutrality uniquely determine the fraction of protons in the system.

Once the value of x_p is known, the neutron, proton and electron number densities can be evaluated and the pressure

$$P = P_n + P_p + P_e \tag{2.22}$$

can be obtained using Eq. (1.28).

Figure 2.1.1 shows the proton and neutron number densities, n_p and n_n (recall that $n_e = n_p$) as a function of matter density ρ. It can be seen that in the range $10^5 \le \rho \le 10^7$ g/cm^3 there are protons only and $\log n_p$ grows linearly with $\log \rho$. At $\rho \sim 10^7$ g/cm^3 neutronization sets in and the neutron number density begins to steeply increase. At $\rho > 10^7$ n_p stays nearly constant, while neutrons dominate.

The equation of state of the β-stable mixture is shown in the upper panel of Fig. 2.1.1. Its main feature is that pressure remains nearly constant as matter density increases by almost two orders of magnitude, in the range $10^7 \le \rho \le 10^9$ g/cm^3. The electron and neutron contributions to the pressure are shown in the lower panel of Fig. 2.1.1. Note that, since charge neutrality requires n_p=n_e, the proton pressure is smaller than the electron pressure by a factor $(m_p/m_e) \sim 2000$.

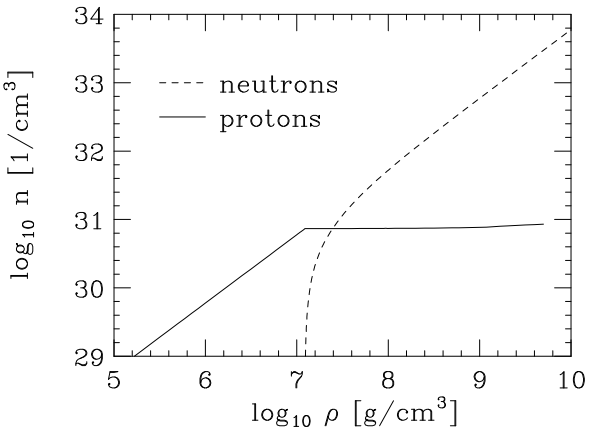

Figure 2.2: Number density of noninteracting protons and neutrons in β-equilibrium as a function of matter density.

2.1.2 Neutronization

The description of β-stable matter in terms of a mixture of degenerate Fermi gases of neutrons, protons and electrons is strongly oversimplified. In reality, electron capture changes a nucleus with given charge Z and mass number A into a different nucleus with the same A and charge (Z−1). Moreover, the new nucleus may be metastable, so that two-step processes of the type

$$^{56}_{26}\mathrm{Fe} \rightarrow {}^{56}_{25}\mathrm{Mn} \rightarrow {}^{56}_{24}\mathrm{Cr} \tag{2.23}$$

can take place. In this case, chemical equilibrium is driven by the mass difference between neighboring nuclei rather than the neutron-proton chemical potential difference.

The measured nuclear charge distributions and masses, $\rho_{ch}(r)$ and $M(Z,A)$, exhibit two very important features

- The charge density is nearly constant within the nuclear volume, its value being roughly the same for all stable nuclei, and drops from ~ 90 % to ~ 10 % of the maximum over a distance R_T ~ 2.5 fm (1 fm = 10×10^{-13} cm), independent of A, called surface thickness (see Fig. 2.4). It can be parametrized in the form

$$\rho_{ch}(r) = \rho_0 \, \frac{1}{1+\mathrm{e}^{(r-\mathrm{R})/\mathrm{D}}} \, , \tag{2.24}$$

  where R = $r_0\mathrm{A}^{1/3}$, with r_0 = 1.07 fm, and D = 0.54 fm. Note that the nuclear charge radius is proportional to $\mathrm{A}^{1/3}$, implying that the nuclear volume increases linearly with the mass number A.

- The (positive) binding energy per nucleon, defined as

$$\frac{B(\mathrm{Z},\mathrm{A})}{A} = \frac{1}{A}\left[\mathrm{Z}m_p + (\mathrm{A}-\mathrm{Z})\,m_n + \mathrm{Z}m_e - M(\mathrm{Z},\mathrm{A})\right] \, , \tag{2.25}$$

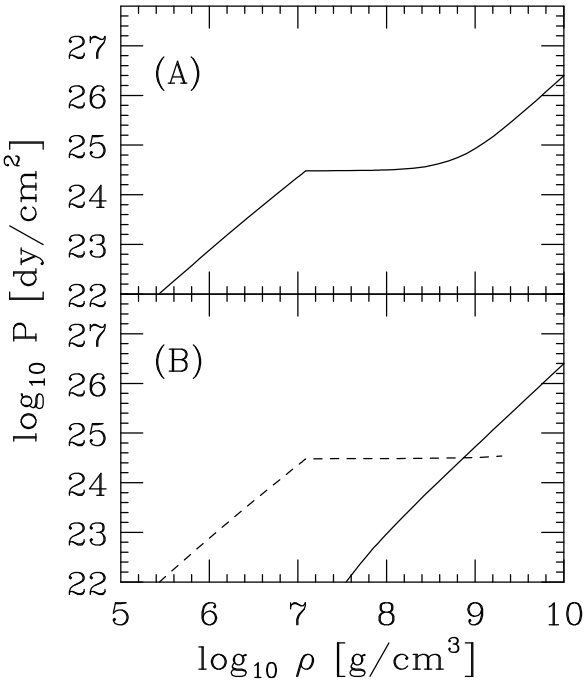

Figure 2.3: (A) Equation of state of a mixture of noninteracting neutrons, electrons and protons in β-equilibrium. (B) Density dependence of the neutron (solid line) and electron (dashed line) contributions to the pressure of β-stable matter.

where $M(\mathrm{Z},\mathrm{A})$ is the measured nuclear mass, is almost constant for A≥ 12 , its value being ~ 8.5 MeV (see Fig. 2.5).

The A and Z dependence of $B(\mathrm{Z},\mathrm{A})$ can be parametrized according to the *semiempirical-mass formula*

$$\frac{B(\mathrm{Z},\mathrm{A})}{A} = \frac{1}{A}\left[\, a_{\mathrm{V}}\mathrm{A} - a_{\mathrm{s}}\mathrm{A}^{2/3} - a_{\mathrm{c}}\frac{\mathrm{Z}^2}{\mathrm{A}^{1/3}} - a_{\mathrm{A}}\frac{(\mathrm{A}-2\mathrm{Z})^2}{4\mathrm{A}} + \lambda\, a_{\mathrm{p}}\frac{1}{\mathrm{A}^{1/2}}\,\right] . \tag{2.26}$$

The first term in square brackets, proportional to A, is called the *volume term* and describes the bulk energy of nuclear matter. The second term, proportional to the nuclear radius squared, is associated with the surface energy, while the third one accounts for the Coulomb repulsion between Z protons uniformly distributed within a sphere of radius R. The fourth term, that goes under the name of *symmetry energy* is required to describe the experimental observation that stable nuclei tend to have the same number of neutrons and protons. Moreover, even-even nuclei (i.e. nuclei having even Z and even A − Z) tend to be more stable than even-odd or odd-odd nuclei. This property is accounted for by the last term in the above equation, where λ −1, 0 and +1 for even-even, even-odd and odd-odd nuclei, respectively. Fig. 2.5 shows the different contributions to $B(\mathrm{Z},\mathrm{A})/\mathrm{A}$, evaluated using Eq. (2.26).

The semi-empirical nuclear mass fomula of Eq. (2.26) can be used to obtain a qualitative description of the neutronization process. The total energy density of the system consisting of nuclei of mass

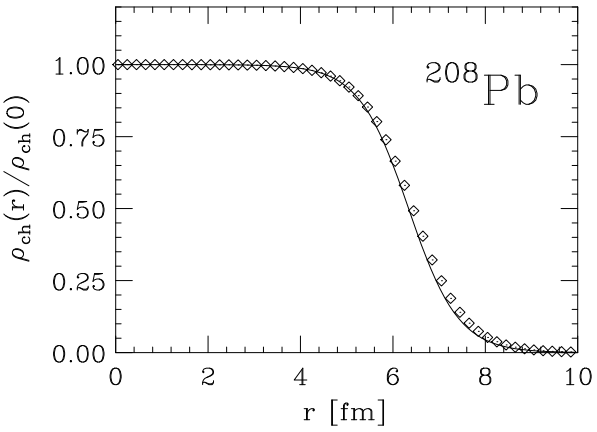

Figure 2.4: Nuclear charge distribution of ^{208}Pb, normalized to $Z/\rho(0)$ (Z = 82). The solid line has been obtained using the parametrization of Eq. (2.24), while the diamonds represent the results of a model independent analysis of electron scattering data.

number A and charge Z arranged in a lattice and surrounded by a degenerate electron gas is

$$\epsilon_T(n_B,\mathrm{A},\mathrm{Z}) = \epsilon_e + \left(\frac{n_B}{\mathrm{A}}\right)[M(\mathrm{Z},\mathrm{A}) + \epsilon_L] \ , \tag{2.27}$$

where ϵ_e is the energy density of the electron gas, Eq. (1.27), n_B and (n_B/A) denote the number densities of nucleons and nuclei, respectively, and ϵ_L is the electrostatic lattice energy per site. As a first approximation, the contribution of ϵ_L will be neglected.

At any given nucleon density n_B the equilibrium configuration corresponds to the values of A and Z that minimize $\epsilon_T(n_B,\mathrm{A},\mathrm{Z})$, i.e. to A and Z such that

$$\left(\frac{\partial \epsilon_T}{\partial Z}\right)_{n_B} = 0 \ , \ \left(\frac{\partial \epsilon_T}{\partial A}\right)_{n_B} = 0 \ . \tag{2.28}$$

Combining the above relationships and using Eq. (2.26) one finds

$$\mathrm{Z} \simeq 3.54 \ A^{1/2}. \tag{2.29}$$

Once Z is known as a function of A, any of the two relationships (2.28) can be used to obtain A as a function of n_B. The mass number A turns out to be an increasing function of n_B, implying that Z also increases with n_B, but at a slower rate. Hence, nuclei become more massive and more and more neutron rich as the nucleon density increases.

The above discussion is obvioulsy still oversimplified. In reality, A and Z are *not* continuous variables and the total energy has to be minimized using the measured nuclear masses, rather than the parametrization of Eq. (2.26), and including the lattice energy, that can be written as

$$\epsilon_L = -K \ \frac{(Ze)^2}{r_s} \tag{2.30}$$

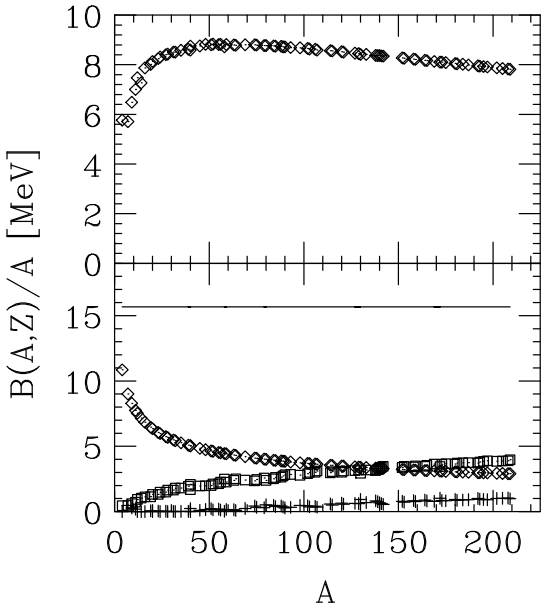

Figure 2.5: Upper panel: A-dependence of the binding energy per nucleon of stable nuclei, evaluated according to Eq. (2.26) with a_V = 15.67 MeV, a_s = 17.23 MeV, a_c = .714 MeV, a_A = 93.15 MeV and a_p = 11.2 MeV. Lower panel: the solid line shows the magnitude of the volume contribution to the binding energy per nucleon, whereas the A-dependence of the surface, coulomb and symmetry contributions are represented by diamonds, squares and crosses, respectively.

where r_s is related to the number density of nuclei through $(4\pi/3)r_s^3 = (n_B/\mathrm{A})^{-1}$ and $K = 0.89593$ for a BCC lattice, yielding the lowest energy. At fixed nucleon number density n_B the total energy density can be written in the form

$$\epsilon_T(n_B,\mathrm{A},\mathrm{Z}) = \epsilon_e + \left(\frac{n_B}{\mathrm{A}}\right)\left[M(\mathrm{Z},\mathrm{A}) - 1.4442(\mathrm{Z}e)^2\left(\frac{n_B}{\mathrm{A}}\right)^{1/3}\right], \tag{2.31}$$

where, for matter density exceeding $\sim 10^6$ g/cm^3, the extreme relativistic limit of the energy density of an electron gas at number density n_e=Zn_B/A (see Section 1.1)

$$\epsilon_e = \frac{3}{4}\left(\mathrm{Z}\frac{n_B}{\mathrm{A}}\right)^{4/3}, \tag{2.32}$$

has to be used.

Collecting together the results of Eqs. (2.30)-(2.32) and expressing n_B in units of $n_{B_0} = 10^{-9}$ fm^{-3} (the number density corresponding to a matter density $\sim 10^6$ g/cm^3), the total *energy per nucleon*, ϵ_T/n_B, can be rewritten in units of MeV as

$$\frac{\epsilon_T}{n_B} = \frac{M(\mathrm{Z},\mathrm{A})}{\mathrm{A}} + \frac{1}{\mathrm{A}^{4/3}}\left[0.4578\,\mathrm{Z}^{4/3} - \frac{\mathrm{Z}^2}{480.74}\right]\left(\frac{n_B}{n_{B_0}}\right)^{1/3}. \tag{2.33}$$

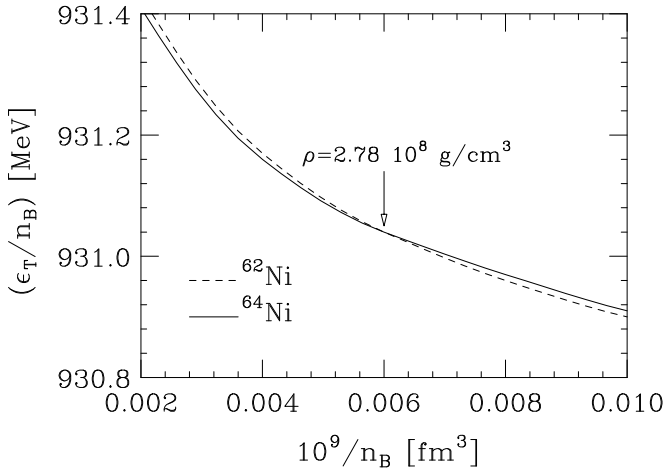

Figure 2.6: Total energy per nucleon of a BCC lattice of ^{62}Ni (dashed line) and ^{64}Ni (solid line) nuclei surrounded by an electron gas, evaluated using eq.(2.33) and plotted versus the inverse nucleon number density.

The average energy per nucleon in a nucleus is about 930 MeV. It can be conveniently written in units of MeV in the form $M(Z,A)/A = 930 + \Delta$. As long as we are dealing with nuclides that are not very different from the stable nuclides, the values of Δ are available in form of tables based on actual measurements or extrapolations of the experimental data.

In practice, ϵ_T/n_B of Eq. (2.33) is computed for a given nucleus (i.e. for given A and Z) as a function of n_B, and plotted versus $1/n_B$ (see Fig. 2.6). The curves corresponding to different nuclei are then compared and the nucleus corresponding to the minimum energy at given n_B can be easily identified. For example, the curves of Fig. 2.6 show the behavior of the energy per particle corresponding to ^{62}Ni and ^{64}Ni, having A−Z = 34 and 36, respectively. It is apparent that a first order phase transition is taking place around the point where the two curves cross one another. The exact densities at which the phase transition occurs and terminates can be obtained using Maxwell's double tangent construction. This method essentially amounts to drawing a straight line tangent to the convex curves corresponding to the two nuclides. In a first order phase transition the pressure remains constant as the density increases. Hence, as all points belonging to the tangent of Maxwell's construction correspond to the same pressure, the onset and termination of the phase transition are simply given by the points of tangency. As expected, at higher density the nucleus with the largest number of neutrons yields a lower energy.

It has to be pointed out that there are limitations to the approach described in this section. Some of the nuclides entering the minimization procedure have ratios Z/A so different from those corresponding to stable nuclei (whose typical value of Z/A is ∼ 0.5, as shown in Fig. 2.7) that the accuracy of the extrapolated masses may be questionable. Obviously, this problem becomes more and more important as the density increases. The study of nuclei far from stability, carried out with radioactive nuclear beams, is regarded as one of the highest priorities in nuclear physics research, and new

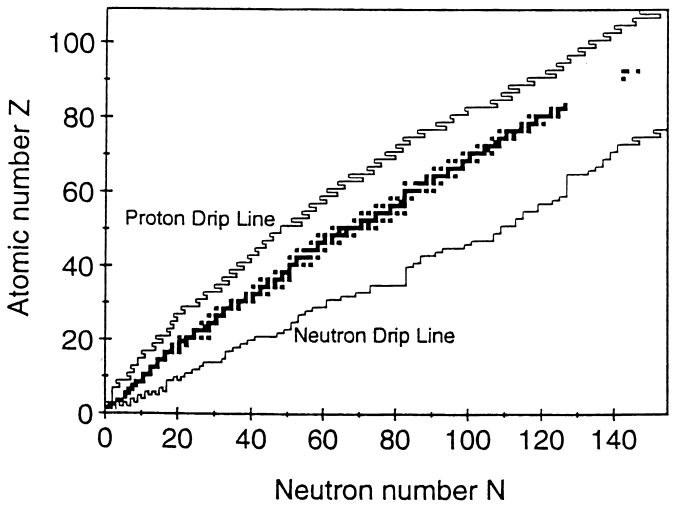

Figure 2.7: Chart of the nuclides. The black squares represent the stable nuclei as a function of Z and N=A−Z. The solid lines correspond to the estimated proton and neutron drip lines.

dedicated experimental facilities are currently being planned both in the U.S. and in Europe.

Table 2.1 reports the sequence of nuclides corresponding to the ground state of matter at subnuclear density, as a function of matter density.

2.2 Inner crust

Table 2.1 shows that as the density increases the nuclides corresponding to the ground state of matter become more and more neutron rich. At $\rho \sim 4.3 \times 10^{11}$ g/cm^3 the ground state corresponds to a Coulomb lattice of ^{118}Kr nuclei, having proton to neutron ratio ~ 0.31 and a slighltly negative neutron chemical potential (i.e. neutron Fermi energy), surrounded by a degenerate electron gas with chemical potential $\mu_e \sim 26$ MeV. At larger densities a new regime sets in, since the neutrons created by electron capture occupy positive energy states and begin to *drip* out of the nuclei, filling the space between them.

At these densities the ground state corresponds to a mixture of two phases: matter consisting of neutron rich nuclei (phase I), with density $\rho_{\rm nuc}$, and a neutron gas of density $\rho_{\rm NG}$ (phase II).

The equilibrium conditions are

$$(\mu_n)_I = (\mu_n)_{II} = \mu_n \tag{2.34}$$

and

$$\mu_p = \mu_n - \mu_e \,, \tag{2.35}$$

where $(\mu_n)_I$ and $(\mu_n)_{II}$ denote the neutron chemical potential in the neutron gas and in the matter of nuclei, respectively.

Nuclide	Z	N = A − Z	Z/A	Δ [MeV]	ρ_{max} [g/cm^3]
^{56}Fe	26	30	.4643	.1616	8.1×10^6
^{62}Ni	28	34	.4516	.1738	2.7×10^8
^{64}Ni	28	36	.4375	.2091	1.2×10^9
^{84}Se	34	50	.4048	.3494	8.2×10^9
^{82}Ge	32	50	.3902	.4515	2.1×10^{10}
^{84}Zn	30	54	.3750	.6232	4.8×10^{10}
^{78}Ni	28	50	.3590	.8011	1.6×10^{11}
^{76}Fe	26	50	.3421	1.1135	1.8×10^{11}
^{124}Mo	42	82	3387	1.2569	1.9×10^{11}
^{122}Zr	40	82	.3279	1.4581	2.7×10^{11}
^{120}Sr	38	82	.3166	1.6909	3.7×10^{11}
^{118}Kr	36	82	.3051	1.9579	4.3×10^{11}

Table 2.1: Sequence of nuclei corresponding to the ground state of matter and maximum density at which they occur. Nuclear masses are given by M(Z,A)/A = (930 + Δ) MeV (from Ref. [10]).

The details of the ground state of matter in the neutron drip regime are specified by the densities ρ, $\rho_{\rm nuc}$ and $\rho_{\rm NG}$, the proton to neutron ratio of the matter in phase I and its surface, whose shape is dictated by the interplay between surface and Coulomb energies.

Recent studies suggest that at densities $4.3\times10^{10} \lesssim \rho \lesssim .75\times10^{14}$ g/cm^3 the matter in phase I is arranged in spheres immersed in electron and neutron gas, whereas at $.75\times10^{14} \lesssim \rho \lesssim 1.2\times10^{14}$ g/cm^3 the energetically favoured configurations exhibit more complicated structures, featuring rods of matter in phase I or alternating layers of matter in phase I and phase II. At $\rho \gtrsim 1.2\times10^{14}$ g/cm^3 there is no separation between the phases, and the ground state of matter corresponds to a homogeneous fluid of neutrons, protons and electrons.

Chapter 3

The neutron star interior

Understandig the properties of matter at densities comparable to the central density of atomic nuclei ($\rho_0 \sim = 2.7 \times 10^{14}$ g/cm^3) is made difficult by *both* the complexity of the interactions *and* the approximations necessarily implied in the theoretical description of quantum mechanical many particle systems. The situation becomes even more problematic as we enter the region of *supranuclear* density, corresponding to $\rho > \rho_0$, as the available empirical information is scarce, and one has to unavoidably resort to a mixture of extrapolation and speculation.

The approach based on non relativistic quantum mechanics and phenomenological nuclear hamiltonians, while allowing for a rather satisfactory description of nuclear bound states and nucleon-nucleon scattering data, fails to fulfill the constraint of causality, as it leads to predict a speed of sound in matter that exceeds the speed of light at large density. On the other hand, the approach based on relativistic quantum field theory, while fulfilling the requirement of causality by construction, assumes a somewhat oversimplified dynamics, not constrained by nucleon-nucleon data. In addition, it is plagued by the uncertainty associated with the use of the mean field approximation, which is long known to fail in strongly correlated systems, such as, for example a van der Waals fluid [11].

In this Chapter, after reviewing the phenomenological constraints on the EOS of cold nuclear matter, we will outline the current understanding of the nucleon-nucleon interaction and the non relativistic and relativistic approaches employed to study the structure of neutron star matter at nuclear and supernuclear density. As anticipated in Section 2.2, in this region a neutron star is believed to consist of a uniform fluid of neutrons, protons and electrons in β-equilibrium.

3.1 Constraints on the nuclear matter EOS

The body of data on nuclear masses can be used to constrain the density depencence predicted by theoretical models of uniform nuclear matter at zero temperature. Note that the zero temperature limit is fully justified, as the typical temperature of the neutron star interior is $\sim 10^9$ °K $\sim .01$ MeV, to be compared to nucleon Fermi energies of tens of MeV.

As we have seen in Section 2.1.2, the A-dependence of the nuclear binding energy is well described by the semiempirical formula (2.26). In the large A limit and neglecting the effect of Coulomb

repulsion between protons, the only term surviving in the case $Z = A/2$ is the term linear in A. Hence, the coefficient a_V can be identified with the binding energy per particle of *symmetric nuclear matter*, an ideal uniform system consisting of equal number of protons and neutrons coupled by strong interactions only. The equilibrium density of such a system, n_0, can be inferred exploiting saturation of nuclear densities, i.e. the fact that the central density of atomic nuclei, measured by elastic electron-nucleus scattering, does not depend upon A for large A (see Fig. 3.1).

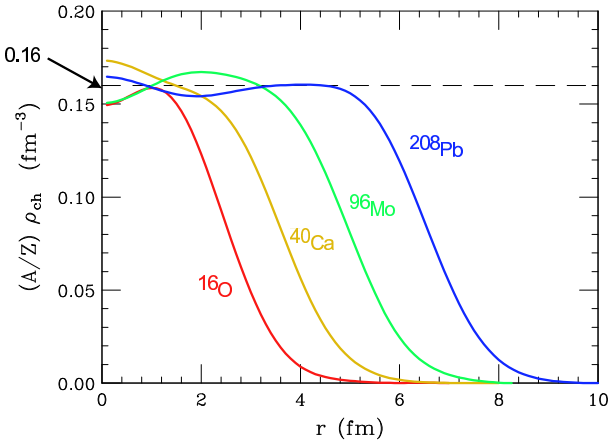

Figure 3.1: Saturation of central nuclear densities measured by elastic electron-nucleus scattering.

The empirical equilibrium properties of symmetric nuclear matter are

$$\left(\frac{E}{A}\right)_{n=n_0} = -16\ \text{MeV}\ ,\quad n_0 \sim .16\ \text{fm}^{-3}\ . \tag{3.1}$$

In the vicinity of the equilibrium density $e = E/A$ can be expanded according to

$$e(n) \approx e_0 + \frac{1}{2}\,\frac{K}{9}\,\frac{(n-n_0)^2}{n_0^2}\ , \tag{3.2}$$

where

$$K = 9\,n_0^2\left(\frac{\partial^2 e}{\partial n^2}\right)_{n=n_0} = 9\left(\frac{\partial P}{\partial n}\right)_{n=n_0} \tag{3.3}$$

is the (in)compressibility module, that can be extracted from the measured excitation energies of nuclear vibrational states. Due to the difficulties implied in the analysis of these experiments, however, empirical estimates of K have a rather large uncertainty, and range from ~ 200 MeV (corresponding to more compressible nuclear matter, i.e. to a *soft* EOS) to ~ 300 MeV (corresponding to a *stiff* EOS).

Unfortunately, the quadratic extrapolation of Eq. (3.2) cannot be expected to work far from equilibrium density. In fact, assuming a parabolic behavior of $e(n)$ at large n ($>> n_0$) leads to predict a speed of sound in matter, c_s, larger than the speed of light, i.e. (compare to Eq. (1.45))

$$c_s^2 = \frac{1}{n}\left(\frac{\partial P}{\partial e}\right) > 1\ , \tag{3.4}$$

regardless of the value of K.

Equation (3.4) shows that causality requires

$$\left(\frac{\partial P}{\partial \epsilon}\right) < 1 \,, \tag{3.5}$$

ϵ being the energy-density. For a relativistic Fermi gas $\epsilon \propto n^{4/3}$, and

$$P \leq \frac{\epsilon}{3} \;\;,\;\; c_s \leq \frac{1}{3} \,. \tag{3.6}$$

where the equal sign corresponds to massless fermions. In the presence of interactions the above limits can be easily exceeded. For example, modeling the repulsion between nucleons in terms of a rigid core leads to predict infinite pressure at finite density.

The relation between microscopic dynamics and speed of sound in matter has been analyzed by Zel'dovich in th early 60s within the framework of relativistic quantum field theory [12].

The model of Ref. [12] describes a system of charged scalar particles of mass M interacting with a massive vector field A^μ. The corresponding field equations are

$$\Box A^\mu + m_v^2 A^\mu = j^\mu \,, \tag{3.7}$$

where m_v is the mass of the vector field. In the case of a point charge at rest at $\mathbf{x} = 0$

$$j_0(\mathbf{x}) = q\delta^{(3)}(\mathbf{x}) \,, \tag{3.8}$$

q being the charge, and Eq.(3.7) has the solution

$$\phi(\mathbf{x}) = q\frac{\mathrm{e}^{-m_v|\mathbf{x}|}}{|\mathbf{x}|} \quad , \quad \mathbf{A} = 0 \,. \tag{3.9}$$

Two charges at rest sitting at positions $\mathbf{x}_1$ and $\mathbf{x}_2$ repel each other, their interaction energy being given by

$$q\phi(x_{12}) = q^2\frac{\mathrm{e}^{-m_v x_{12}}}{x_{12}} \,, \tag{3.10}$$

with $x_{12} = |\mathbf{x}_1| - \mathbf{x}_2$. Note that the effects of self interactions are included in the mass M.

The total energy of a system of N charges can be found using the superposition principle, with the result

$$E = NM + \frac{q^2}{2}\sum_{i\neq j=1}^{N}\frac{\mathrm{e}^{-m_v x_{ij}}}{x_{ij}} \,. \tag{3.11}$$

Denoting by n the density of charges and assuming that

$$n^{-1/3} < m_v^{-1} \,, \tag{3.12}$$

we can resort to the mean field approximation, and write the energy of one charge in the form

$$e = M + q^2\frac{n}{2}\int d^3x\frac{\mathrm{e}^{-m_v x}}{x} = M + 2\pi q^2\frac{n}{m_v^2} \,. \tag{3.13}$$

Finally, from the above equation we can readily obtain the expresions of energy density and pressure

$$\epsilon = ne = nM + 2\pi q^2 \frac{n^2}{m_v^2} \,, \tag{3.14}$$

$$P = n^2 \left(\frac{\partial e}{\partial n}\right) = 2\pi q^2 \frac{n^2}{m_v^2} \,, \tag{3.15}$$

implying that, in the limit of large n, $P \to \epsilon$.

Assuming that the energy density be related to number density through the power law

$$\epsilon = \frac{E}{V} = an^\nu \,, \tag{3.16}$$

energy per particle and pressure can be written

$$e = \frac{E}{N} = a\nu^{n-1} \,, \tag{3.17}$$

$$P = n^2 \left(\frac{\partial e}{\partial n}\right) = (n-1)an^\nu = (n-1)\epsilon \,. \tag{3.18}$$

From the above relations we easily see that that $\nu = 4/3$ corresponds to $P = \epsilon/3$ and that the limiting case $c_s = 1$, i.e. $(\partial P)/(\partial \epsilon) = 1$ is reached when $\nu = 2$. Powers higher than $\nu = 2$ are forbidden by causality.

In the model proposed by Zel'dovich matter consists of baryons interacting through exchange of a massive vector meson described by the lagrangian density

$$\mathscr{L}_V = -\frac{1}{4} F_{\mu\nu} F^{\mu\nu} - \frac{1}{2}\mu^2 A_\mu A^\mu \,, \tag{3.19}$$

where $A^\mu \equiv (\phi, \mathbf{A})$ and μ is the meson mass. The corresponding field equation is

$$(\partial^\nu \partial_\nu + \mu^2) A_\mu = g J_\mu \,, \tag{3.20}$$

g being the coupling constant. In the simple case of a point source located at $\mathbf{x} = 0$

$$J_\mu \equiv (J_0, \mathbf{J}) \equiv (\delta(\mathbf{x}), 0) \,, \tag{3.21}$$

and the solution of (3.20) is

$$\phi(\mathbf{x}') = g \, \frac{\mathrm{e}^{-\mu|\mathbf{x}'-\mathbf{x}|}}{|\mathbf{x}'-\mathbf{x}|} \quad , \quad \mathbf{A} = 0 \,. \tag{3.22}$$

Two charges at rest separated by a distance r repel each other with a force of magnitude

$$F = -g^2 \frac{d}{dr} \frac{\mathrm{e}^{-\mu r}}{r} \,, \tag{3.23}$$

and the corresponding interaction energy is

$$g\phi = g^2 \frac{\mathrm{e}^{-\mu r}}{r} \,. \tag{3.24}$$

In the case of N particles of mass M, as the equation of motion (3.20) is linear, we can use the superposition principle and write the total energy as ($r_{ij} = |\mathbf{r}_i - \mathbf{r}_j|$)

$$E = NM + g^2 \sum_{j>i=1}^{N} \frac{\mathrm{e}^{-\mu r_{ij}}}{r_{ij}} \,. \tag{3.25}$$

Let us now make the further assumption that the average particle density be such that

$$\left(\frac{1}{n}\right)^{1/3} < \frac{1}{\mu} \,. \tag{3.26}$$

The above equation implies that the meson field changes slowly over distances comparable to the average particle separation. If this is the case we can use the mean field approximation and rewrite Eq. (3.25) in the form

$$e = \frac{E}{N} = M + \frac{g^2}{2} \int d^3 r \frac{\mathrm{e}^{-\mu r}}{r} = m + 2\pi g^2 \frac{n}{\mu} \,. \tag{3.27}$$

The corresponding expression of the energy density and pressure read

$$\epsilon = ne = nM + 2\pi g^2 \frac{n^2}{\mu} \tag{3.28}$$

and

$$P = n^2 \left(\frac{\partial e}{\partial n}\right) = 2\pi g^2 \frac{n^2}{\mu} \,. \tag{3.29}$$

From the above equations it follows that, in the large n limit $P \to \epsilon$, inplying in turn $c_s \to 1$. In conclusion, Zel'dovich model shows that the causality limit, corresponding to $\epsilon \propto n^2$, is indeed attained in a simple semirealistic theory, in which nucleons are assumed to interact through exchange of a vector meson.

3.2 The nucleon-nucleon interaction

The main features of the nucleon-nucleon (NN) interaction, inferred from the analysis of nuclear systematics, may be summarized as follows.

- The *saturation* of nuclear density (see Fig. 3.1), i.e. the fact that density in the interior of atomic nuclei is nearly constant and independent of the mass number A, tells us that nucleons cannot be packed together too tightly. Hence, at short distance the NN force must be repulsive. Assuming that the interaction can be described by a non relativistic potential v depending on the interparticle distance, $\mathbf{r}$, we can then write:

$$v(\mathbf{r}) > 0 \quad , \quad |\mathbf{r}| < r_c \,, \tag{3.30}$$

  r_c being the radius of the repulsive core.

- The fact that the nuclear binding energy per nucleon is roughly the same for all nuclei with A≥ 20, its value being
$$\frac{B(\mathrm{Z},\mathrm{A})}{\mathrm{A}} \sim 8.5\ \mathrm{MeV}\,, \tag{3.31}$$
suggests that the NN interaction has a finite range r_0, i.e. that
$$v(\mathbf{r}) = 0 \quad , \quad |\mathbf{r}| > r_0\,. \tag{3.32}$$

- The spectra of the so called *mirror nuclei*, i.e. pairs of nuclei having the same A and charges differing by one unit (implying that the number of protons in a nucleus is the same as the number of neutrons in its mirror companion), e.g. $^{15}_{7}$N (A = 15, Z = 7) and $^{15}_{8}$O (A = 15, Z = 8), exhibit striking similarities. The energies of the levels with the same parity and angular momentum are the same up to small electromagnetic corrections, showing that protons and neutrons have similar nuclear interactions, i.e. that nuclear forces are *charge symmetric*.

Charge symmetry is a manifestation of a more general property of the NN interaction, called *isotopic invariance*. Neglecting the small mass difference, proton and neutron can be viewed as two states of the same particle, the nucleon (N), described by the Dirac equation obtained from the lagrangiam density
$$\mathscr{L} = \overline{\psi}_N \left(i\gamma^\mu \partial_\mu - m\right)\psi_N \tag{3.33}$$
where
$$\psi_N = \begin{pmatrix} p \\ n \end{pmatrix}, \tag{3.34}$$
p and n being the four-spinors associated with the proton and the neutron, respectively. The lagrangian density (3.33) is invariant under the SU(2) global phase transformation
$$U = \mathrm{e}^{i\alpha_j \tau_j}\,, \tag{3.35}$$
where $\boldsymbol{\alpha}$ is a constant (i.e. independent of x) vector and the τ_j ($j = 1,2,3$) are Pauli matrices. The above equations show that the nucleon can be described as a doublet in isospin space. Proton and neutron correspond to isospin projections $+1/2$ and $-1/2$, respectively. Proton-proton and neutron-neutron pairs always have total isospin T=1 whereas a proton-neutron pair may have either $T = 0$ or $T = 1$. The two-nucleon isospin states $|T, T_3\rangle$ can be summarized as follows
$$\begin{aligned} |1,1\rangle &= |pp\rangle \\ |1,0\rangle &= \frac{1}{\sqrt{2}}\left(|pn\rangle + |np\rangle\right) \\ |1,-1\rangle &= |nn\rangle \\ |0,0\rangle &= \frac{1}{\sqrt{2}}\left(|pn\rangle - |np\rangle\right)\,. \end{aligned}$$
Isospin invariance implies that the interaction between two nucleons separated by a distance $r = |\mathbf{r}_1 - \mathbf{r}_2|$ and having total spin S depends on their total isospin T but not on T_3. For example, the potential $v(\mathbf{r})$ acting between two protons with spins coupled to $S = 0$ is the same as the potential acting between a proton and a neutron with spins and isospins coupled to $S = 0$ and $T = 1$.

3.3 The two-nucleon system

The details of the NN interaction can be best studied in the two-nucleon system. There is *only one* NN bound state, the nucleus of deuterium, or deuteron (^{2}H), consisting of a proton and a neutron coupled to total spin and isospin $S = 1$ and $T = 0$, respectively. This is clear manifestation of the fact that nuclear forces are *spin dependent*.

Another important piece of information can be inferred from the observation that the deuteron exhibits a nonvanishing electric quadrupole moment, implying that its charge distribution is not spherically symmetryc. Hence, the NN interaction is *noncentral*.

Besides the properties of the two-nucleon bound state, the large data base of phase shifts measured in NN scattering experiments ($\sim$ 4000 data points corresponding to energies up to 350 MeV in the lab frame) provides valuable additional information on the nature of NN forces.

The theoretical description of the NN interaction was first attempted by Yukawa in 1935. He made the hypotesis that nucleons interact through the exchange of a particle, whose mass μ can be related to the interaction range r_0 according to

$$r_0 \sim \frac{1}{\mu} \,. \tag{3.36}$$

Using $r_0 \sim 1$ fm, the above relation yields $\mu \sim 200$ MeV (1 fm = 197.3 MeV).

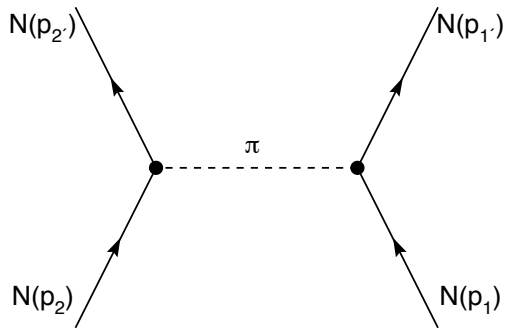

Figure 3.2: Feynman diagram describing the one-pion-exchange process between two nucleons. The corresponding amplitude is given by Eq. (3.37).

Yukawa's idea has been successfully implemented identifying the exchanged particle with the π meson (or *pion*), discovered in 1947, whose mass is $m_\pi \sim 140$ MeV. Experiments show that the pion is a spin zero pseudoscalar particle[1] (i.e. it has spin-parity 0^-) that comes in three charge states, denoted π^+, π^- and π^0. Hence, it can be regarded as an isospin T=1 triplet, the charge states being associated with isospin projections T_3=+ 1, 0 and -1, respectively.

The simplest π-nucleon coupling compatible with the observation that nuclear interactions conserve parity has the pseudoscalar form $ig\gamma^5\boldsymbol{\tau}$, where g is a coupling constant and $\boldsymbol{\tau}$ describes the

[1] The pion spin has been deduced from the balance of the reaction $\pi^+ + {}^2\mathrm{H} \leftrightarrow p + p$, while its intrinsic parity was determined observing the π^- capture from the K shell of the deuterium atom, leading to the appearance of two neutrons: $\pi^- + d \rightarrow n + n$.

isospin of the nucleon. With this choice for the interaction vertex, the amplitude of the process depicted in Fig. 3.2 can readily be written, using standard Feynman's diagram techniques, as

$$\langle f|M|i\rangle = -ig^2 \, \frac{\bar{u}(p_2',s_2')\gamma_5 u(p_2,s_2)\,\bar{u}(p_1',s_1')\gamma_5 u(p_1,s_1)}{k^2-m_\pi^2} \, \langle \boldsymbol{\tau}_1\cdot\boldsymbol{\tau}_2\rangle \, , \tag{3.37}$$

where $k = p_1' - p_1 = p_2 - p_2'$, $k^2 = k_\mu k^\mu = k_0^2 - |\vec{k}|^2$, $u(p,s)$ is the Dirac spinor associated with a nucleon of four momentum $p \equiv (\vec{p}, E)$ (E=$\sqrt{\mathbf{p}^2+m^2}$) and spin projection s and

$$\langle \boldsymbol{\tau}_1\cdot\boldsymbol{\tau}_2\rangle = \eta_{2'}^\dagger \boldsymbol{\tau}\eta_2 \, \eta_{1'}^\dagger \boldsymbol{\tau}\eta_1 \, , \tag{3.38}$$

η_i being the two-component Pauli spinor describing the isospin state of particle i.

In the nonrelativisti limit, Yukawa's theory leads to define a NN interaction potential that can be written in coordinate space as

$$\begin{aligned} v_\pi &= \frac{g^2}{4m^2}\,(\boldsymbol{\tau}_1\cdot\boldsymbol{\tau}_2)(\boldsymbol{\sigma}_1\cdot\nabla)(\boldsymbol{\sigma}_2\cdot\nabla)\,\frac{e^{-m_\pi r}}{r} \\ &= \frac{g^2}{(4\pi)^2}\,\frac{m_\pi^3}{4m^2}\,\frac{1}{3}(\boldsymbol{\tau}_1\cdot\boldsymbol{\tau}_2)\left\{\left[(\boldsymbol{\sigma}_1\cdot\boldsymbol{\sigma}_2)+S_{12}\left(1+\frac{3}{x}+\frac{3}{x^2}\right)\right]\frac{e^{-x}}{x}\right. \\ &\qquad \left. -\frac{4\pi}{m_\pi^3}(\boldsymbol{\sigma}_1\cdot\boldsymbol{\sigma}_2)\delta^{(3)}(\mathbf{r})\right\} \, , \end{aligned} \tag{3.39}$$

where $x = m_\pi|\mathbf{r}|$ and

$$S_{12} = \frac{3}{r^2}(\boldsymbol{\sigma}_1\cdot\mathbf{r})(\boldsymbol{\sigma}_2\cdot\mathbf{r}) - (\boldsymbol{\sigma}_1\cdot\boldsymbol{\sigma}_2) \, , \tag{3.40}$$

is reminiscent of the operator describing the noncentral interaction between two magnetic dipoles. A detailed derivation of Eq.(3.39) can be found in Appendix A.

For $g^2/(4\pi) = 14$, the above potential provides an accurate description of the long range part ($|\mathbf{r}| > 1.5$ fm) of the NN interaction, as shown by the very good fit of the NN scattering phase shifts in states of high angular momentum. In these states, due to the strong centrifugal barrier, the probability of finding the two nucleons at small relative distances becomes in fact negligibly small.

At medium- and short-range other more complicated processes, involving the exchange of two or more pions (possibly interacting among themselves) or heavier particles (like the ρ and the ω mesons, whose masses are $m_\rho = 770$ MeV and $m_\omega = 782$ MeV, respectively), have to be taken into account. Moreover, when their relative distance becomes very small ($|\mathbf{r}| \lesssim 0.5$ fm) nucleons, being composite and finite in size, are expected to overlap. In this regime, NN interactions should in principle be described in terms of interactions between nucleon constituents, i.e. quarks and gluons, as dictated by *quantum chromodynamics* (QCD), which is believed to be the fundamental theory of strong interactions.

Phenomenological potentials describing the *full* NN interaction are generally written as

$$v = \widetilde{v}_\pi + v_R \, , \tag{3.41}$$

where $\widetilde{v}_\pi$ is the one pion exchange potential, defined by Eqs. (3.39) and (3.40), stripped of the δ-function contribution, whereas v_R describes the interaction at medium and short range. The spin-isospin dependence and the noncentral nature of the NN interactions can be properly described

rewriting Eq. (3.41) in the form

$$v_{ij} = \sum_{ST} \left[v_{TS}(r_{ij}) + \delta_{S1} v_{tT}(r_{ij}) S_{12} \right] P_S \Pi_T \ , \tag{3.42}$$

S and T being the total spin and isospin of the interacting pair, respectively. In the above equation P_S ($S = 0, 1$) are the spin projection operators

$$P_0 = \frac{1}{4}(1 - \boldsymbol{\sigma}_1 \cdot \boldsymbol{\sigma}_2) \ \ , \ \ P_1 = \frac{1}{4}(3 + \boldsymbol{\sigma}_1 \cdot \boldsymbol{\sigma}_2) \ , \tag{3.43}$$

satisfying

$$P_0 + P_1 = 1 \ , \ P_S |S'\rangle = \delta_{SS'} |S'\rangle \ , \ P_S P_{S'} = P_S \delta_{SS'} \ , \tag{3.44}$$

and Π_T are the isospin projection operators that can be written as in Eq. (3.43) replacing $\boldsymbol{\sigma} \rightarrow \boldsymbol{\tau}$. The functions $v_{TS}(r_{ij})$ and $v_{Tt}(r_{ij})$ describe the radial dependence of the interaction in the different spin-isospin channels and reduce to the corresponding components of the one pion exchange potential at large r_{ij}. Their shapes are chosen in such a way as to reproduce the available NN data (deuteron binding energy, charge radius and quadrupole moment and the NN scattering phase shifts).

Substitution of Eq. (3.43) and the corresponding expressions for the isospin projection operators allows one to rewrite Eq. (3.42) in the form

$$v_{ij} = \sum_{n=1}^{6} v^{(n)}(r_{ij}) O_{ij}^{(n)} \ , \tag{3.45}$$

where

$$O_{ij}^{(n)} = 1, \ (\boldsymbol{\tau}_i \cdot \boldsymbol{\tau}_j), \ (\boldsymbol{\sigma}_i \cdot \boldsymbol{\sigma}_j), \ (\boldsymbol{\sigma}_i \cdot \boldsymbol{\sigma}_j)(\boldsymbol{\tau}_i \cdot \boldsymbol{\tau}_j), \ S_{ij}, \ S_{ij}(\boldsymbol{\tau}_i \cdot \boldsymbol{\tau}_j) \ , \tag{3.46}$$

and the $v^{(n)}(r_{ij})$ are linear combination of the $v_{TS}(r_{ij})$ and $v_{tT}(r_{ij})$. Note that the operatos defined in Eq. (3.46) form an algebra, as they satisfy the relation

$$O_{ij}^{(n)} O_{ij}^{(m)} = \sum_{\ell} K_{nm\ell} O_{ij}^{(\ell)} \ , \tag{3.47}$$

where the coefficients $K_{nm\ell}$ can be easily obtained from the properties of Pauli matrices. Equations (3.47) can be exploited to greatly simplify the calculation of nuclear observables based on the representation (3.45)-(3.46) of the NN potential.

The typical shape of the NN potential in the state of relative angular momentum $\ell = 0$ and total spin and isospin $S = 0$ and $T = 1$ is shown in Fig. 3.3. The short range repulsive core, to be ascribed to heavy meson exchange or to more complicated mechanisms involving nucleon constituents, is followed by an intermediate range attractive region, largely due to two-pion exchange processes. Finally, at large interparticle distance the one-pion-exchange mechanism dominates. Note the similarity with the van der Waals potential of Fig. 1.1.

3.4 non relativistic many-body theory

Within non relativistic many-body theory (NMBT), nuclear systems are described as a collection of pointlike nucleons interacting through the hamiltonian

$$H = \sum_{i=1}^{\mathrm{A}} \frac{\mathbf{p}_i^2}{2m} + \sum_{j>i=1}^{\mathrm{A}} v_{ij} + \dots \ , \tag{3.48}$$

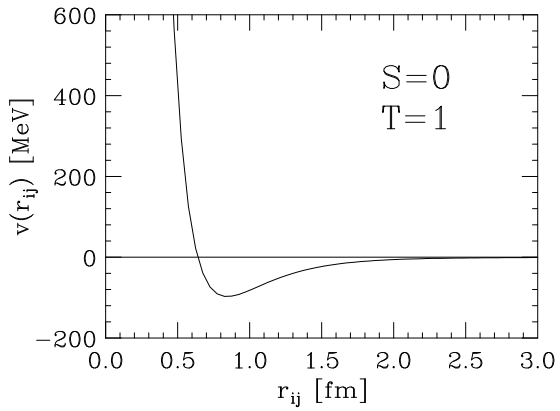

Figure 3.3: Radial dependence of the NN potential describing the interaction between two nucleons in the state of relative angular momentum $\ell = 0$, and total spin and isospin $S = 0$ and $T = 1$.

where $\mathbf{p}_i$ denotes the momentum carried by the i-th nucleon, v_{ij} is the two-body potential describing NN interactions the and the ellipsis refers to the possible existence of interactions involving more than two nucleons.

The validity of the assumptions implied in the treatment of nucleons as pointlike particles, in spite of their finite size, can be gauged using the empirical information provided by elastic electron-proton scattering experiments. The measured cross section are in fact simply related to the proton charge form factor, the Fourier transform of which yields the charge distribution in coordinate space. Figure 3.4 illustrates the overlap between the charge distributions of two protons separated by a distance $1 < d < 2$ fm. The results of theoretical calculations, yielding an average nucleon-nucleon separation distance ~ 2.5 fm in isospin symmetric nuclear matter at equilibrium desity, suggest that the finite size of the nucleon may not play a critical role up to densities $\rho \lesssim 3\rho_0$.

Unfortunately, solving the Schrödinger equation

$$H|\Psi_0\rangle = E_0|\Psi_0\rangle \ . \tag{3.49}$$

for the ground state of a nucleus, using the hamiltonian (3.48) and the NN potential of Eqs.(3.45) and (3.46), is only possible for not too large A. The numerical solution is trivial for A=2 only. For A=3 Eq. (3.49) can still be solved using deterministic approaches, while for A>3 sthocastic methods, such as the Green Function Monte Carlo method, have to be employed. The results of these calculations will be briefly reviewed in the next Section.

3.4.1 The few-nucleon systems

The NN potential determined from the properties of the two-nucleon system can be used to solve Eq. (3.49) for $A > 2$. In the case $A = 3$ the problem can be still solved exactly, but the resulting ground state energy, E_0, turns out to be slightly different from the experimental value. For example, for ^3He one typically finds $E_0 = 7.6$ MeV, to be compared to $E_{exp} = 8.48$ MeV. In order to exactly reproduce

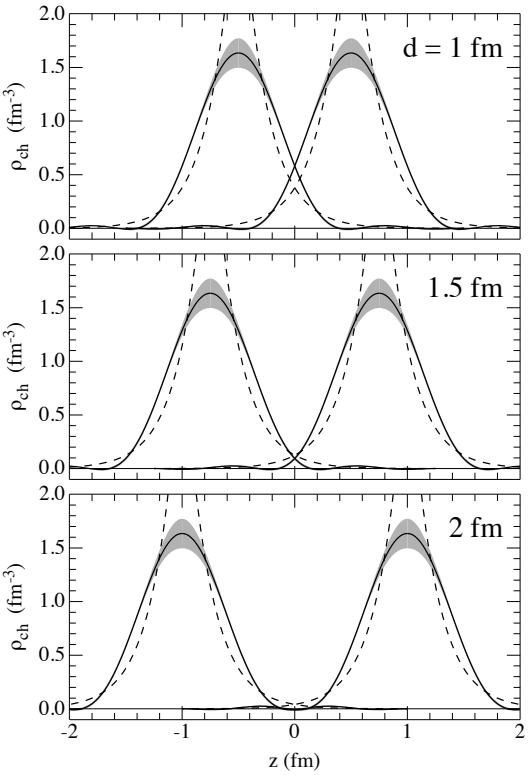

Figure 3.4: Overlap between the charge distributions of two protons separated by a distance $1 < d < 2$ fm. The shaded area corresponds to the experimental error, while the dashed lines have been obtained using a simple dipole parametrization of the proton charge form factor.

E_{exp} one has to add to the nuclear hamiltonian a term containing three-nucleon interactions described by a potential V_{ijk}. The most important process leading to three nucleon interactions is the two-pion exchange associated with the excitation of a nucleon resonance in the intermediate state, depicted in Fig. 3.5.

The three-nucleon potential is usually written in the form

$$V_{ijk} = V_{ijk}^{2\pi} + V_{ijk}^{N} \,, \tag{3.50}$$

where the first contribution takes into account the process of Fig. 3.5 while V_{ijk}^{N} is purely phenomenological. The two parameters entering the definition of the three-body potential are adjusted in such a way as to reproduce the properties of ^3H and $3He$. Note that the inclusion of V_{ijk} leads to a very small change of the total potential energy, the ratio $\langle V_{ijk}\rangle / \langle v_{ij}\rangle$ being ~ 2 %.

For $A > 3$ the Scrödinger equation is no longer exactly solvable. The ground state energy of nuclei having $A \geq 4$ can be estimated from Ritz principle, stating that the expectation value of the hamiltonian in the trial state $|\Psi_V\rangle$ satisfies

$$E_V = \frac{\langle \Psi_V | H | \Psi_V \rangle}{\langle \Psi_V | \Psi_V \rangle} \geq E_0 \,, \tag{3.51}$$

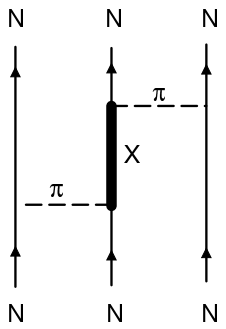

Figure 3.5: Diagrammatic representation of the process providing the main contribution to the three-nucleon interaction. The thick solid line corresponds to an excited state of the nucleon.

E_0 being the ground state energy. Obviously, the larger the overlap $\langle\Psi_0|\Psi_V\rangle$ the closer E_V is to E_0.

In the variational approach based on Eq. (3.51) E_0 is estimated carrying out a functional minimization of E_V. The trial ground state is written in such a way as to reflect the structure of the nuclear interaction hamiltonian. For few nucleon systems it takes the form

$$|\Psi_V\rangle = (1+U)\,|\Psi_P\rangle\,, \tag{3.52}$$

where

$$|\Psi_P\rangle = F|\Phi_A(JJ_3TT_3)\rangle\,. \tag{3.53}$$

In the above equations $|\Phi_A(JJ_3TT_3)\rangle$ is a shell model state, describing A independent particles coupled to total angular momentum J and total isospin T, with third components J_3 and T_3, while the operators U and F take into acount the correlation structure induced by the two- and three-nucleon potentials, respectively. The dominant correlation effects, associated with the NN potential v_{ij}, are described by the operator F, which is usually written

$$F = \mathscr{S}\prod_{j>i=1}^{A} f_{ij}\,, \tag{3.54}$$

where $\mathscr{S}$ is the symmetrization operator and (compare to Eq. (3.45))

$$f_{ij} = \sum_{n=1}^{6} f^{(n)}(r_{ij})O_{ij}^{(n)}\,. \tag{3.55}$$

The shape of the radial correlation functions $f^{(n)}$ are determined by minimizing the expectation value E_V. In few nucleon systems this procedure is implemented choosing suitable analytical expressions involving few adjustable parameters.

The main features of the $f^{(n)}$ are dictated by the behaviour of the corresponding component of the potential v_{ij}. For example, due to the presence of the strong repulsive core $f^{(n)}(r) \ll 1$ at $r \lesssim 1$ fm. A typical set of radial correlation functions is shown in Fig. 3.6.

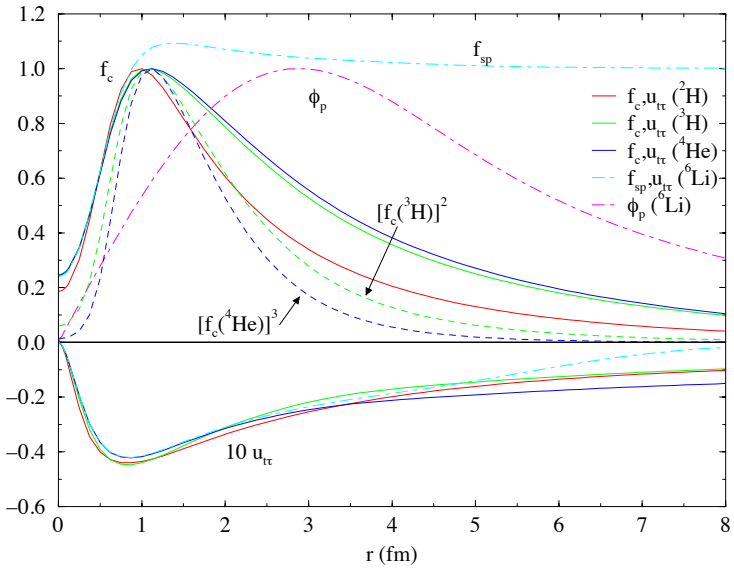

Figure 3.6: Correlation functions in few nucleon systems: the central and tensor-isospin components $f^{(1)}$ and $f^{(4)}$ are denoted by f_c and $u_{t\tau}$, respectively. The dashed lines show $f_c^2(^3\mathrm{H})$ and $f_c^3(^4\mathrm{He})$ to illustrate the large r behavior. The dot-dashed line marked ϕ_p shows the independent particle model wave function for ^{6}Li.

The main difficulty of the variational approach is the calculation of the expectation value E_V, involving an integration over $3A$ space coordinate as well as a sum over the spin-isospin degrees of freedom, which makes the dimensionality of the problem very difficult to handle for $A \geq 8$.

To understand this problem, let us write the variational state in the form

$$|\Psi_V\rangle = \sum_n \Psi_n(R)|n\rangle \,, \tag{3.56}$$

where the sum includes all possible spin-isospin states, labelled by the index n, and $R \equiv \{\mathbf{r}_1, \ldots, \mathbf{r}_A\}$ specifies the space configuration of the system. For example, in the case of ^3He ($J = T = 1/2$) one finds

$$\begin{aligned} |1\rangle &= |\uparrow p \uparrow n \downarrow n\rangle \\ |2\rangle &= |\downarrow p \uparrow n \downarrow n\rangle \\ |3\rangle &= |\downarrow n \uparrow p \downarrow n\rangle \\ \ldots &= \ldots\ldots \,, \end{aligned} \tag{3.57}$$

The possible spin states of A spin-1/2 particles are 2^A and, since Z of the A nucleons can be protons, there are $A!/Z!(A-Z)!$ isospin states. Hence, the sum over n in Eq. (3.56) involves

$$M = 2^A \, \frac{A!}{Z!(A-Z)!} \,, \tag{3.58}$$

contributions.

In the representation of Eq. (3.56) the nuclear hamiltonian H is a $M \times M$ matrix whose elements depend upon R. To obtain E_V one has to evaluate the $M \times M$ integrals

$$\int dR \Psi_n^\dagger(R) H_{nm} \Psi_m(R) \,, \tag{3.59}$$

whose calculation is carried out using the Monte Carlo (MC) method.

The expectation value of any operator O in the state Ψ_V can be written in the form

$$\begin{aligned} \langle O \rangle &= \sum_{m,n} \int dR \left[\frac{\Psi_m^\dagger(R) O_{mn}(R) \Psi_n(R)}{P_{mn}(R)} \right] P_{mn}(R) \\ &= \sum_{m,n} \int dR \, \widetilde{O}_{mn}(R) P_{mn}(R) \,, \end{aligned} \tag{3.60}$$

with

$$\widetilde{O}_{mn} = \frac{\Psi_m^\dagger(R) O_{mn}(R) \Psi_n(R)}{P_{mn}(R)} \,, \tag{3.61}$$

the probability distribution $P_{mn}(\mathbf{R})$ being given by

$$P_{mn}(R) = |\mathrm{Re}(\Psi_m^\dagger(R) \Psi_n(R))| \,. \tag{3.62}$$

Let $\{R_p\} \equiv \{R_1, \ldots, R_{N_c}\}$ be a set of N_c configurations drawn from the probability distribution of Eq. (3.60), i.e. such that the probability that a configuration $\widetilde{R}$ belongs to the set $\{R_p\}$ is proportional to $P_{mn}(R)$. It then follows that

$$\int dR \, \widetilde{O}_{mn}(R) P_{mn}(R) = \lim_{N_c \to \infty} \frac{1}{N_c} \sum_{p=1}^{N_c} \widetilde{O}_{mn}(R_p) \,. \tag{3.63}$$

The above procedure, called Variational Monte Carlo (VMC) method, allows one to obtain estimates of the ground state energy E_0 whose accuracy is limited by the statistical error associated with the use of a finite configuration set and by the uncertainty in the choice of the trial wave function. The second source of error can be removed using the Green Function Monte Carlo (GFMC) approach.

Let $\{|\Psi_m\rangle\}$ be the complete set of eigenstates of the nuclear hamiltonian, satisfying

$$H|\Psi_m\rangle = E_m|\Psi_m\rangle \,. \tag{3.64}$$

The trial variational wave function can obviously be expanded according to

$$|\Psi_V\rangle = \sum_n \beta_n \, |\Psi_m\rangle \,, \tag{3.65}$$

implying

$$\lim_{\tau \to \infty} \mathrm{e}^{-H\tau} |\Psi_V\rangle = \lim_{\tau \to \infty} \sum_n \beta_n \, \mathrm{e}^{-E_m \tau} |\Psi_m\rangle = \beta_0 \, \mathrm{e}^{-E_0 \tau} |\Psi_0\rangle \,. \tag{3.66}$$

Hence, evolution of the variational ground state to infinite imaginary time projects out the *true* ground state of the nuclear hamiltonian and allows one to extract the corresponding eigenvalue.

The calculation is carried out dividing the imaginary time interval τ in N steps of length $\Delta\tau = \tau/N$ to rewrite

$$e^{-H\tau} = \left(e^{-H\Delta\tau}\right)^N . \tag{3.67}$$

The state at imaginary time $(i+1)\Delta\tau$ is can be obtained from the one corresponding to $\tau = i\Delta\tau$ through the relation

$$|\Psi_V^{i+1}\rangle = e^{-H\Delta\tau}|\Psi_V^i\rangle , \tag{3.68}$$

that can be rewritten ($|RST\rangle$ specifies the configuration of the system in coordinate, spin and isospin space)

$$\langle R'S'T'|\Psi_V^{i+1}\rangle = \sum_{ST}\int dR\, \langle R'S'T'|e^{-H\Delta\tau}|RST\rangle\langle RST|\Psi_V^i\rangle , \tag{3.69}$$

or

$$\Psi_{V,S'T'}^{i+1}(R) = \sum_{ST}\int dR\, G_{S'T',ST}(R',R)\Psi_{V,ST}^i(R) , \tag{3.70}$$

The Green's function appearing in the above equation, yielding the amplitude for the system to evolve from $|RST\rangle$ to $|R'S'T'\rangle$ during the imaginary time interval $\Delta\tau$, is defined as

$$G_{S'T',ST}(R',R) = \langle R'S'T'|e^{-H\Delta\tau}|RST\rangle . \tag{3.71}$$

The GFMC approach has been succesfully employed to describe the ground state and the low lying excited states of nuclei having A up to 8. The results of these calculations, summarized in Table 3.1 and Fig. 3.7, show that the non relativistic approach, based on a dynamics modeled to reproduce the properties of two- and three-nucleon systems, has a remarkable predictive power.

$^AZ(J^\pi;T)$	VMC (Ψ_T)	VMC (Ψ_V)	GFMC	Expt
^{2}H($1^+;0$)	–2.2248(5)			–2.2246
^{3}H($(1/2)^+;1/2$)	–8.15(1)	–8.32(1)	–8.47(1)	–8.48
^{4}He($0^+;0$)	–26.97(3)	–27.78(3)	–28.34(4)	–28.30
^{6}He($0^+;1$)	–23.64(7)	–24.87(7)	–28.11(9)	–29.27
^{6}Li($1^+;0$)	–27.10(7)	–27.83(5)	–31.15(11)	–31.99
^{7}He($(3/2)^-;3/2$)	–18.05(11)	–19.75(12)	–25.79(16)	–28.82
^{7}Li($(3/2)^-;1/2$)	–31.92(11)	–33.04(7)	–37.78(14)	–39.24
^{8}He($0^+;2$)	–17.98(8)	–19.31(12)	–27.16(16)	–31.41
^{8}Li($2^+;1$)	–28.00(14)	–29.76(13)	–38.01(19)	–41.28
^{8}Be($0^+;0$)	–45.47(16)	–46.79(19)	–54.44(19)	–56.50

Table 3.1: Experimental and quantum Monte Carlo ground state energies of nuclei with A=2-8 in MeV. The columns marked VMC(Ψ_V) and GFMC show the VMC and GFMC results, respectively.

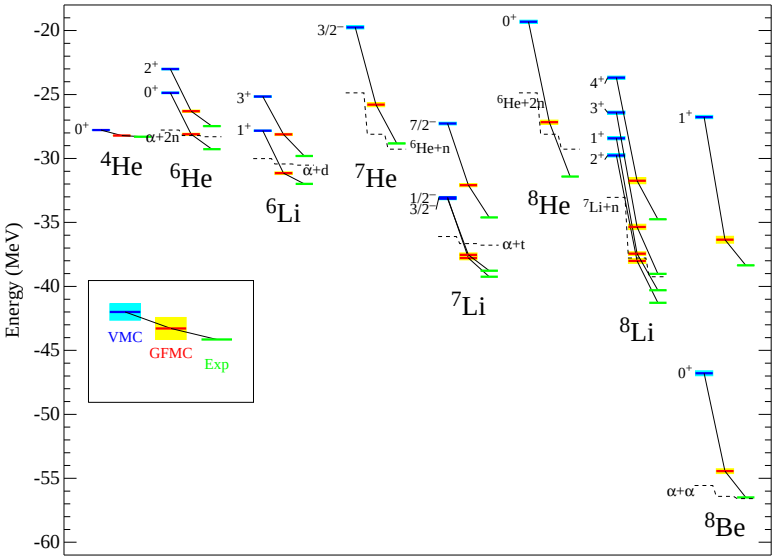

Figure 3.7: VMC and GFMC energies of nuclei with $A \leq 8$ compared to experiment.

3.4.2 Nuclear matter

In the case of neutron stars, correponding to A $\sim 10^{57}$, the computational techniques described in Section 3.4.1 cannot be applied and approximations need to be made.

In the simplest scheme the complicated NN potential is replaced by a *mean field*. This amount to substituting

$$\sum_{j>i=1}^{A} v_{ij} \rightarrow \sum_{i=1}^{A} U_i \,, \tag{3.72}$$

in Eq. (3.48), witht the potential U chosen in such a way that the *single particle* hamiltonian

$$h_0 = \frac{p^2}{2m} + U \,, \tag{3.73}$$

be diagonalizable. Within this framework the nuclear ground state wave function reduces to a Slater determinant, constructed using the A lowest energy eigenstates of h_0:

$$|\Psi_0\rangle = \frac{1}{\sqrt{A!}} \det\{\phi_i\} \,, \tag{3.74}$$

the ϕ_i's (i = 1, 2,..., A) being solutions of the Schrödinger equation

$$h_0|\phi_i\rangle = \epsilon_i|\phi_i\rangle \,, \tag{3.75}$$

and the corresponding ground state energy is given by

$$E_0 = \sum_{i=1}^{A} \epsilon_i \ . \tag{3.76}$$

This procedure is the basis of the nuclear shell model, that has been succesfully applied to explain many nuclear properties.

Matter in the neutron star interior, however, is a uniform, dense nuclear fluid, whose single particle wave functions are known to be plane waves, as dictated by translational invariace. Shell effects are not expected to play a major role in such a system. On the other hand, strong correlations between nucleons induced by the NN potential, not taken into account within the mean field approximation, become more and more important as the density increases, and can not be disregarded.

Let us first consider symmetric nuclear matter, defined as a uniform extended system containing equal numbers of proton and neutrons which interact through strong interactions only. Neglecting, for the sake of simplicity, three-nucleon forces, the nuclear matter hamiltonian can be written as in Eq.(3.48) with v_{ij} denoting the NN potential. In absence of interactions, the wave function is a Slater determinant of single particle states

$$\varphi_{\mathbf{k}\sigma\tau}(\mathbf{r}) = \frac{1}{\sqrt{V}} e^{\mathbf{k}\cdot\mathbf{r}} \chi_\sigma \eta_\tau \ , \tag{3.77}$$

where χ and η are the Pauli spinors describing spin and isospin, respectively, and $|\mathbf{k}| < k_F = (3\pi^2 n/2)^{1/3}$, n being the matter density.

The main problem associated with the application of many-body perturbation theory to nuclear matter is the presence of the strongly repulsive core in the NN potential (see Section 3.2 and Fig. 3.3), that makes the matrix elements

$$\langle \varphi_{\mathbf{k_1}'\sigma_{1'}\tau_{1'}} \varphi_{\mathbf{k_2}'\sigma_{2'}\tau_{2'}} | v_{12} | \varphi_{\mathbf{k}_1\sigma_1\tau_1} \varphi_{\mathbf{k}_2\sigma_2\tau_2} \rangle \ , \tag{3.78}$$

very large or even divergent. As we will see, this difficulty can be circumvented either through a proper redefintion of the interaction potential or changing the basis of states describing the "unperturbed" system.

A. G-matrix perturbation theory

Within the first approach the hamiltonian is first split in two pieces according to

$$H = H_0 + H_1 \ , \tag{3.79}$$

with

$$H_0 = \sum_{i=1}^{N} (K_i + U_i) \ , \tag{3.80}$$

where $K = -\nabla^2/2m$ is the kinetic energy operator, and

$$H_1 = \sum_{j>i=1}^{N} v_{ij} - \sum_{i=1}^{N} U_i \ , \tag{3.81}$$

with the single particle potential generally chosen in such a way as to make the perturbative expansion rapidly convergent. The interaction hamiltonian H_1 is then treated perturbatively, summing up infinite set of diagrams to overcome the problems assciated with the calculation of the matrix elements (3.78). This procedure leads to the integral equation defining the G-matrix

$$G(W) = v - v\,\frac{Q}{W}\,G\,. \tag{3.82}$$

The G-matrix, as diagrammatically illustrated in Fig. 3.8, is the operator describing NN scattering in the nuclear medium. The quantity W appearing in Eq. (3.82) is the energy denominator associated with the propagator of the intermediate state, while the operator Q prevents scattering to states in the Fermi sea, forbidden by Pauli exclusion principle.

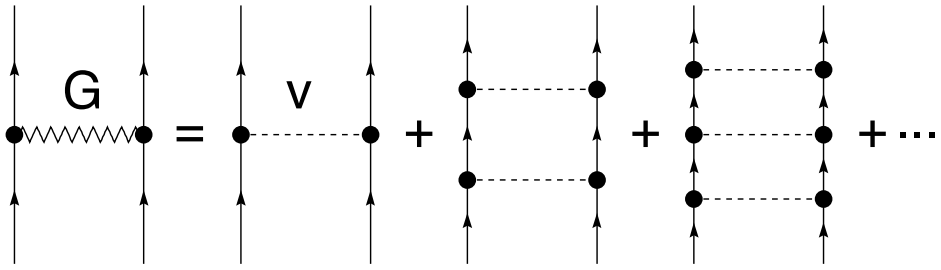

Figure 3.8: Diagrammatic representation of Eq. (3.82).

The state describing two interacting nucleons ψ_{ij} can be expressed in terms of G through the Bethe-Golstone equation

$$\psi_{ij} = \phi_{ij} - \frac{Q}{W} G\,\psi_{ij}\,, \tag{3.83}$$

where $\phi_{ij} = \varphi_i\varphi_j$, with $\varphi_i = \varphi_{\mathbf{k}_i\sigma_i\tau_i}$ given by Eq. (3.77), is the corresponding unperturbed state. From Eq. (3.83) it follows that the matrix elements of G between unperturbed states

$$\langle\phi_{i'j'}|G|\phi_{ij}\rangle = \langle\phi_{i'j'}|v|\psi_{ij}\rangle\,, \tag{3.84}$$

are well behaved.

Although the expansion in powers of G is still not convergent, the terms in the perturbative series can be grouped in such a way as to obtain a convergent expansion in powers of the quantity

$$\kappa = n\sum_{ij}\int d^3r|\phi_{ij}(r) - \psi_{ij}(r)|^2\,, \tag{3.85}$$

where the sum is extended to all states belonging to the Fermi sea. The definition shows that κ measures the average distortion of the two-nucleon wave function produced by NN forces.

Nuclear matter calculations carried out within G-matrix perturbation theory include contributions of order κ^3 to the energy per nucleon. The results show that the convergence strongly depends on the choice of the single particle potential U.

B. CBF perturbation theory

In the alternative approach, called Correlated Basis Functions (CBF) perturbation theory, the non-perturbative effects arising from the short range repulsive core of the interaction potential are incorporated in the basis functions. The unperturbed Fermi gas states $|n_0\rangle$ are replaced by the set of correlated states

$$|n\rangle = \frac{F|n_0\rangle}{\langle n_0|F^\dagger F|n_0\rangle^{1/2}} , \tag{3.86}$$

where F is the *correlation operator*, whose structure reflects the complexity of the NN potential. In most nuclaer matter applications F is written in the form

$$F = \mathscr{S} \prod_{j>i=1}^{A} f_{ij} , \tag{3.87}$$

where

$$f_{ij} = \sum_n f^{(n)}(r_{ij}) O^{(n)}_{ij} , \tag{3.88}$$

$\mathscr{S}$ is the operator that symmetrizes the product on its right hand side and the operators $O^{(n)}$ are defined in Eq. (3.47).

The correlated states (3.86) form a complete set but are *not* orthogonal to one another. However, they can be orthogonalized using standard techniques of many-body perturbation theory.

The radial shapes of the $f^{(n)}(r)$ are determined minimizing the expectation value $E_V = \langle 0|H|0\rangle$. In nuclear matter, this procedure leads to a set of Euler-Lagrange equations, whose solutions satisfy the boundary conditions

$$\lim_{r\to\infty} f^{(n)}(r) = \begin{cases} 1 & n=1 \\ 0 & n>1 \end{cases} . \tag{3.89}$$

The short range behaviour of the two-nucleon correlation functions is such that the quantity

$$f^\dagger_{ij} H_{ij} f_{ij} = f^\dagger_{ij} \left(\frac{\mathbf{p}_i^2}{2m} + \frac{\mathbf{p}_j^2}{2m} + v_{ij} \right) f_{ij}, \tag{3.90}$$

which reduces to H_{ij} at large interparticle distances, is well behaved as $r \to 0$.

Once the correlated basis has been defined, the nuclear hamiltonian can be split in two pieces according to Eq. (3.79), where H_0 and H_1 are now defined as the diagonal and off diagonal part of H in the correlated basis, respectively. We can then write

$$\langle m|H_0|n\rangle = \delta_{mn}\langle m|H|n\rangle \tag{3.91}$$

$$\langle m|H_1|n\rangle = (1-\delta_{mn})\,\langle m|H|n\rangle . \tag{3.92}$$

If the two-body correlation function has been properly chosen, i.e. if E_V is close to the eigenvalue E_0, the correlated states have large overlaps with the true eigenstates of the nuclear hamiltonian and the

matrix elements of H_1 are small. Hence, the perturbative expansion in powers of H_1 is expected to be rapidly convergent.

The explicit calculation of matrix elements of H between correlated states involves prohibitive difficulties, as it requires integrations over the coordinates of a huge number of particles. It is usually performed expanding the matrix element in a series whose terms represent the contributions of subsystems (clusters) containing an increasing number (2, 3, ..., A) of nucleons. The terms in the series can be classified according to their topological structure and summed up to all orders solving a set of coupled integral equations, called Fermi Hyper-Netted Chain (FHNC) equations.

3.5 Relativistic mean field theory: the $\sigma - \omega$ model

The theoretical approach described in the previous section is based on the assumption that the degrees of freedom associated with the carriers of the NN interaction can be eliminated in favor of a static NN potential. While this procedure has proved exceedingly succesful at $\rho \sim \rho_0$, as matter density (and therefore the nucleon Fermi momentum) increases the relativistic propagation of the nucleons, as well as the retarded propagation of the virtual meson fields giving rise to nuclear forces, are expected to become more and more significant.

In principle, relativistic quantum field theory provides a well defined theoretical framework in which relativistic effects can be taken into account in a fully consistent fashion. Due to the complexity and non perturbative nature of the strong interaction, however, the *ab initio* approach to the nuclear many problem, based on the QCD lagrangian, involves prohibitive difficulties. In fact, even the structure of individual hadrons, like the proton or the π meson, is not yet understood at a fully quantitative level in terms of the elementary QCD degrees of freedom. Let alone the structure of highly condensed hadronic matter at supernuclear densities.

It has to be pointed out, however, that when dealing with condensed matter it is often convenient to replace the lagrangian describing the interactions between elementary constituents, be it solvable or not, with properly constructed *effective interactions*. For example, the properties of highly condensed systems bound by electromagnetic interactions are most successfully explained using effective interatomic potentials. In spite of the fact that the lagrangian of quantum electrodynamics is very well known and can be treated in perturbation theory, nobody in his right mind would ever use it to carry out explicit calculations of the bulk properties of condensed matter.

The fact that most of the time nucleons in nuclear matter behave as individual particles interacting through boson exchange suggests that the fundamental degrees of freedom of QCD, quarks and gluons, may indeed be replaced by nucleons and mesons, to be regarded as the degrees of freedom of an *effective* field theory.

In this section we will describe a simple model in which nuclear matter is viewed as a uniform system of nucleons, described by Dirac spinors, interacting through exchange of a scalar and a vector meson, called σ and ω, respectively.

The basic element of the σ-ω model is the lagrangian density

$$\mathscr{L} = \mathscr{L}_N + \mathscr{L}_B + \mathscr{L}_{int} \,, \tag{3.93}$$

where $\mathscr{L}_N$, $\mathscr{L}_B$ and $\mathscr{L}_{int}$ describe free nucleons and mesons and their interactions, respectively. The

dynamics of the free nucleon field is dictated by the Dirac lagrangian of Eq. (3.33)

$$\mathscr{L}_N(x) = \overline{\psi}(x)\,(i\partial\!\!\!/ - m)\,\psi(x)\,, \tag{3.94}$$

where the nucleon field, denoted by $\psi(x)$, combines the two four-component Dirac spinors describing proton and neutron, as in Eq. (3.34). The meson lagrangian reads

$$\begin{aligned}\mathscr{L}_B(x) &= \mathscr{L}_\omega(x) + \mathscr{L}_\sigma(x) \\ &= -\frac{1}{4}F^{\mu\nu}(x)F_{\mu\nu}(x) + \frac{1}{2}m_\omega^2 V_\mu(x)V^\mu(x) \\ &+ \frac{1}{2}\partial_\mu\phi(x)\partial^\mu\phi(x) - \frac{1}{2}m_\sigma^2\phi(x)^2\end{aligned} \tag{3.95}$$

where

$$F_{\mu\nu}(x) = \partial_\nu V_\mu(x) - \partial_\mu V_\nu(x)\,, \tag{3.96}$$

$V_\mu(x)$ and $\sigma(x)$ are the vector and scalar meson fields, respectively, and m_ω and m_σ the corresponding masses.

In specifying the form of the interaction lagrangian we will require that, besides being a Lorentz scalar, $\mathscr{L}_{int}(x)$ gives rise to a Yukawa-like meson exchange potential in the static limit. Hence, we write

$$\mathscr{L}_{int}(x) = g_\sigma\phi(x)\overline{\psi}(x)\psi(x) - g_\omega V_\mu(x)\overline{\psi}(x)\gamma^\mu\psi(x)\,, \tag{3.97}$$

where g_σ and g_ω are coupling constants and the choice of signs reflect the fact that the NN interaction contains both attractive and repulsive contributions.

The equations of motion for the fields follow from the Euler-Lagrange equations associated with the lagrangian density of Eq. (3.93). The meson fields satisfy

$$(\Box + m_\sigma^2)\phi(x) = g_\sigma\,\overline{\psi}(x)\psi(x) \tag{3.98}$$

and

$$(\Box + m_\omega^2)V_\mu(x) - \partial_\mu(\partial^\nu V_\nu) = g_\omega\,\overline{\psi}(x)\gamma_\mu\psi(x)\,, \tag{3.99}$$

while the evolution of the nucleon field is dictated by the equation

$$\left[\left(\partial\!\!\!/ - g_\omega\gamma_\mu V^\mu(x)\right) - \left(m - g_\sigma\phi(x)\right)\right]\psi(x) = 0\,. \tag{3.100}$$

The above coupled equations are fully relativistic and Lorentz covariant. However, their solution involves prohibitive difficulties, that can not be circumvented using approximations based on perturbation theory. Here we will restrict ourselves to the discussion of a different scheme, known as *mean field* approximation and widely used to solve Eqs. (3.98)-(3.100), that essentially amounts to treat $\phi(x)$ and $V_\mu(x)$ as classical fields.

We replace the meson field with their mean values in the ground state of uniform nuclear matter

$$\phi(x) \to \langle\phi(x)\rangle\,, \quad V_\mu(x) \to \langle V_\mu(x)\rangle\,, \tag{3.101}$$

where $\langle\phi(x)\rangle$ and $\langle V_\mu(x)\rangle$ must be computed from the equations of motion. In uniform nuclear matter the baryon and scalar densities, $n_B = \langle\psi^\dagger\psi\rangle$ and $n_s = \langle\overline{\psi}\psi\rangle$, as well as the current $j_\mu = \langle\overline{\psi}\gamma_\mu\psi\rangle$, are

constants, independent of x. In addition, rotation invariance implies $\langle\overline{\psi}\gamma_i\psi\rangle = 0$ ($i = 1,\ 2,\ 3$). As a consequence, the mean values of the meson fields satisfy the relations

$$m_\sigma^2\ \langle\phi\rangle = g_\sigma\langle\overline{\psi}\psi\rangle \tag{3.102}$$

$$m_\omega^2\ \langle V_0\rangle = g_\omega\langle\psi^\dagger\psi\rangle \tag{3.103}$$

$$m_\omega^2\ \langle V_i\rangle = g_\omega\langle\overline{\psi}\gamma_i\psi\rangle = 0\,,\quad i = 1,\ 2,\ 3\,. \tag{3.104}$$

The nucleon equation of motion, rewritten in terms of the mean values of the meson fields, reads

$$\left[\left(\not{\partial} - g_\omega\gamma_\mu\langle V^\mu\rangle\right) - \left(m - g_\sigma\langle\phi\rangle\right)\right]\psi(x) = 0\,. \tag{3.105}$$

In uniform matter, the nucleon states must be eigenstates of the four-momentum operator, that can be written as

$$\psi_{\mathbf{k}}\mathrm{e}^{ikx} = \psi_{\mathbf{k}}\mathrm{e}^{ik_\mu x^\mu} = \psi_{\mathbf{k}}\mathrm{e}^{i(k_0 t - \mathbf{k}\cdot\mathbf{r})}\,, \tag{3.106}$$

the four-spinors $\psi_{\mathbf{k}}$ being solutions of

$$\begin{aligned}&\left[\left(\not{k} - g_\omega\gamma_\mu\langle V^\mu\rangle\right) - \left(m - g_\sigma\langle\phi\rangle\right)\right]\psi_{\mathbf{k}}\\ &\quad = \left[\gamma_\mu\left(k^\mu - g_\omega\langle V^\mu\rangle\right) - \left(m - g_\sigma\langle\phi\rangle\right)\right]\psi_{\mathbf{k}} = 0\,.\end{aligned} \tag{3.107}$$

The above equation can be recast in a form reminiscent of the Dirac equation for a non interacting nuleon. Defining

$$K_\mu = k_\mu - g_\omega\langle V^\mu\rangle \tag{3.108}$$

$$m^* = m - g_\sigma\langle\phi\rangle\,, \tag{3.109}$$

we obtain

$$\left(\not{K} - m^*\right)\psi_{\mathbf{k}} = 0. \tag{3.110}$$

The corresponding energy eigenvalues can be easily using

$$\begin{aligned}\left(\not{K} + m^*\right)\left(\not{K} - m^*\right) &= \not{K}\not{K} - m^{*2} = K_\mu K_\nu\gamma^\mu\gamma^\nu - m^{*2}\\ &= K_\mu K_\nu\frac{\gamma^\mu\gamma^\nu + \gamma^\nu\gamma^\mu}{2} - m^{*2}\\ &= K_\mu K^\mu - m^{*2}\,.\end{aligned} \tag{3.111}$$

Substitution in Eq.(3.110) yields

$$\left(K_\mu K^\mu - m^{*2}\right)\psi_{\mathbf{k}} = 0\,, \tag{3.112}$$

implying

$$\left(K_\mu K^\mu - m^{*2}\right) = 0\,, \tag{3.113}$$

and

$$K_0^2 = (k_0 - g_\omega\langle V_0\rangle)^2 = |\mathbf{k}|^2 + m^{*2} = E_{\mathbf{k}}^2\,. \tag{3.114}$$

It follows that the energy eigenvalues associated with nucleons and antinucleons can be written

$$e_{\mathbf{k}} = g_\omega\langle V_0\rangle + E_{\mathbf{k}}\,, \tag{3.115}$$

and

$$\overline{e}_{\mathbf{k}} = g_\omega \langle V_0 \rangle - E_{\mathbf{k}} \,, \tag{3.116}$$

respectively. The above equations give the nucleon and antinucleon energies in terms of the mean values of the meson fields, which are in turn defined in terms of the ground state expectation values of the nucleon densities and current, according to Eqs. (3.102)-(3.104).

The ground state expectation value of an operator $\overline{\psi}\Gamma\psi$ can be evaluated exploiting the fact that each nucleon state is specified by its momentum, $\mathbf{k}$, and spin-isospin projections. Denoting the average of $\overline{\psi}\Gamma\psi$ in a single particle state by $\langle\overline{\psi}\Gamma\psi\rangle_{\mathbf{k}\alpha}$, where the index α labels the spin-isospin state, we can write the ground state expectation value as

$$\langle\overline{\psi}\Gamma\psi\rangle = \sum_\alpha \int \frac{d^3k}{(2\pi)^3} \, \langle\overline{\psi}\Gamma\psi\rangle_{\mathbf{k}\alpha} \, \theta(e_F - e_{\mathbf{k}}) \,, \tag{3.117}$$

where the θ-function restricts the momentum integration to the region corresponding to energies lower than the Fermi energy e_F.

To obtain the single particle average $\langle\overline{\psi}\gamma_\mu\psi\rangle_{\mathbf{k}\alpha}$, we use Eq. (3.110), implying

$$k_0 = \gamma_0 \left(\boldsymbol{\gamma}\cdot\mathbf{k} + g_\omega \gamma_\mu \langle V^\mu \rangle + m^* \right) \,. \tag{3.118}$$

The quantity defined by the above equation can be regarded as the single nucleon hamiltonian, whose eigenvalues are given by (compare to Eq. (3.115))

$$\langle k_0 \rangle_{\mathbf{k}\alpha} = \langle \psi^\dagger k_0 \psi \rangle_{\mathbf{k}\alpha} = g_\omega \langle V_0 \rangle \pm E_{\mathbf{k}} \,. \tag{3.119}$$

The ground state expectation value of the baryon density can be readily evaluated from Eqs. (3.118) and (3.119) noting that

$$\begin{aligned} \frac{\partial}{\partial\langle V_0\rangle} \langle \psi^\dagger k_0 \psi \rangle_{\mathbf{k}\alpha} &= \frac{\partial}{\partial\langle V_0\rangle} \left(g_\omega \langle V_0 \rangle + E_{\mathbf{k}} \right) = g_\omega \\ &= \langle \psi^\dagger \frac{\partial k_0}{\partial\langle V_0\rangle} \psi \rangle_{\mathbf{k}\alpha} = g_\omega \langle \psi^\dagger \psi \rangle_{\mathbf{k}\alpha} \,, \end{aligned} \tag{3.120}$$

implying

$$\langle \psi^\dagger \psi \rangle_{\mathbf{k}\alpha} = 1 \,. \tag{3.121}$$

It follows that n_B can be obtained using Eq. (3.117), leading to

$$n_B = \langle \psi^\dagger \psi \rangle = \nu \int \frac{d^3k}{(2\pi)^3} \theta(e_F - e_{\mathbf{k}}) \,, \tag{3.122}$$

where ν is the degeneracy of the momentum eigenstate ($\nu = 2$ and 4 for pure neutron matter and isospin symmetric nuclear matter, respectively).

The same procedure can be applied to calculate the ground state expectation value $\langle\overline{\psi}\gamma^i\psi\rangle$ ($i = 1, 2, 3$). Taking the derivative with respect to k_i we find

$$\begin{aligned} \frac{\partial}{\partial k_i} \langle \psi^\dagger k_0 \psi \rangle_{\mathbf{k}\alpha} &= \frac{\partial}{\partial k_i} \left(g_\omega \langle V_0 \rangle + E_{\mathbf{k}} \right) = \frac{\partial E_{\mathbf{k}}}{\partial k_i} \\ &= \langle \psi^\dagger \frac{\partial k_0}{\partial k_i} \psi \rangle_{\mathbf{k}\alpha} = \langle \psi^\dagger \gamma^0 \gamma^i \psi \rangle_{\mathbf{k}\alpha} = \langle \overline{\psi}\gamma^i \psi \rangle_{\mathbf{k}\alpha} \,, \end{aligned} \tag{3.123}$$

leading to

$$\begin{aligned}\langle\overline{\psi}\gamma^i\psi\rangle &= \nu\int\frac{d^3k}{(2\pi)^3}\left(\frac{\partial E_{\mathbf{k}}}{\partial k_i}\right)\theta(e_F-e_{\mathbf{k}})\\ &= \frac{\nu}{(2\pi)^3}\int\prod_{j\neq i}dk_j\int dE_{\mathbf{k}}\,\theta(e_F-e_{\mathbf{k}})=0\,.\end{aligned}\tag{3.124}$$

The above result follows from the fact that, by definition, $e_{\mathbf{k}}\equiv e_F-g_\omega\langle V_0\rangle$ everywhere on the boundary of the integration region. The vanishing of the baryon current had been anticipated noting that in uniform matter the mean values of the space components of the vector field vanish, i.e. that $\langle V_i\rangle=0$. As a consequence, the energy eigenvalues depend upon the magnitude of the nucleon momentum only, according to

$$e_{\mathbf{k}}=e_k=g_\omega\langle V_0\rangle+\sqrt{|\mathbf{k}|^2+(m-g_\sigma\langle\phi\rangle)^2}\,,\tag{3.125}$$

and the occupied region of momentum space is a sphere. Eq. (3.122) then shows that in symmetric nuclear matter, with Z=(A−Z)=A/2, the baryon density takes the familiar form $n_B=2k_F^3/(3\pi^2)$, k_F being the Fermi momentum.

Finally, the scalar density $n_s=\langle\overline{\psi}\psi\rangle$ can be evaluated from the derivative of $\langle\psi^\dagger k_0\psi\rangle_{\mathbf{k}\alpha}$ with respect to m:

$$\frac{\partial}{\partial m}\langle\psi^\dagger k_0\psi\rangle_{\mathbf{k}\alpha}=\frac{\partial E_{\mathbf{k}}}{\partial m}=\langle\psi^\dagger\frac{\partial k_0}{\partial m}\psi\rangle_{\mathbf{k}\alpha}=\langle\psi^\dagger\gamma_0\psi\rangle_{\mathbf{k}\alpha}=\langle\overline{\psi}\psi\rangle_{\mathbf{k}\alpha}\,,\tag{3.126}$$

yielding

$$\langle\overline{\psi}\psi\rangle_{\mathbf{k}\alpha}=\frac{(m-g_\sigma\langle\phi\rangle)}{\sqrt{|\mathbf{k}|^2+(m-g_\sigma\langle\phi\rangle)^2}}\,,\tag{3.127}$$

and

$$\langle\overline{\psi}\psi\rangle=\frac{\nu}{2\pi^2}\int_0^{k_F}k^2dk\,\frac{(m-g_\sigma\langle\phi\rangle)}{\sqrt{|\mathbf{k}|^2+(m-g_\sigma\langle\phi\rangle)^2}}\,.\tag{3.128}$$

Collecting together the results of Eqs. (3.122), (3.124) and (3.128) we can rewrite the equations of motion (3.98)-(3.100) in the form

$$g_\sigma\langle\phi\rangle=\left(\frac{g_\sigma}{m_\sigma}\right)^2\frac{\nu}{2\pi^2}\int_0^{k_F}|\mathbf{k}|^2d|\mathbf{k}|\,\frac{(m-g_\sigma\langle\phi\rangle)}{\sqrt{|\mathbf{k}|^2+(m-g_\sigma\langle\phi\rangle)^2}}\,,\tag{3.129}$$

$$g_\omega\langle V_0\rangle=\left(\frac{g_\omega}{m_\omega}\right)^2n_B=\left(\frac{g_\omega}{m_\omega}\right)^2\nu\,\frac{k_F^3}{6\pi^2}\,,\tag{3.130}$$

$$m_\omega^2\langle V_i\rangle=0,\quad i=1,2,3\,.\tag{3.131}$$

Note that, while Eqs. (3.130) and (3.131) are trivial, Eq. (3.129) implies a self-consistency requirement on the mean value of the scalar field, whose value has to satisfy a transcendental equation.

To obtain the equation of state, i.e. the relation between pressure and density (or energy density) of matter, in quantum field theory we start from the energy-momentum tensor, that for a generic Lagrangian $\mathscr{L}=\mathscr{L}(\phi,\partial_\mu\phi)$ can be written

$$T^{\mu\nu}=\frac{\partial\mathscr{L}}{\partial(\partial_\mu\phi)}\partial^\nu\phi-g^{\mu\nu}\mathscr{L}\,,\tag{3.132}$$

$g^{\mu\nu}$ being the metric tensor.

In a uniform system the expectation value of $T^{\mu\nu}$, is directly related to the energy density, ϵ, and pressure, P, through

$$\langle T_{\mu\nu}\rangle = u_\mu u_\nu\,(\epsilon + P) - g_{\mu\nu}P\,, \tag{3.133}$$

where u denotes the four velocity of the system, satisfying $u_\mu u^\mu = 1$. It follows that in the reference frame in which matter is at rest $\langle T_{\mu\nu}\rangle$ is diagonal and

$$\epsilon = \langle T_{00}\rangle = \langle\overline{\psi}\gamma_0 k_0\psi\rangle - \langle\mathscr{L}\rangle\,, \tag{3.134}$$

$$P = \frac{1}{3}\langle T_{ii}\rangle = \frac{1}{3}\langle\overline{\psi}\gamma_i k_i\psi\rangle + \langle\mathscr{L}\rangle\,. \tag{3.135}$$

Within the mean field approximation, the lagrangian density of the σ-ω model reduces to

$$\mathscr{L}_{MF} = \overline{\psi}\left[i\partial\!\!\!/ - g_\omega\gamma^0\langle V_0\rangle - (m - g_\sigma\langle\phi\rangle)\right]\psi - \frac{1}{2}m_\sigma^2\langle\phi\rangle^2 + \frac{1}{2}m_\omega^2\langle V_0\rangle^2\,, \tag{3.136}$$

implying

$$T^{\mu\nu}_{MF} = i\overline{\psi}\gamma^\mu\partial^\nu\psi - g^{\mu\nu}\left[-\frac{1}{2}m_\sigma^2\langle\phi\rangle^2 - \frac{1}{2}m_\omega^2\langle V_0\rangle^2\right]\,. \tag{3.137}$$

As a consequence, Eqs. (3.134) and (3.135) become

$$\epsilon = -\langle\mathscr{L}_{MF}\rangle + \langle\overline{\psi}\gamma_0 k_0\psi\rangle \tag{3.138}$$

$$P = \langle\mathscr{L}_{MF}\rangle + \frac{1}{3}\langle\overline{\psi}\gamma_i k_i\psi\rangle, \tag{3.139}$$

where (use Eqs. (3.119), (3.125) and (3.130))

$$\begin{aligned}
\langle\overline{\psi}\gamma_0 k_0\psi\rangle &= \frac{\nu}{2\pi^2}\int_0^{k_F}|\mathbf{k}|^2 d|\mathbf{k}|\left[\sqrt{|\mathbf{k}|^2 + (m - g_\sigma\langle\phi\rangle)^2} + g_\omega\langle V_0\rangle\right] \\
&= g_\omega\langle V_0\rangle n_B + \frac{\nu}{2\pi^2}\int_0^{k_F}|\mathbf{k}|^2 d|\mathbf{k}|\,\sqrt{|\mathbf{k}|^2 + (m - g_\sigma\langle\phi\rangle)^2} \\
&= \frac{g_\omega^2}{m_\omega^2}n_B^2 + \frac{\nu}{2\pi^2}\int_0^{k_F}|\mathbf{k}|^2 d|\mathbf{k}|\,\sqrt{|\mathbf{k}|^2 + (m - g_\sigma\langle\phi\rangle)^2}\,,
\end{aligned} \tag{3.140}$$

and (use eq.(3.124))

$$\langle\overline{\psi}\gamma_i k_i\psi\rangle = \langle\overline{\psi}(\boldsymbol{\gamma}\cdot\mathbf{k})\psi\rangle = \frac{\nu}{2\pi^2}\int_0^{k_F} d|\mathbf{k}|\,\frac{|\mathbf{k}|^4}{\sqrt{|\mathbf{k}|^2 + (m - g_\sigma\langle\phi\rangle)^2}}\,. \tag{3.141}$$

Substitution of the above equations into Eqs. (3.138)-(3.139) finally yields (use Eq. (3.136) and the equation of motion for the nucleon field)

$$\epsilon = \frac{1}{2}\frac{m_\sigma^2}{g_\sigma^2}(m - m^*)^2 + \frac{1}{2}\frac{g_\omega^2}{m_\omega^2}n_B^2 + \frac{\nu}{2\pi^2}\int_0^{k_F}|\mathbf{k}|^2 d|\mathbf{k}|\,\sqrt{|\mathbf{k}|^2 + m^{*2}} \tag{3.142}$$

$$P = -\frac{1}{2}\frac{m_\sigma^2}{g_\sigma^2}(m - m^*)^2 + \frac{1}{2}\frac{g_\omega^2}{m_\omega^2}n_B^2 + \frac{1}{3}\frac{\nu}{2\pi^2}\int_0^{k_F} d|\mathbf{k}|\,\frac{|\mathbf{k}|^4}{\sqrt{|\mathbf{k}|^2 + m^{*2}}} \tag{3.143}$$

The first two contributions to the right hand side of the above equations arise from the mass terms associated with the vector and scalar fields, while the remaining term gives the energy density and pressure of a relativistic Fermi gas of nucleons of mass m^* given by (see Eq. (3.129))

$$\begin{aligned} m^* &= m - \frac{g_\sigma^2}{m_\sigma^2}\frac{\nu}{2\pi^2}\int_0^{k_F} |\mathbf{k}|^2 d|\mathbf{k}| \, \frac{m^*}{\sqrt{|\mathbf{k}|^2 + m^{*2}}} \\ &= m - \frac{g_\sigma^2}{m_\sigma^2}\frac{m^*}{\pi^2}\left[k_F e_F^* - m^{*2}\ln\left(\frac{k_F + e_F^*}{m^*}\right)\right] , \end{aligned} \tag{3.144}$$

with $e_F^* = \sqrt{k_F^2 + m^{*2}}$. Equations (3.142)-(3.144) yield energy density and pressure of nuclear matter as a function of the baryon number density n_B (recall: $k_F = (6\pi^2 n_B/\nu)^{(1/3)}$). The values of the unknown coefficients (m_σ^2/g_σ^2) and (m_ω^2/g_ω^2) can be determined by a fit to the empirical saturation properties of nuclear matter, i.e. requiring

$$\frac{B}{A} = \frac{\epsilon(n_0)}{n_0} - m = -16\,\text{MeV} \tag{3.145}$$

with $n_0 = .16\,\text{fm}^{-3}$. This procedure leads to the result

$$\frac{g_\sigma^2}{m_\sigma^2}\, m^2 = 267.1 \quad , \quad \frac{g_\omega^2}{m_\omega^2}\, m^2 = 195.9\,. \tag{3.146}$$

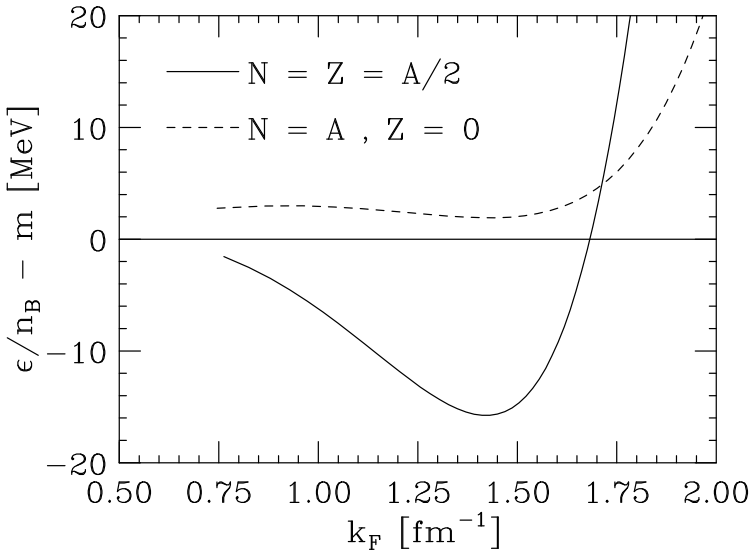

Figure 3.9: Fermi momentum dependence of the binding energy per nucleon of symmetric nuclear matter (solid line) and pure neutron matter (dashed line) evaluated using the $\sigma - \omega$ model and the mean field approximation.

Fig. 3.9 shows the binding energies of symmetric nuclear matter (solid line) and pure neutron matter (dashed line) predicted by the $\sigma - \omega$ model, plotted against the Fermi momentum k_F. Note that pure neutron matter is always unbound.

Chapter 4

Exotic forms of matter

As the density increases up to values well beyond nuclear saturation density, different forms of matter, containing hadrons other than protons and neutrons, can become energetically favoured. Strange hadrons are produced through weak interaction processes, such as

$$p + e \rightarrow \Lambda^0 + \nu_e \,, \tag{4.1}$$

$$p + e \rightarrow \Sigma^0 + \nu_e, \tag{4.2}$$

$$n + e \rightarrow \Sigma^- + \nu_e. \tag{4.3}$$

For example, the reaction (4.1), leading to the appearance of a Σ^-, sets in as soon as the sum of the proton and electron chemical potentials exceeds the rest mass of the produced baryon, M_{Σ^-} [1] . The results of theoretical calculations suggest that this condition is typically fulfilled at densities $n \gtrsim 2n_0$.

At even larger density ($n > 4n_0$) a new transition, to a phase in which quarks are no longer clustered into hadrons is eventually expected to take place.

4.1 Stability of strange hadronic matter

The properties of baryons with non zero strangeness, also referred to as hyperons, are summarised in Table 4.1.

The mechanism responsible for the stability of strange hadronic matter matter—driven by the Fermi-Dirac statistics obeyed by the constituent particles —is analog to the one leading to neutronization, discussed in Chapter 2.

Let us consider a system consisting of B baryonic species $b_1 \ldots b_B$ and L leptonic species $\ell_1 \ldots \ell_L$, in equilibrium with respect to the weak interaction processes

$$b_i \rightarrow b_j + \ell_k + \overline{\nu}_\ell \,, \tag{4.4}$$

$$b_j + \ell_k \rightarrow b_i + \nu_\ell \,, \tag{4.5}$$

with $i, j = 1 \ldots B$ and $k = 1 \ldots L$. The ground state of system, specified by the densities of the constituent particles, n_{b_i} and n_{ℓ_i}, is determined through minimisation of the energy density, with the

[1] Recall that we always assume that neutrinos have vanishing chemical potentials.

	Charge	Mass [MeV]	Valence quark structure	Strangeness
Λ^0	0	1115.7	uds	-1
Σ^-	-1	1197.4	dds	-1
Σ^0	0	1192.6	uds	-1
Σ^+	+1	1189.4	uus	-1
Ξ^0	0	1314.8	dss	-2
Ξ^-	-1	1321. 3	dss	-2

Table 4.1: Properties of strange Baryions.

constraints dictated from conservation of the baryon density, n_B, and charge neutrality, implying

$$\sum_{i=1}^{B} n_{b_i} = n_B \,, \tag{4.6}$$

$$\sum_{i=1}^{B} Q_{b_i} n_{b_i} + \sum_{i=1}^{L} Q_{\ell_i} n_{\ell_i} = 0 \,, \tag{4.7}$$

where Q_{b_i} and Q_{ℓ_i} denote the electric charge of the i-th baryonic and leptonic species, respectively.

Minimization of energy density ϵ with respect to the densities n_{b_i} and n_{ℓ_i} with the above constraints results in $L+B$ equations involving the chemical potentials of the constituents

$$\mu_{b_i} = \frac{\partial \epsilon}{\partial n_{b_i}} \quad , \quad \mu_{\ell_i} = \frac{\partial \epsilon}{\partial n_{\ell_i}} \,,$$

and two Lagrange multipliers, denoted λ_B and λ_Q. There are as many independent chemical potentials as there are conserved quantities. All other chemical potentials can be expressed in terms of the independent ones.

To see how the determination of matter composition works, consider, as an example, a system of protons (p), neutrons (n), electrons (e), muons (μ), and hyperons Σ^- and Λ^0. In addition to Eqs.(4.6) and (4.7), which in this case take the form

$$n_n + n_p + n_\Lambda + n_\Sigma = n_B \,,$$

and

$$n_p - n_e - n_m u - n_\Sigma = 0 \,,$$

we obtain $B+L-2=4$ equations involving the chemical potentials

$$\begin{aligned} \mu_p &= \mu_n - \mu_e \,, \\ \mu_{\Sigma^-} &= \mu_n + \mu_e \,, \\ \mu_{\Lambda^0} &= \mu_n \,, \\ \mu_\mu &= \mu_e \,, \end{aligned}$$

showing that there are in fact only two independent chemical potentials, e.g. μ_n and μ_p.

In principle, for any given baryon density, n_B, the densities of the constituent particles can be determined from the above equations. Treating all constituents as non interacting particles, one finds that Σ^- and Λ^0 appear at densities $\sim 4n_0$ and $\sim 8n_0$, respectively, n_0 being the equilibrium density of isospin-symmetric nuclear matter.

Note that the density at which the production of a strange hadron is expected to occur do not depend on its mass only. Let us consider the Λ^0 and Σ^- hyperons, whose appearance becomes energetically favoured as soon as the threshold conditions

$$\mu_n + \mu_e = M_{\Sigma^-} \,,$$
$$\mu_n = M_{\Lambda^0} \,,$$

are fulfilled. From the above relations it follows that, in spite of the larger mass, the threshold density of Σ^- production is in fact lower than that of Λ^0 production if the electron chemical potential is such that

$$\mu_e > M_{\Sigma^-} - M_{\Lambda^0} \approx 80 \text{ MeV} \,.$$

Treating the electron as a non interacting particle, the corresponding electron density can be easily obtained, and the threshold condition takes the form

$$\mu_e = \sqrt{p_{Fe}^2 + m_e^2} \approx p_{Fe} = (3\pi^2 n_e)^{1/3} > 80 \text{ MeV} \,,$$

implying

$$n_e \gtrsim 2 \times 10^{-3} \text{ fm}^{-3} \,.$$

Under the reasonable assumption that the electron density be of the order of one percent of the baryon density, the above estimate corresponds to $n_B > 0.2$ fm$^{-3} \gtrsim n_0$, a density that is certainly reached in compact stars.

4.1.1 Hyperon interactions

While lepton interactions can be safely neglected, the interactions of baryons, including hyperons must be properly taken into account in the calculation of the corresponding chemical potentials. The maximum mass of a star consisting of non interacting neutrons, protons and leptons, obtained by solving the Tolman-Oppenheimer-Volkoff equations discussed in Section 1.5, turns out to be $M_{\max} \sim 0.8\, M_\odot$—to be compared with the *canonical* value of the neutron star mass, $M \sim 1.4\, M_\odot$, resulting from observations—and the appearance of strange baryons, leading to a softening of the EoS, makes things worse, bringing the value of $M_{\max}$ down to $\sim 0.7\, M_\odot$.

In principle, the EoS of strange hadronic matter can be studied using either non relativistic many-body theory or relativistic mean field theory, as discussed in Sections 3.4 and 3.5, respectively. However, the former approach requires the determination of the potentials describing hyperon-nuleon (YN) and hyperon-hyperon (YY) interactions, while the latter involves the YN and YY coupling constants.

Experimental data providing information on YN and YY information are scarce and not very accurate. Studies of hypernuclei and Λp scattering suggest that the Λp interaction is weaker than the pn and pp interactions.

Some insight on the relation between strong interactions in the nucleon and hyperon sectors can be obtained from an admittedly crude argument based on the quark model of hadrons. According to this model, the π-meson is a quark-antiquark system, and the composition of the three charge states is given by

$$\pi^+ = u\bar{d} \quad , \quad \pi^- = d\bar{u} \quad , \quad \pi^0 = \frac{1}{\sqrt{2}}(u\bar{u} - d\bar{d}) \, ,$$

where u and d denote the up and down quark, respectively. As discussed in Chapter 3, the intermediate-range NN force can be described in terms of exchange of a quark-antiquark system, modelled by a scalar meson whose structure can be written in the form

$$\sigma = \frac{1}{\sqrt{2}}(u\bar{u} + d\bar{d}) \, ,$$

which is essentially the number operator of non-strange quarks. Since nucleons contain three non-strange quarks, while the Λ and Σ^- only contain two, it follows that the coupling constants of the Λp or Σp interaction mediated by the σ-meson is 2/3 of the corresponding pp coupling constant. In the language of nuclear many body theory, this argument leads to predict the following simple relations between the interaction potentials

$$v_{\Lambda N} = v_{\Sigma N} = \frac{2}{3} v_{NN} \, ,$$
$$v_{\Lambda\Lambda} = v_{\Lambda\Sigma} = v_{\Sigma\Sigma} = \frac{4}{9} v_{NN} \, ,$$

where N denotes either a proton on or a neutron.

More realistic and accurate models of the YN potentials, referred to as Jülich and Nijmegen models, have been developed exploiting all the available information on YN scattering and hypernuclear properties. Unfortunately, the predictions of the two models are appreciably different. Using the Jülich potential leads to predict Σ^- and Λ appearance at density $\sim 2n_0$ and $\sim 3n_0$, respectively, whereas the corresponding quantities obtained from the Nijmegen potential are $\sim 1.5n_0$ and $\sim 4n_0$. Figure 4.1 illustrates the typical composition of matter resulting from a calculation carried out using the formalism of nuclear many-body theory, a realistic nuclear Hamiltonian and the Nijmegen model of YN interactions.

Recently, it has been suggested that the inclusion of a purely phenomenological three body force, involving two nucleons and a Λ hyperon, is needed to achieve an accurate description of the Λ binding energy in a variety of nucleons. The results of a quantum Monte Carlo calculation performed taking into account ΛNN interactions are displayed in Fig. 4.2

4.2 Deconfinement and quark matter

The *ab initio* description of the QCD phase diagram would require numerical simulations on a lattice [13, 14]. However, application of this approach in the region corresponding to non vanishing chemical potential presents severe difficulties. Therefore, most studies of the properties of quark matter are carried out within simplified models, inspired to QCD and involving a set of of parameters, the values of which are determined in such a way as to reproduce the observed properties of hadrons.

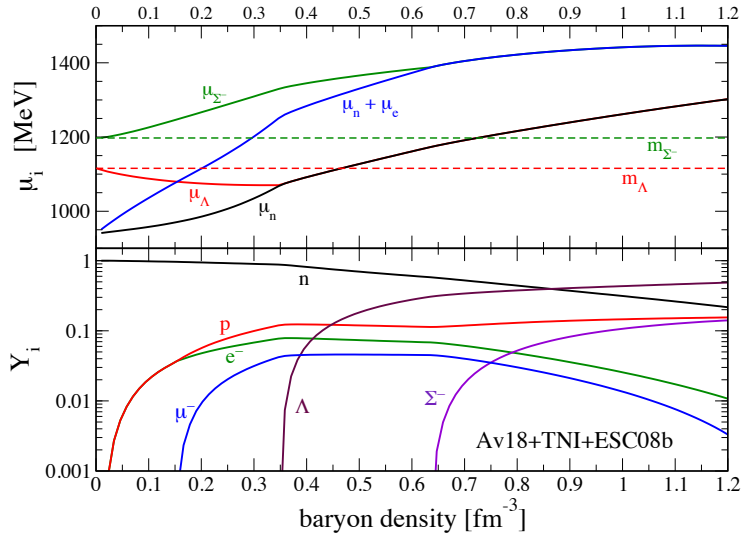

Figure 4.1: The bottom panel shows the composition of strange hadronic matter obtained from non relativistic nuclear many-body theory using the Nijmegen model of YN interactions. The density dependence of the chemical potentials is illustrated in the upper panel. Three-body forces involving nucleons and hyperons are not taken into account.

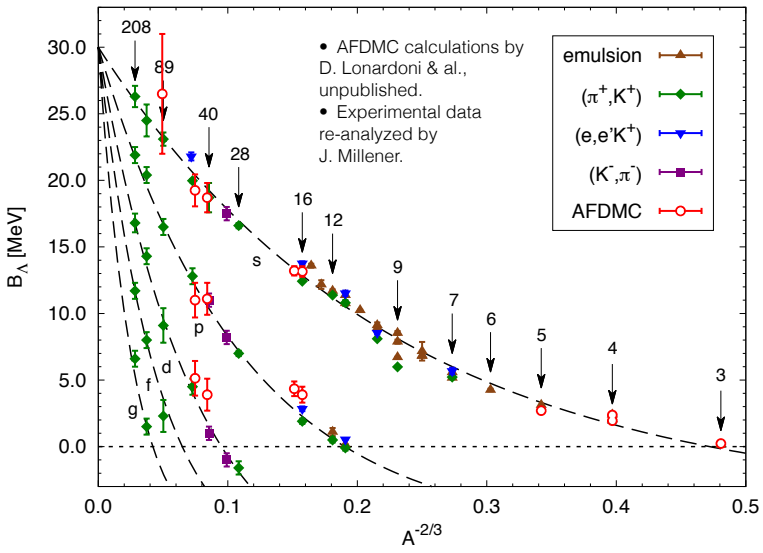

Figure 4.2: Λ binding energy as a function of $A^{-2/3}$. The results of quantum Monte Carlo calculations, labelled AFDMC, are compared to data collected using different experimental techniques.

4.2.1 The bag model

In this section, we will analyse a model developed in the 1970s at the Massachusetts Institute of Technology (MIT)—referred to as *bag model*—in which the main features of QCD are taken into account in a rather crude fashion. It is remarkable that, in spite of its simplicity, the MIT bag model provides a reasonable description of the hadronic spectrum.

Within the MIT bag model, the fundamental properties of QCD, that is, asymptotic freedom and confinement, translate into two simple hypoteses:

- the QCD vacuum exerts a pressure on any quark aggregate of vanishing color charge, thus confining it to a finite region in space: the bag;
- within the bag, gluon-excgange interactions between quarks are negligible, or tractable at lowest order of perturbation theory.

In the simplest implementation of the above scenario, in which the quarks within the bag are described of non-interacting particles obeying Fermi statistics, the thermodynamic potential can be computed explicitly.

Consider a system consisting of N_f types of fermions with masses m_i, described by the Dirac Lagrangian density

$$\mathscr{L} = \sum_{i=1}^{N_f} \bar{q}^i (i\partial\!\!\!/ - m_i) q^i \,. \tag{4.8}$$

The formalism suitable to describe fermion fields, satisfying anticommutation rules, is based on the use of Grassman variables η_i $(i = 1,\ldots,N)$, whose gaussian integral is given by [15, 16]

$$\int d\eta_1^\dagger d\eta_1 \cdot d\eta_N^\dagger d\eta_N \mathrm{e}^{\eta_i^\dagger A^{ij} \eta_j} = \det(A) \,. \tag{4.9}$$

Exploiting the techniques descrided in Appendix C we can therefore write the partition function of the system in the form [15]

$$\mathscr{Z} = \prod_i \int i\mathscr{D} q^{i\dagger} \int \mathscr{D} q^i \exp\left[\int_0^\beta d\tau \int d^3x \, \bar{q}^i \Big(-\gamma^0 \partial_\tau + i\vec{\gamma}\cdot\vec{\nabla} - m_i + \mu_i \gamma^0 \Big) q^i \right] , \tag{4.10}$$

where the integration is extended to all paths satisfying the antiperiodicity conditions $q^i(\vec{x},0) = -q^i(\vec{x},\beta)$.

We can now transform to momentum space using the expansion

$$q_\alpha^i(\vec{x},\tau) = \frac{1}{\sqrt{V}} \sum_{n,\vec{p}} e^{i(\vec{p}\cdot\vec{x} + E_{in}\tau)} \tilde{q}_{\alpha n}^i(\vec{p}) \,, \tag{4.11}$$

where α is the index associated with the components of Dirac's spinors, and the antiperiodicity constraint requires

$$E_{in} = (2n+1)\pi T \,. \tag{4.12}$$

Using Eq.(4.9) we obtain the partition function

$$\mathscr{Z} = \prod_{i,\alpha,\vec{p},n} \int i\mathscr{D}(\tilde{q}_{\alpha n}^i)^\dagger \int \mathscr{D}\tilde{q}_{\alpha n}^i \exp i \sum_{in\vec{p}} (\tilde{q}_{\alpha n}^i)^\dagger D^{\alpha\rho} \tilde{q}_{\rho n}^i = \det(D) \tag{4.13}$$

with

$$D = -i\beta\left[(-iE_{in}+\mu_i) - \gamma^0\vec{\gamma}\cdot\vec{p} - m_i\gamma^0\right] . \tag{4.14}$$

In addition, exploiting the operatorial relation

$$\ln[\det(D)] = \mathrm{Tr}\,[\ln(D)] \tag{4.15}$$

we can now derive from Eq.(4.14) the thermodynamic potential, defined as

$$\Omega = -T\ln\mathcal{Z} = -PV . \tag{4.16}$$

The results is

$$\begin{aligned}\Omega &= -T\ln[\det(D)] = -2T\sum_{i,n,\vec{p}}\ln\{\beta^2[(E_{in}+\mu_i)^2+E_{ip}^2]\} \\ &= -T\sum_{i,n,\vec{p}}\ln\{\beta^2[E_{in}^2+(E_{ip}-\mu_i)^2]\}+\ln\{\beta^2[E_{in}^2+(E_{ip}+\mu_i)^2]\} ,\end{aligned} \tag{4.17}$$

where $E_{ip} = \sqrt{|\vec{p}|^2+m_i^2}$. Using Eq.(4.12). we can rewrite the logarithms appearing on the right hand side of Eq.(4.17) in the form

$$\begin{aligned}&\ln\left[(2n+1)^2\pi^2+\beta^2(E_{ip}\pm\mu_i)^2\right] \\ &\qquad = \int_1^{\beta^2(E_{ip}\pm\mu_i)^2}\frac{d\theta^2}{\theta^2+(2n+1)^2\pi^2}+\ln[1+(2n+1)^2\pi^2] ,\end{aligned} \tag{4.18}$$

which allows us to perform the sum over n, because

$$\sum_{n=-\infty}^{\infty}\frac{1}{\theta^2+(2n+1)^2\pi^2} = \frac{1}{\theta}\left(\frac{1}{2}-\frac{1}{e^{\theta+1}}\right) . \tag{4.19}$$

By integrating over the variable θ we obtain an expression for the logarithm of the partition function which involves terms independent of β and the chemical potentials μ_i. These contributions do not affect the thermodynamics, because, after being exponentiated, can be included in the normalization of the partition function.Neglecting these terms we find

$$\Omega = -6TV\sum_{i=1}^{N_f}\int\frac{d^3p}{(2\pi)^3}[\beta E_{ip}+\ln(1+\mathrm{e}^{-\beta(E_{ip}-\mu_i)})+\ln(1+\mathrm{e}^{-\beta(E_{ip}+\mu_i)})] , \tag{4.20}$$

where the factor $6 = 2\times 3$ accounts for the degeneracy associated with colour and spin degrees of freedom, the second and third terms on the right hand side represent the contributions arising from particles and antiparticles, respectively, and the first term contributes to the vacuum energy.

From Eq.(C.6), establishing the relation between pressure, thermodynamic potential and partition function, we finally obtain

$$P_0 = 6\,T\sum_i\int\frac{d^3p}{(2\pi)^3}\Big\{\ln\left[1+\exp\beta(E_{ip}-\mu_i)\right]+\ln\left[1+\exp\beta(E_{ip}+\mu_i)\right]\Big\} . \tag{4.21}$$

Within the bag model, we have to add to the pressure P_0, corresponding to a gas of non interacting quarks and antiquarks, three additional contributions: δP_{glue}, describing the pressure of a

gluon gas (which can be computed using a technique similar to that employed to obtain Eq. (4.21)—), δP_{pert} taking into account perturbative corrections arising from strong interaction processes associated with gluon exchange, and the constant term $-B$, which parametrises the pressure exerted by the QCD vacuum on the perturbative vacuum within the bag. Therefore, we can write

$$P = P_0 + \delta P_{\text{glue}} + \delta P_{\text{pert}} - B \,, \tag{4.22}$$

with [15]

$$\delta P_{\text{gluoni}} = -16 \int \frac{d^3 p}{(2\pi)^3} \ln[1 - \mathrm{e}^{-\beta p}] \,. \tag{4.23}$$

Consider now the simplest implementation of the model, in which the number of flavours is limited to two—u and d, with $m_u = m_d = 0$ and $\mu_u = \mu_d = \mu$—and perturbative gluon exchange is neglected. Under these simplifying assumptions, the calculation of the pressure can be carried out analytically, with the result [17]

$$P = -B + 37 \frac{\pi^2}{90} T^4 + \mu^2 T^2 + \frac{\mu^4}{2\pi^2} \,. \tag{4.24}$$

The factor 37 in front of the term proportional to T^4 results from the sum $16 + 21$, where $16 = 8 \times 2$ is the number of gluonic degrees of freedom and 21 is obtained by multiplying the number of degrees of freedom associated with quarks and antiquarks ($24 = 2 \times 3 \times 2 \times 2$) by the factor 7/8 typical of Fermi statistics.

Equation (4.24) can be exploited to obtain a qualitative description of the QCD phase diagram. Assuming that a pion gas with vanishing potential provides a schematic representation of the hadronic phase, we can write the corresponding pressure in the form [15]

$$P_{\text{had}} = 3 \frac{\pi^2}{90} T^4 \,, \tag{4.25}$$

where 3 is the number of pionic degrees of freedom, that is, the number of isospin states. Gibb's equilibrium condition is represented by the curve of Fig. 4.3, computed using the value $B = 57.5$ MeV/fm^3, resulting from a fit to the masses and magnetic moments of light hadrons [18].

4.2.2 The equation of state of quark matter

The thermodynamic functions describing a many-particle system at temperature $T = 1/\beta$ can be obtained from the grand partition function, defined as

$$Z = \mathrm{Tr}\left[\exp\left(-\beta(H - \sum_i \mu_i N_i)\right)\right] \,, \tag{4.26}$$

where H is the hamiltonian operator and μ_i and N_i are the chemical potential and the number operator associated with particles of species i, respectively.

For example, pressure (P) and energy density (ϵ) can be defined in terms of the Gibbs free energy, Ω, which is in turn related to Z through

$$\Omega = -\frac{1}{\beta} \ln Z \,, \tag{4.27}$$

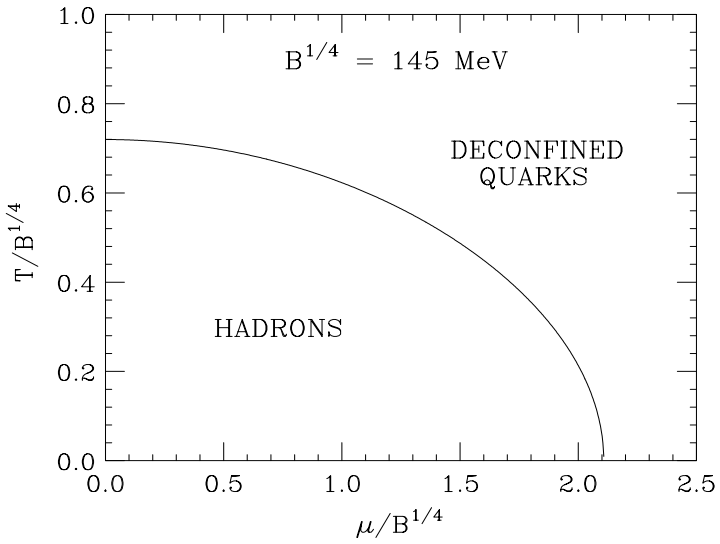

Figure 4.3: Diagramma di fase del bag model con $N_f = 2$, ottenuto ponendo $m_u = m_d = 0$, $\mu_u = \mu_d = \mu$ e $B = 57.5$ MeV/fm^3 (corrispondente a $B^{1/4} = 145$ MeV). La fase adronica è descritta come un gas di pioni a potenziale chimico nullo.

according to

$$P = -\frac{\Omega}{V}\,, \tag{4.28}$$

and

$$\epsilon = \Omega - \sum_i \left(\frac{\partial\Omega}{\partial\mu_i}\right)_{T,V}\,, \tag{4.29}$$

where V is the volume occupied by the system.

In the case of quark matter, due to the properties of QCD described in Section XXXX, Ω consists of two contributions. One of them, that will be denoted Ω_{pert}, is tractable in perturbation theory, while the second one takes into acount nonperturbative effects induced by the properties of the QCD vacuum.

The relation (4.28) between pressure and Gibbs free energy and the interpretation of the bag constant discussed in Section 4.2.1 suggest that within the MIT bag model the difference between Ω and Ω_{pert} can be identified with the bag constant, i.e. that

$$\Omega = \Omega_{pert} + VB\,. \tag{4.30}$$

The perturbative contribution can be expanded according to

$$\Omega_{pert} = V \sum_f \sum_n \Omega_f^{(n)}\,, \tag{4.31}$$

where the index f specifies the quark flavor, while $\Omega_f^{(n)}$ is the n-th order term of the perturbative expansion in powers of the strong coupling constant, α_s.

The EOS of quark matter can be obtained from the relations linking pressure and energy density to Ω:

$$P = -\frac{\Omega}{V} = -B - \sum_f \sum_n \Omega_f^{(n)} \,. \tag{4.32}$$

$$\epsilon = \frac{\Omega}{V} - \sum_f \left(\frac{\partial \Omega}{\partial \mu_f} \right) = -P + \sum_f \mu_f n_f \,, \tag{4.33}$$

n_f and μ_f being the density and chemical potential of the quarks of flavor f.

The lowest order contribution at $T = 0$, reads (compare to Eqs. (1.29) and (1.30))

$$\begin{aligned} \Omega_f^{(0)} &= -\frac{1}{\pi^2}\left[\frac{1}{4}\mu_f \sqrt{\mu_f^2 - m_f^2}\left(\mu_f^2 - \frac{5}{2}m_f^2\right) \right. \\ &\left. + \frac{3}{8} m_f^4 \log \frac{\mu_f + \sqrt{\mu_f^2 - m_f^2}}{m_f} \right] , \end{aligned} \tag{4.34}$$

where m_f is the quark mass.

Substituting Eq. (4.34) into Eqs. (4.32) and (4.33) and taking the limit of massless quarks one finds the EOS

$$P = \frac{\epsilon - 4B}{3} \,. \tag{4.35}$$

The contribution of first order in α_s, arising from the one-gluon exchange processes discussed in Appendix **??**, reads

$$\begin{aligned} \Omega_f^{(1)} &= \frac{2\alpha_s}{\pi^3}\left[\frac{3}{4}\left(\mu_f \sqrt{\mu_f^2 - m_f^2} - m_f^2 \log \frac{\mu_f + \sqrt{\mu_f^2 - m_f^2}}{m_f} \right)^2 \right. \\ &\left. - \frac{1}{2}(\mu_f^2 - m_f^2)^2 \right] . \end{aligned} \tag{4.36}$$

The chemical potentials appearing in Eqs.(4.34) and (4.36) can be written

$$\mu_f = e_{F_f} + \delta\mu_f = \sqrt{m_f^2 + p_{F_f}^2} + \delta\mu_f, \tag{4.37}$$

where the first term is the Fermi energy of a gas of noninteracting quarks of mass m_f at density $n_f = p_{F_f}^3/\pi^2$, whereas the second term is a perturbative correction of order α_s, whose explicit expression is

$$\delta\mu_f = \frac{2\alpha_s}{3\pi^2}\left[p_{F_f} - 3\frac{m_{F_f}^2}{e_{F_f}} \log\left(\frac{e_{F_f} + p_{F_f}}{m_f} \right) \right] . \tag{4.38}$$

Including both $\Omega_f^{(0)}$ and $\Omega_f^{(1)}$ in Eqs. (4.32) and (4.33) and taking again the limit of vanishing quark masses one finds

$$P = \frac{1}{4\pi^2}\left(1 - \frac{2\alpha_s}{\pi} \right) \sum_f \mu_f^4 - B \tag{4.39}$$

$$\epsilon = \frac{3}{4\pi^2}\left(1-\frac{2\alpha_s}{\pi}\right)\sum_f \mu_f^4 + B\,. \tag{4.40}$$

Comparison to Eq. (4.35) shows that the EOS of a system of massless quarks in unaffected by one-gluon exchange interactions.

For any baryon density, quark densities are dictated by the requirements of baryon number conservation, charge neutrality and weak equilibrium. In the case of two flavors, in which only the light up and down quarks are present, we have

$$n_B = \frac{1}{3}(n_u + n_d)\,, \tag{4.41}$$

$$\frac{2}{3}n_u - \frac{1}{3}n_d - n_e = 0 \tag{4.42}$$

$$\mu_d = \mu_u + \mu_e\,, \tag{4.43}$$

where n_e and μ_e denote the density and chemical potential of the electrons produced through

$$d \rightarrow u + e^- + \overline{\nu}_e\,. \tag{4.44}$$

Note that we have not taken into account the possible appearance of muons, as in the density region relevant to neutron stars μ_e never exceeds the muon mass.

As the baryon density increases, the d-quark chemical potential reaches the value $\mu_d = m_s$, m_s being the mass of the strange quark. The energy of quark matter can then be lowered turning d-quarks into s-quarks through

$$d + u \rightarrow u + s\,. \tag{4.45}$$

In presence of three flavors, Eqs. (4.41)-(4.43) become

$$n_B = \frac{1}{3}(n_u + n_d + n_s)\,, \tag{4.46}$$

$$\frac{2}{3}n_u - \frac{1}{3}n_d - \frac{1}{3}n_s - n_e = 0 \tag{4.47}$$

$$\mu_d = \mu_s = \mu_u + \mu_e\,. \tag{4.48}$$

Unfortunately, the parameters entering the bag model EOS are only loosely constrained by phenomenology and their choice is somewhat arbitrary.

As quarks are confined and not observable as individual particles, their masses are not directly measurable and must be inferred from hadron properties. The Particle Data Group reports masses of a few MeV for up and down quarks and 60 to 170 MeV for the strange quark. At typical neutron stars densities heavier quarks do not play a role.

The strong coupling constant α_s can be obtained from the renormalization group equation

$$\alpha_s = \frac{12\pi}{(33-2N_f)\ln(\overline{\mu}^2/\Lambda^2)}\,, \tag{4.49}$$

where $N_f = 3$ is the number of active flavors, Λ is the QCD scale parameter and $\overline{\mu}$ is an energy scale typical of the relevant density region (e.g. the average quark chemical potential). Using $\Lambda \sim 100 \div 200$ MeV and setting $\overline{\mu} = \mu_d \sim \mu_u$ at a typical baryon density $n_B \sim 4n_0$ one gets $\alpha_s \sim 0.4 \div 0.6$.

The values of the bag constant resulting from fits of the hadron spectrum range between ~ 57 MeV/fm^3, with $\Lambda = 220$ MeV, and ~ 350 MeV/fm^3 , with $\Lambda = 172$ MeV. However, the requirement that the deconfinement transition does not occur at density ~ n_0 constrains B to be larger than ~ 120−150 MeV/fm^3, and lattice results suggest a value of ~ 210 MeV/fm^3.

Figure 4.4 shows the energy density of neutral quark matter in weak equilibrium as a function of baryon density, for different values of B and α_s. Comparison between the dotdash line and those corresponding to $\alpha_s \neq 0$ shows that perturbative gluon exchange, whose inclusion produces a sizable change of slope, cannot be simulated by adjusting the value of the bag constant and must be explicitly taken into account.

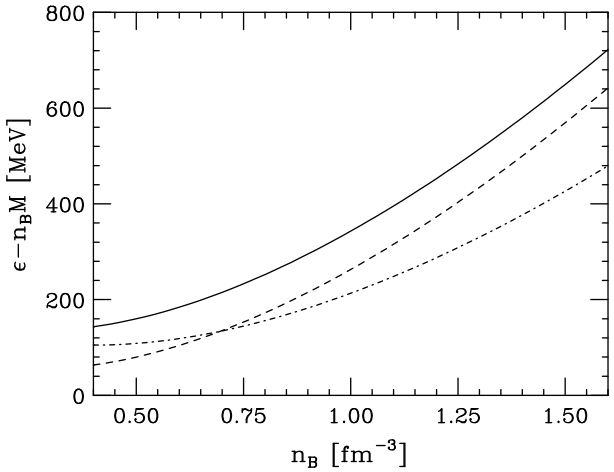

Figure 4.4: Energy density of neutral quark matter in weak equilibrium as a function of baryon number density. The solid and dashed lines have been obtained setting $\alpha_s = 0.5$ and $B = 200$ and 120 MeV/fm^3, respectively, while the dashdot line corresponds to $\alpha_s = 0$ and $B = 200$ MeV/fm^3. The quark masses are $m_u = m_d = 0$, $m_s = 150$ MeV.

The composition of charge neutral quark matter in weak equilibrium obtained from the MIT bag model is shown in Fig. 4.5. Note that at large densities quarks of the three different flavors are present in equal number, and leptons are no longer needed to guarantee charge neutrality.

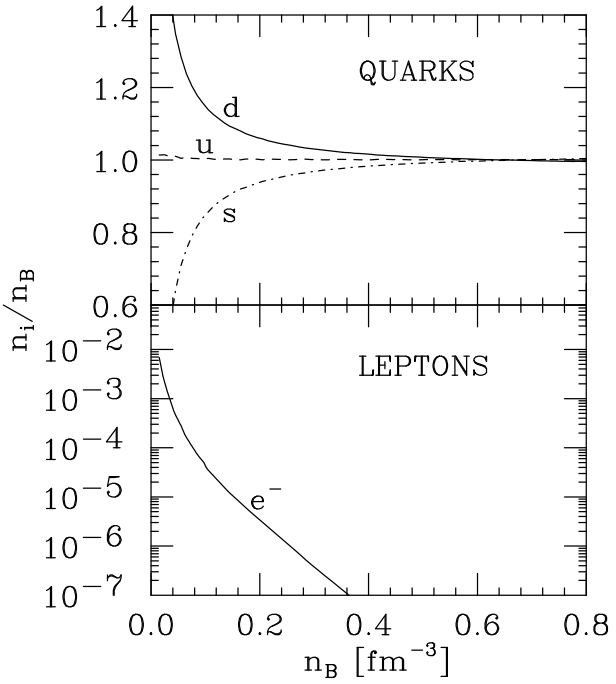

Figure 4.5: Composition of charge neutral matter of u, d and s quarks and electrons in weak equilibrium, obtained from the MIT bag model setting $m_u = m_d = 0$, $m_s = 150$ MeV, $B = 200$ MeV/fm^3 and $\alpha_s = 0.5$.

Chapter 5

Cooling mechanisms

The physical processes leading to neutron star cooling are driven by the emission of neutrinos (and antineutrinos) produced through a variety of mechanisms, depending on the different forms of matter present in the crust and the core of the star.

In this Chapter, we will briefly describe the emission processes taking place in the core, where matter is believed to consist mainly of neutrons, with a small fraction of protons and leptons, the abundance of which is determined by the requirements of weak equilibrium and charge neutrality. These processes turn out to be dominant, and can be described within a realistic and consistent model of the microscopic dynamics.

5.1 Direct Urca process

The most efficient neutrino and antineutrino production mechanisms, dubbed direct Urca processes, are the simplest weak processes taking place in matter consisting of neutrons, protons and leptons: neutron β-decay and electron capture by protons

$$n \to p + e + \bar{\nu}_e\,, \qquad p + e \to n + \nu_e\,. \tag{5.1}$$

At β-equilibrium, the above reactions take place at the same rate, and the chemical potentials of the participating particles satisfy the condition[1]

$$\mu_n = \mu_p + \mu_e\,. \tag{5.2}$$

Because at equilibrium the rate of production of neutrinos and antineutrinos is the same, the total neutrino emissivity, Q_D, is simply twice the emissivity associated with neutron β-decay, discussed in Appendix B

$$Q_D = 2\int \frac{d\mathbf{p}_n}{(2\pi)^3}\, dW_{i\to f}\, E_\nu\, f_n\,(1-f_p)\,(1-f_e)\,. \tag{5.3}$$

[1] We will always assume that neutrinos and antineutrinos be non degenerate, i.e. that they have vanishing chemical potential.

In the above equation $dW_{i\to f}$ is the differential probability of β-decay, f_j is the equilibrium Fermi-Dirac distribution of the particles of species j and E_ν denotes the neutrino energy. Note that the calculation of Q_D requires the evaluation of a twelve-dimensional integration, which can be reduced to a eight-dimensional one exploiting energy and momentum conservation.

The calculation of Eq.(5.3) can be greatly simplified, and treated analytically, using the approximation known as phase space decomposition, which is expected to be applicable to strongly degenerate fermions. This scheme is based on the tenet that, as at the temperatures typical of neutron stars both nucleons and leptons are strongly degenerate, the main contribution to the emissivity is provided by particles occupying quantum states in the vicinity of the Fermi surface. As a consequence, one can set $|\mathbf{p}_j| \approx p_{F_j}$, implying in turn that the energy scale relevant to the process is driven by the temperature, i.e. that $E_\nu \sim T$. As the neutrino momentum is also of order T, it can safely be neglected, with respect to the momenta of the degenerate fermions, in the argument of the momentum conserving δ-function.

The differential transition probability reads

$$dW_{i\to f} = 2\pi\,\delta(E_n - E_p - E_e - E_\nu)\,\delta(\mathbf{p}_n - \mathbf{p}_p - \mathbf{p}_e)\,|M_{fi}|^2\,4\pi E_\nu^2\,dE_\nu\,\frac{d\mathbf{p}_p}{(2\pi)^3}\,\frac{d\mathbf{p}_e}{(2\pi)^3}\,, \tag{5.4}$$

with $|M_{fi}|^2 = 2G^2(1+3g_A^2)$, where $G = G_F\cos\theta_c$, G_F and θ_c being the Fermi constant and Cabibbo's angle, respectively, while g_A is the axial vector coupling constant.

Equation (5.4) can be cast in the form

$$dW_{i\to f}\,\frac{d\mathbf{p}_n}{(2\pi)^3} = \frac{1}{(2\pi)^8}\,\delta(E_n - E_p - E_e - E_\nu)\,\delta(\mathbf{p}_n - \mathbf{p}_p - \mathbf{p}_e) \tag{5.5}$$

$$\times\,|M_{fi}|^2\,4\pi E_\nu^2\,dE_\nu\,\prod_{j=1}^{3} p_{Fj}\,m_j^*\,dE_j\,d\Omega_j\,, \tag{5.6}$$

where$d\Omega_j$ is the differential solid angle specifying the direction of the momentum $\mathbf{p}_j$, $m_j^* = p_{Fj}/v_{Fj}$ is the effective mass of the particles of species j and $v_{Fj} = (\partial E_j/\partial p_j)_{p=p_{Fj}}$ denotes the corresponding Fermi velocity.

Substutution of Eq.(5.5) in the definition of the neutrino emissivity, Eq.(5.3), leads to the result

$$Q_D = \frac{2}{(2\pi)^8}\,T^8\,A\,I\,|M_{fi}|^2\,\prod_{j=1}^{3} p_{Fj}\,m_j^*\,, \tag{5.7}$$

with

$$A = 4\pi\int d\Omega_1\,d\Omega_2\,d\Omega_3\,\delta(\mathbf{p}_n - \mathbf{p}_p - \mathbf{p_e})\,, \tag{5.8}$$

and

$$I = \int_0^\infty dx_\nu\,x_\nu^3\left[\prod_{j=1}^{3}\int_{-\infty}^{\infty} dx_j\,f_j\right]\,\delta(x_1 + x_2 + x_3 - x_\nu)\,. \tag{5.9}$$

The definition of A, Eq.(5.8), involves the integration on angular variables, while the calculation of I, defined by Eq.(5.9), requires integration over the adimensional variables $x_\nu = E_\nu/T$ and $x_j = (E_j - \mu_j)/T$. The details of the calculations of both A and I are described in Appendix D. The final results are

$$A = \frac{32\pi^3}{p_{Fn}\, p_{Fp}\, p_{Fe}}\,\Theta_{npe} \quad , \quad I = \frac{457\pi^6}{5040}\,, \tag{5.10}$$

where the function

$$\Theta_{npe} = \begin{cases} 1 & \text{se } p_{Fn} \le p_{Fp} + p_{Fe} \\ 0 & \text{otherwise} \end{cases}\,, \tag{5.11}$$

enforces the threshold condition that must be satisfied to fulfill he requirement of momentum conservation.

The resulting expression of the emissivity is

$$\begin{aligned} Q_D &= \frac{457}{10080}\, G_F^2 \cos^2\theta_c\, (1+3g_A^2)\, \frac{m_n^*\, m_p^*\, m_e^*}{\hbar^{10}\, c^3}\, (K_B T)^6\, \Theta_{npe} \\ &\simeq 4.00\times 10^{27} \left(\frac{n_e}{n_0}\right)^{1/3} \frac{m_n^*\, m_p^*}{m_n^2}\, T_9^6\, \Theta_{npe}\, \mathrm{erg\,cm^{-3}\,s^{-1}}\,, \end{aligned} \tag{5.12}$$

where, as usual, $n_0 = 0.16\, fm^{-3}$ is the equilibrium density of isospin symmetric nuclear matter, obtained from extrapolation of the central density of atomic nuclei and the semi empiric mass formula, while T_9 denotes the temperature measured in units of 10^9K. Note that the emissivity depends on temperature according to the power law $Q_D \propto T_9^6$. The power six can be easily explained on the basis of simple phase space considerations.

Integration over the momenta of the three strongly degenerate fermions participating in the process contributes a term $\propto T^3$, as the integration region is restricted to a thin shell of size $\sim T$ around the Fermi surface. On the other hand, the integration over the momentum of the non degenerate neutrino is not restricted, so that its contribution is $\propto T^3$. Taking into account that the energy conserving δ-function brings about a factor T^{-1}, that cancels the factor T arising from the neutrino energy, one gets the expected $\propto T^6$ dependence. This example illustrates how neutrino emissivity in neutron star matter is strongly affected by degeneracy.

5.1.1 Threshold of the direct Urca process

The main feature of the direct Urca process is the occurrence of a threshold, reflected by the presence of the step function Θ_{npe} in Eq. (5.12). Because the neutrino emissivity associated with this process, when active, dominates by many order of magnitude, it is very important to understand the implications of the threshold condition.

As we have already seen, the occurrence of the direct Urca process requires that the Fermi momenta of the degenerate fremions, p_{Fn}, p_{Fp} e p_{Fe}, fulfill the triangular condition $p_{Fn} \le p_{Fp} + p_{Fe}$. At densities around the equilibrium density of isospin symmetric nuclear matter, n_0, this requirement is not met. However, several models of the nuclear equation of state predict that the Fermi momenta p_{Fp} and p_{Fe} can grow faster than p_{Fn} with increasing density, thus allowing the onset of the process.

The Urca process is active when the proton fraction reaches a critical value. In the case of matter consisting of neutrons, protons and electrons (npe matter), electric neutrality implies $p_{Fp} = p_{Fe}$ and the triangular condition simplifies to $p_{Fp} \geq p_{Fn}/2$. It follows that the proton and neutron densities must be such that $n_p \geq n_n/8$. In terms of proton fraction this inequality reads

$$x_p = \frac{n_p}{n_n + n_p} \geq \frac{1}{9} \,. \tag{5.13}$$

If the electron chemical potential exceeds the muon rest mass, $m_\mu = 105.7$ Mev, a different kind of direct Urca process is energetically allowed, in addition to the one described above

$$n \to p + \mu + \bar{\nu}_\mu \,, \qquad p + \mu \to n + \nu_\mu \,. \tag{5.14}$$

The emissivity associated with the above processes can be written in the same form as Eq. (5.12), since the condition of β-equilibrium requires $\mu_\mu = \mu_e$, implying in turn $m_\mu^* = m_e^*$. The threshold function alone is modified to $\Theta_{np\mu}$, as the appearance of muons affects the critical value of the proton fraction, which grows until it reaches the upper limit $x_p = 1/[1 + (1 + 2^{-1/3})^3] \approx 0.148$ when $\mu_\mu \gg m_\mu$.

As mentioned in the previous Chapters, early models of neutron star matter were largely based on the non interacting Fermi gas description. Within this oversimplified picture, the proton fraction never exceeds the threshold of direct Urca processes. However, in the 1980s [19] and early 1990s [20] it was shown that inclusion of the effects of strong interactions – through models of nuclear dynamics predicting large symmetry energies – leads to a sizeable increase of the proton fraction. The resulting values of x_p turn out to be above the direct Urca threshold in a density region which is believed to be attained in the neutron star core.

Figure 5.1 shows the proton, electron and muon fractions in cold, i.e. $T = 0$, nuclear matter obtained from the equation of state of Ref. [21]. It clearly appears that the horizontal lines corresponding to the thresholds of direct electron and muon Urca processes are crossed at densities in the range $0.6 \lesssim n \lesssim 0.9$ fm^{-3}.

The density dependence of the of the neutron Fermi momentum is displayed in Fig. 5.2. For comparison, the quantities $p_{Fp} + p_{Fe}$ and $p_{Fp} + p_{F\mu}$ are also shown. It can be seen that the triangular condition on the Fermi momenta is fulfilled at density ~ 0.7 fm^{-3} and ~ 0.9 fm^{-3} for the electron and muon Urca process, respectively.

5.2 Modified Urca processes

If the direct Urca process is not allowed, the most efficient mechanism of neutrino emission is the *modified* Urca process, in which momentum conservation is made possible by the presence of an additional, spectator, nucleon.

The modified Urca reactions involve a nucleon-nucleon collision associated with β-decay or capture

$$n + n \to p + n + e + \bar{\nu}_e \quad , \quad p + n + e \to n + n + \nu_e \,, \tag{5.15}$$

$$n + p \to p + p + e + \bar{\nu}_e \quad , \quad p + p + e \to n + p + \nu_e \,. \tag{5.16}$$

where the two lines correspond to the neutron and proton branches, respectively. As we will see, the addition of the spectator nucleon dramatically slows down the reaction rate.

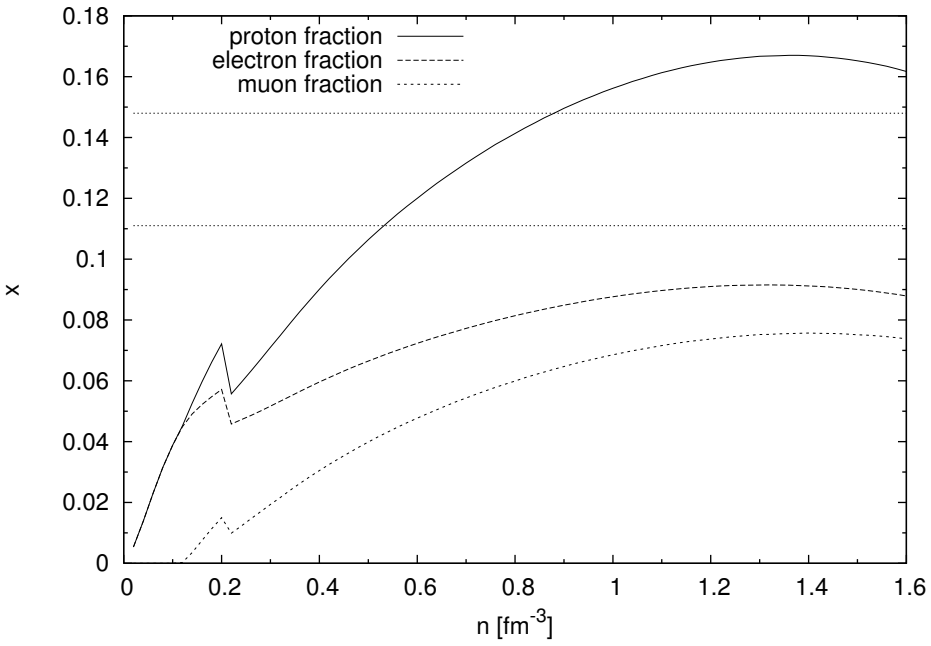

Figure 5.1: Proton, electron and muon fractions predicted by the model of Ref. [21]. The two horizontal lines show the thresholds of the direct Urca processes involving electrons and muons.

In the following, modified Urca processes will be denoted by the label MN, where M stands for *modified*, whereas $N = n$ and p refers to the neutron or proton branch. Both branches include the direct and inverse reactions, the rates of which at equilibrium are the same. Hence, only one rate is to be computed, and multiplied by a factor two to get the total emission rate.

Neutrino emissivity can be written in the usual form

$$Q^{MN} = 2\int \left[\prod_{j=1}^{4} \frac{d\mathbf{p}_j}{(2\pi)^3}\right] \frac{d\mathbf{p}_e}{(2\pi)^3}\,\frac{d\mathbf{p}_\nu}{(2\pi)^3}\,E_\nu\,(2\pi)^4\,\delta(E_f - E_i)$$
$$\times\,\delta(\mathbf{p}_f - \mathbf{p}_i)\,f_1\,f_2\,(1-f_3)\,(1-f_4)\,(1-f_e)\,\frac{1}{2}|M_{fi}|^2\,, \tag{5.17}$$

where the indices i and f refer to the initial and final states and $|M_{fi}|^2$ is the squared modulus of the ampletude associated with the process. The additional factor 2 is a symmetry factor, the inclusion of which is needed to avoid double counting in collisions involving identical particles.

One can proceed following the same procedure employed in the discussion of the direct Urca process (see Appendix D), and rewrite the emissivity associated with the direct reaction in the form

$$Q^{MN} = \frac{1}{(2\pi)^{14}}\,T^8\,A\,I\,\langle|M_{fi}|^2\rangle\,\prod_{j=1}^{5} p_{Fj}\,m_j^*\,, \tag{5.18}$$

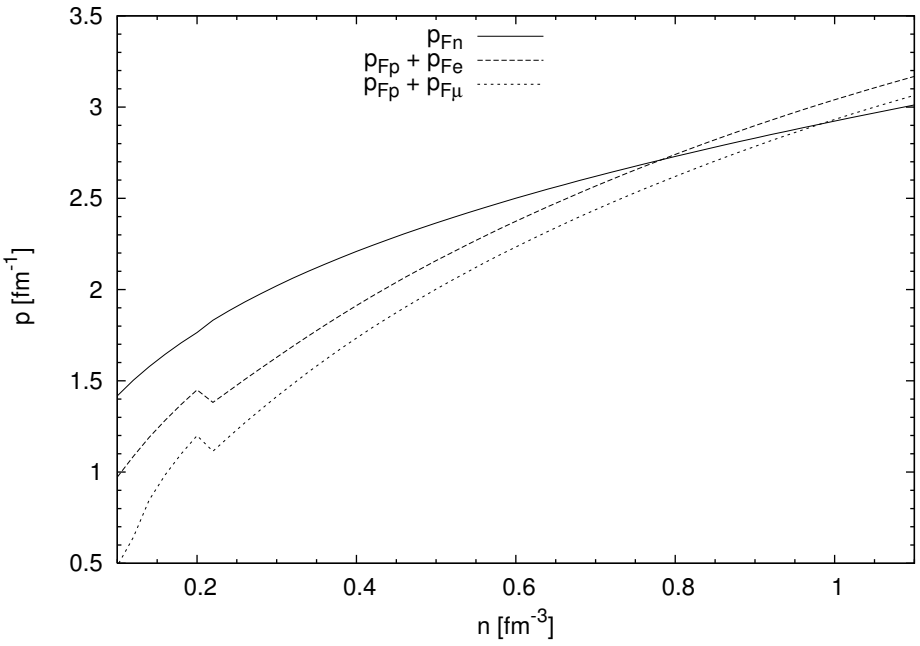

Figure 5.2: Density dependence of p_{Fn}, $p_{Fp} + p_{Fe}$ and $p_{Fp} + p_{F\mu}$, obtained from the model of Ref. [21]. The triangular conditions on the Fermi momenta are fulfilled at densities larger than the values at which the dashed and dotted lines cross the solid line.

with

$$A = 4\pi \left[\prod_{j=1}^{5} \int d\Omega_j \right] \delta(\mathbf{P}_f - \mathbf{P}_i) \,, \tag{5.19}$$

$$\langle |M_{fi}|^2 \rangle = \frac{4\pi}{A} \left[\prod_{j=1}^{5} \int d\Omega_j \right] \delta(\mathbf{P}_f - \mathbf{P}_i) \, |M_{fi}|^2 \tag{5.20}$$

and

$$I = \int_0^\infty dx_\nu \, x_\nu^3 \left[\prod_{j=1}^{5} \int_{-\infty}^{\infty} dx_j \, f_j \right] \delta\left(\sum_{j=1}^{5} x_j - x_\nu \right) . \tag{5.21}$$

Note that, as the magnitudes of the momenta of the degenerate fermions, $\mathbf{p}_j$ are set to be equal to the corresponding Fermi momenta, the quantities A and $\langle |M_{fi}|^2 \rangle$ only involve integrations over the angles specifying the directions of the particle momenta.

In the evaluation of A, the integration over the neutrino momentum can be readily carried out, as $\mathbf{p}_\nu$ is neglected in the δ-function. Because, in general, $|M_{fi}|^2$ depends on the momenta, we have introduced the the squared modulus of the angle-averaged matrix element, $\langle |M_{fi}|^2 \rangle$.

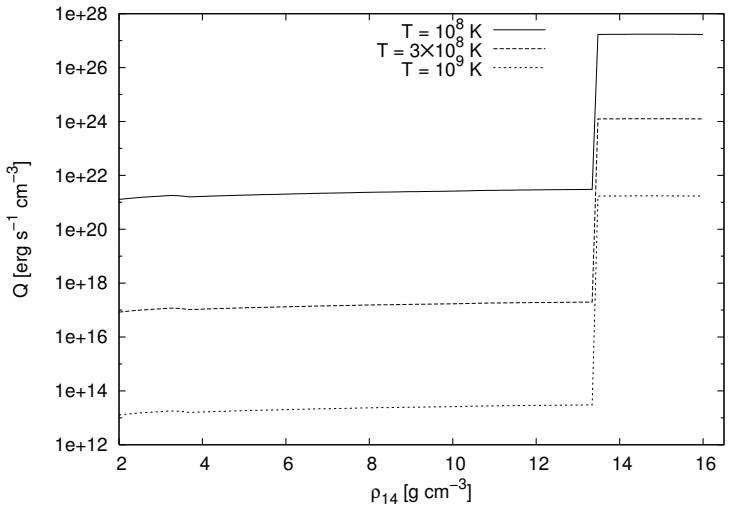

Figure 5.3: Neutrino emissivity obtained from the dynamical model of Ref [21]. The direct Urca process set in at density ~ 1.3 g cm^{-3}. Below threshold the dominant emission mechanism is the modified Urca process.

Calculation of the integral of Eq. (5.21) yields (see Appendix D)

$$I = \frac{11513\,\pi^8}{120960}\,. \tag{5.22}$$

At this stage the neutron and proton branches require separate discussions.

5.2.1 Neutron branch

Let us consider the first reaction of Eq. (5.15). We label with 1 and 2 the neutrons in the initial state, while 3 and 4 refer to the neutron and proton in the final state, respectively. The calculation of

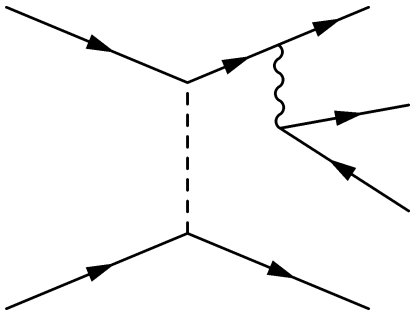

Figure 5.4: Feynman diagram illustrating the first reaction of Eq. (5.15)

A can be performed, with the result

$$A_n = \frac{2\pi(4\pi)^4}{p_{Fn}^3} \,. \tag{5.23}$$

Recall that the above expression should be modified at high density, if direct the Urca process sets in. In this case, modified Urca processes would give a negligible contribution to the emissivity.

The evaluation of the matrix elements M_{fi} involves non trivial difficulties, as it includes strong interactions. The nucleon-nucleon interaction, discussed in Chapter 2, features a long range component arising from one-pion-exchange (OPE) processes, taken into account within Yukawa's theory, and a short range, strongly repulsive, component, that is generally described within phenomenological approaches.

The long range contribution has been estimated in the classic work of Friman and Maxwell [22], treating nucleons as non relativistic particles and assuming that all lepton momenta can be neglected. The result, obtained averaging over the direction of the neutrino momentum, can be written in the form

$$|M_{fi}^{MN}|^2 = \frac{16\,G^2}{E_e^2}\left(\frac{f_\pi}{m_\pi}\right)^4 g_A^2\,F_A \,, \tag{5.24}$$

where m_π is the pion mass, $f_\pi \approx 1$ and

$$F_A = \frac{4\mathbf{Q}_1^4}{(\mathbf{Q}_1^2+m_\pi^2)^2} + \frac{4\mathbf{Q}_2^4}{(\mathbf{Q}_2^2+m_\pi^2)^2} + \frac{(\mathbf{Q}_1\cdot\mathbf{Q}_2)^2 - 3\mathbf{Q}_1^2\mathbf{Q}_2^2}{(\mathbf{Q}_1^2+m_\pi^2)(\mathbf{Q}_2^2+m_\pi^2)} \,, \tag{5.25}$$

with $\mathbf{Q}_1 = \mathbf{p}_1 - \mathbf{p}_3$ e $\mathbf{Q}_2 = \mathbf{p}_1 - \mathbf{p}_4$.

The first contribution arises from the amplitude of the reaction with $1 \to 3$ and $2 \to 4$, whereas the second one is associated with the exchange process, in which $1 \to 4$ and $2 \to 3$. Finally, the third contribution takes into account interference between the two amplitudes. In addition, Friman and Maxwell neglect the proton momentum, setting $|\mathbf{Q}_1| = |\mathbf{Q}_2| \approx p_{Fn}$ e $\mathbf{Q}_1\cdot\mathbf{Q}_2 \approx p_{Fn}^2/2$. Their final result reads

$$|M_{fi}^{Mn}|^2 = 16\,G^2\left(\frac{f_\pi}{m_\pi}\right)^4 \frac{g_A^2}{E_e^2}\,\frac{21}{4}\,\frac{p_{Fn}^4}{(p_{Fn}^2+m_\pi^2)^2} \,. \tag{5.26}$$

Being independent of the directions of the momenta, the above expression can be moved out of the integral appearing in Eq, (5.20), with the result $\langle|M_{fi}^{Mn}|^2\rangle = |M_{fi}^{Mn}|^2$. Comparison between the above result and the exact solution, obtained through numerical integration, shows that the approximation employed in Ref. [22] are remarkably accurate. The discrepancy turns out to be few percent at $n \sim n_0$, and $\sim 10\%$ at $n \sim 3n_0$.

In conclusion, the emissivity associated with the neutron branch of the modified Urca process obtained by Frimam and Maxwell is

$$\begin{aligned} Q^{Mn} &= \frac{11513}{30240}\,\frac{G_F^2\cos^2\theta_C\,g_A^2\,m_n^{*3}\,m_p^*}{2\pi}\left(\frac{f_\pi}{m_\pi}\right)^4 \frac{p_{Fp}(k_B T)^8}{\hbar^{10}\,c^8}\,\alpha_n\,\beta_n \\ &\approx 8.1\times 10^{21}\left(\frac{m_n^*}{m_n}\right)^3\left(\frac{m_p^*}{m_p}\right)\left(\frac{n_p}{n_0}\right)^{1/3} T_9^8\,\alpha_n\,\beta_n \;\; erg\,cm^{-3}\,s^{-1} \,, \end{aligned} \tag{5.27}$$

with $\alpha_n = 1.13$ e $\beta_n = 0.68$.

5.2.2 Proton branch

Let us now consider the second reaction of (5.16). We will label 1 e 2 the initial state protons 3 and 4 the final state proton and neutron, respectively.

The calculation of A turns out to be more compilex, with respect to the case of the neutron branch. We find

$$A_p = \frac{2(2\pi)^5}{p_{Fn}\, p_{Fp}^3\, p_{Fe}} \left(p_{Fe} + 3p_{Fp} - p_{Fn}\right)^2 \Theta_{Mp}\,, \tag{5.28}$$

where $\Theta_{Mp} = 1$ if the proton branch is allowed by momentum conservation and $\Theta_{Mp} = 1$ otherwise. The triangular condition translates into the inequality $p_{Fn} < 3p_{Fp} + p_{Fe}$. Note that the expression of A_p should also be modified at densities larger than that corresponding to the threshold of the direct Urca process. However, in this density region the contribution of the modified Urca processes turns out to be negligible.

The calculation of the squared matrix element yields a result identical to (5.24). Replacing $|\mathbf{Q}_1| = |\mathbf{Q}_2| \approx p_{Fn} - p_{Fp}$ (maximum momentum trasfer) and $\mathbf{Q}_1 \cdot \mathbf{Q}_2 = -(p_{Fn} - p_{Fp})^2$, one obtains an expression similar to Eq. (5.26), apart from the replacements of 21/4 with 6 e p_{Fn} with $p_{Fn} - p_{Fp}$. Neglecting the angular dependence of the matrix element has been shown to be a good approximation in both the neutron and neutron branches.

The proton branch emissivity can be obtained from the corresponding neutron branch result exploiting the *rescaling* rule

$$\begin{aligned}\frac{Q^{Mp}}{Q^{Mn}} &= \frac{\langle |M_{fi}^{Mp}|^2 \rangle}{\langle |M_{fi}^{Mn}|^2 \rangle} \left(\frac{m_p^*}{m_n^*}\right)^2 \frac{(p_{Fe} + 3p_{Fp} - p_{Fn})^2}{8\, p_{Fe}\, p_{Fp}} \Theta_{Mp} \\ &\approx \left(\frac{m_p^*}{m_n^*}\right)^2 \frac{(p_{Fe} + 3p_{Fp} - p_{Fn})^2}{8\, p_{Fe}\, p_{Fp}} \Theta_{Mp}\,. \end{aligned} \tag{5.29}$$

In applications, it is common practice setting $\langle |M_{fi}^{Mp}|^2 \rangle = \langle |M_{fi}^{Mn}|^2 \rangle$, as illustrated by that the last line of Eq. (5.29).

The main difference between the two branches is the presence of a threshold for the proton branch. In npe matter, this condition reduces to $p_{Fn} < 4p_{Fp}$, corresponding to a critical proton fraction $x = 1/65 = 0.0154$, which is believed to be attained almost everywhere in the neutron star core. Once the modified Urca process is active in the proton branch, the associated emissivity slowly grows, starting from zero and eventually becoming comparable to the the emissivity associated with the neutron branch, in the vicinity of the threshold of the direct Urca process.

In conclusion, it has to be pointed out that the temperature dependence of the emissivity of the modified Urca process is a power law T^8. The additional factor T^2, with respect to the direct Urca process, is to be ascribed to the presence of two additional degenerate fermions.

5.3 Neutrino bremsstrahlung in nucleon-nucleon collisions

To complete the discussion of neutrino emission processes in the neutron star core, we need to consider neutron bremsstrahlung associated with nucleon-nucleon collisions

$$n+n \to n+n+\nu+\bar{\nu}\,, \quad n+p \to n+p+\nu+\bar{\nu}\,, \quad p+p \to p+p+\nu+\bar{\nu}\,. \tag{5.30}$$

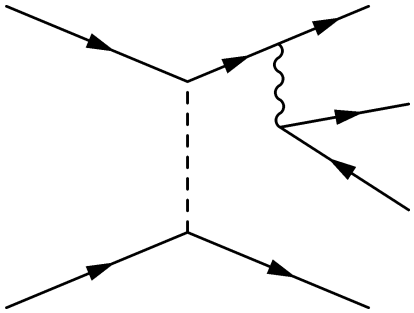

Figure 5.5: Feynman diagram illustrating the first reaction of 5.30.

In these reactions, the scattering process driven by strong interactions leads to the production of a neutrino-antineutrino pair, of any flavour. Neutrino bremsstrahlung has no threshold, and is therefore active at any densities. In addition, unlike the processes discussed above, does not change the composition of matter.

The emissivity associated with bremsstrahlung can be written in the form

$$Q^{NN} = \int \left[\prod_{j=1}^{4} \frac{d\mathbf{p}_j}{(2\pi)^3}\right] \frac{d\mathbf{p}_\nu}{(2\pi)^3}\,\frac{d\mathbf{p'}_\nu}{(2\pi)^3}\,\omega_\nu\,(2\pi)^4\,\delta(E_f-E_i) \\ \times\,\delta(\mathbf{P}_f-\mathbf{P}_i)\,f_1\,f_2\,(1-f_3)\,(1-f_4)\,\frac{1}{s}|M_{fi}|^2\,, \tag{5.31}$$

where the index j labels nucleons, $\mathbf{p}_\nu$ and $\mathbf{p'}_\nu$ are the neutrino and antineutrino momenta, $\omega_\nu = E_\nu + E'_\nu$ is the energy carried by the neutron pair and the symmetry factor s ($s=1$ for the np channel and $s=4$ for the nn and pp channels) is meant to avoid double counting. In the non relativistic limit, the squared matrix element, after spin summation, reads

$$|M_{fi}|^2 = |\tilde{M}_{fi}|^2/\omega_\nu^2\,. \tag{5.32}$$

The factor ω_ν^2 in the denominator comes from the propagator of the virtual nucleon appearing in the Feynman diagram.

Neglecting the momenta of the neutrinos with respect to those of the nucleons, $|\tilde{M}_{fi}|^2$ become independent of $\mathbf{p}_\nu$ e $\mathbf{p'}_\nu$. As a consequence, the integration over the neutrinos phase-space yields

$$\int_0^\infty E_\nu^2\,dE_\nu \int_0^\infty E'_\nu\,dE'_\nu \cdots = \frac{1}{30}\int_0^\infty \omega_\nu^5\,d\omega_\nu \cdots\,, \tag{5.33}$$

and the emissivity takes the form (we follow the decomposition approximation again)

$$Q^{NN} = \frac{(2\pi)^4}{(2\pi)^1 8}\,\frac{1}{30}\,A\,I\,\frac{1}{s}\langle|\tilde{M}_{fi}|^2\rangle\,T^8\prod_{j=1}^{4} m_j^*\,p_{Fj}\,, \tag{5.34}$$

con

$$A = (4\pi)^2\int d\Omega_1\,d\Omega_2\,d\Omega_3\,d\Omega_4\,\delta(\mathbf{p}_1+\mathbf{p}_2-\mathbf{p}_3-\mathbf{p}_4)\,, \tag{5.35}$$

$$\langle|\tilde{M}_{fi}|^2\rangle = \frac{(4\pi)^2}{A}\int d\Omega_1\,d\Omega_2\,d\Omega_3\,d\Omega_4\,\delta(\mathbf{p}_1+\mathbf{p}_2-\mathbf{p}_3-\mathbf{p}_4)\,|\tilde{M}_{fi}|^2\,, \tag{5.36}$$

$$I = \int_0^\infty dx_\nu\,x_\nu^4\left[\prod_{j=1}^{4}\int_{-\infty}^{+\infty} dx_j\,f_j\right]\delta\left(\sum_{j=1}^{4} x_j - x_\nu\right) = \frac{164\pi^8}{945}\,. \tag{5.37}$$

Recall that $x_j = (E_j-\mu_j)/T$ is the dimensionless nucleon energy, while $x_\nu = \omega_\nu/T$ is the corresponding variable for neutrinos. The result of the angular integrations is

$$A_{nn} = \frac{(4\pi)^5}{2\,p_{Fn}^3}\,,\qquad A_{np} = \frac{(4\pi)^5}{2\,p_{Fn}^2\,p_{Fp}}\,,\qquad A_{pp} = \frac{(4\pi)^5}{2\,p_{Fp}^3}\,. \tag{5.38}$$

Phase-space decomposition provides the rules to rescale the different processes

$$\frac{Q^{np}}{Q^{nn}} = 4\,\frac{\langle|\tilde{M}_{fi}^{np}|^2\rangle}{\langle|\tilde{M}_{fi}^{nn}|^2\rangle}\left(\frac{m_p^*}{m_n^*}\right)^2\frac{p_{Fp}}{p_{Fn}}\quad,\quad \frac{Q^{pp}}{Q^{nn}} = 4\,\frac{\langle|\tilde{M}_{fi}^{pp}|^2\rangle}{\langle|\tilde{M}_{fi}^{nn}|^2\rangle}\left(\frac{m_p^*}{m_n^*}\right)^4\frac{p_{Fp}}{p_{Fn}}\,. \tag{5.39}$$

Within the OPE dynamical model, the squared matrix element turns out to be

$$|\tilde{M}_{fi}^{NN}|^2 = 16\,G_F^2\,g_A^2\left(\frac{f_\pi}{m_\pi}\right)^4 F_{NN}\,, \tag{5.40}$$

with

$$F_{NN} = \frac{\mathbf{Q}_1^4}{(\mathbf{Q}_1^2+m_\pi^2)^2} + \frac{\mathbf{Q}_2^4}{(\mathbf{Q}_2^2+m_\pi^2)^2} + \frac{\mathbf{Q}_1^2\mathbf{Q}_2^2 - 3(\mathbf{Q}_1\cdot\mathbf{Q}_2)^2}{(\mathbf{Q}_1^2+m_\pi^2)(\mathbf{Q}_2^2+m_\pi^2)} \tag{5.41}$$

for nn e pp processes, and

$$F_{NN} = \frac{\mathbf{Q}_1^4}{(\mathbf{Q}_1^2+m_\pi^2)^2} + \frac{2\mathbf{Q}_2^4}{(\mathbf{Q}_2^2+m_\pi^2)^2} - 2\,\frac{\mathbf{Q}_1^2\mathbf{Q}_2^2 - (\mathbf{Q}_1\cdot\mathbf{Q}_2)^2}{(\mathbf{Q}_1^2+m_\pi^2)(\mathbf{Q}_2^2+m_\pi^2)}\,, \tag{5.42}$$

for the np process. Recall that $\mathbf{Q}_1 = \mathbf{p}_1-\mathbf{p}_3$, $\mathbf{Q}_2 = \mathbf{p}_1-\mathbf{p}_4$ and , in the strong degeneracy limit, $\mathbf{Q}_1\cdot\mathbf{Q}_2 = 0$.

After averaging the squared matrix element over the directions of the nucleon momenta, one obtains

$$\langle|\tilde{M}_{fi}^{NN}|^2\rangle = 161,G_F^2\,g_A^2\left(\frac{f_\pi}{m_\pi}\right)^4\langle F_{NN}\rangle\,, \tag{5.43}$$

where

$$\langle F_{NN}\rangle = 3 - \frac{5}{q}\arctan q + \frac{1}{1+q^2} + \frac{1}{q\sqrt{2+q^2}}\arctan\left(q\sqrt{2+q^2}\right), \tag{5.44}$$

for nn or pp processes, and

$$\langle F_{NN}\rangle = 1 - \frac{3\arctan q}{2q} + \frac{1}{2(1+q^2)} + \frac{2\,p_{Fn}^4}{(p_{Fn}^2+m_\pi^2)^2} - \left(1-\frac{\arctan q}{q}\right)\frac{2\,p_{Fn}^2}{p_{Fn}^2+m_\pi^2}, \tag{5.45}$$

with $q_N = 2p_{Fn}/m_\pi$, for the np process.

Note that Eq. (5.44) has been derived within the model under consideration, while Eq. (5.45) has been obtained assuming $p_{Fp} \ll p_{Fn}$. However, this approximation is applicable at densities $n \lesssim 3n_0$.

To summarise the calculation of neutrino emissivity, we can refer again to the treatment of Friman and Maxwell. In the nn channel they neglect the exchange contribution to the squared matrix element (5.44), average over the directions of the nucleon momenta and set $n = n_0$. Finally, they plug $\langle|\tilde{M}_{fi}|^2\rangle$ obtained within this scheme into the expression of Q^{nn}, with an arbitrary correction factor β_{nn}, meant to take into account all neglected effects (correlations, repulsive component of the nucleon-nuhcleon interaction ...). The same procedure is applied to the np contribution, in which the interference term of Eq. (5.45) is omitted.

The pp process, not taken into account in Ref. [22], has been studied by Yakovlev and Levenfish [23]. Their results read

$$\begin{aligned} Q^{nn} &= \frac{41}{14175}\frac{G_F^2 g_A^2 m_n^{*4}}{2\pi\hbar^{10}c^8}\left(\frac{f_\pi}{m_\pi}\right)^4 p_{Fn}\,\alpha_{nn}\beta_{nn}(k_B T)^8\mathscr{N}_\nu \\ &\approx 7.5\times10^{19}\left(\frac{m_n^*}{m_n^*}\right)^4\left(\frac{n_n}{n_0}\right)^{1/3}\alpha_{nn}\beta_{nn}\mathscr{N}_\nu T_9^8 \;\; erg\,cm^{-3}\,s^{-1}, \end{aligned} \tag{5.46}$$

$$\begin{aligned} Q^{nn} &= \frac{82}{14175}\frac{G_F^2 g_A^2 m_n^{*2} m_p^{*2}}{2\pi\hbar^{10}c^8}\left(\frac{f_\pi}{m_\pi}\right)^4 p_{Fp}\,\alpha_{np}\beta_{np}(k_B T)^8\mathscr{N}_\nu \\ &\approx 1.5\times10^{20}\left(\frac{m_n^* m_p^*}{m_n m_p}\right)^2\left(\frac{n_p}{n_0}\right)^{1/3}\alpha_{np}\beta_{np}\mathscr{N}_\nu T_9^8 \;\; erg\,cm^{-3}\,s^{-1}, \end{aligned} \tag{5.47}$$

$$\begin{aligned} Q^{pp} &= \frac{41}{14175}\frac{G_F^2 g_A^2 m_p^{*4}}{2\pi\hbar^{10}c^8}\left(\frac{f_\pi}{m_\pi}\right)^4 p_{Fp}\,\alpha_{pp}\beta_{pp}(k_B T)^8\mathscr{N}_\nu \\ &\approx 7.5\times10^{19}\left(\frac{m_p^*}{m_p^*}\right)^4\left(\frac{n_p}{n_0}\right)^{1/3}\alpha_{pp}\beta_{pp}\mathscr{N}_\nu T_9^8 \;\; erg\,cm^{-3}\,s^{-1}, \end{aligned} \tag{5.48}$$

where m_π is the π^0 mass and $\mathscr{N}_\nu$ is the number of neutrino flavours. The dimensionless flavours α_{NN} are obtained from estimates of the matrix elements at $n = n_0$. Their values are $\alpha_{nn} = 0.59$, $\alpha_{np} = 1.06$, $\alpha_{pp} = 0.11$.

The emissivities of all process turn out to be comparable, with $Q^{pp} < Q^{np} < Q^{nn}$.

Note that the emissivity is always $\propto T^8$. This result can be explained with the usual phase-space consideration. The four degenerate nucleons contributecontribuiscono a power T^4 and the two neutrinos a power T^6. The squared matrix element is proportional to ω_ν^{-2}, i.e. to T^{-2}, which remove the power T^2 in excess.

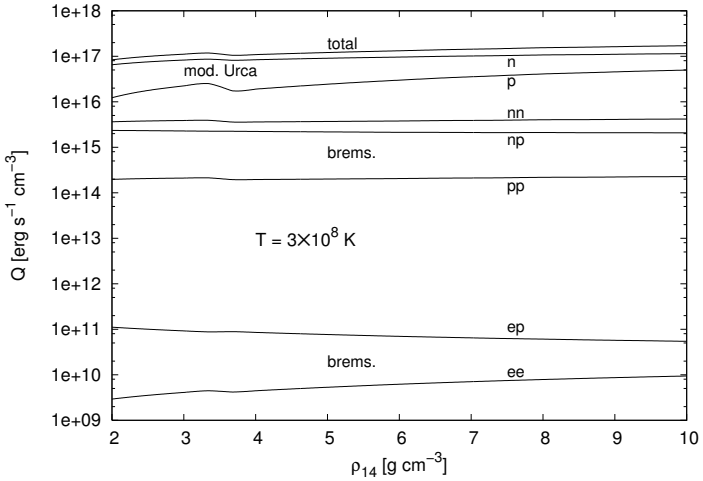

Figure 5.6: Density dependence of the neutrino emissivity in the neutron star core, associated with different mechanisms. The density range is restricted to the region in which the direct Urca process is not allowed. The most effective mechanism is the modified Urca processes, while the contribution arising from bremsstrahlung of neutrino-antineutrino pairs in nucleon-nucleon collisions is more than one order of magnitude smaller. The emissivity from bremsstrahlung in scattering processes driven by electromagnetic interactions appears to be negligible.

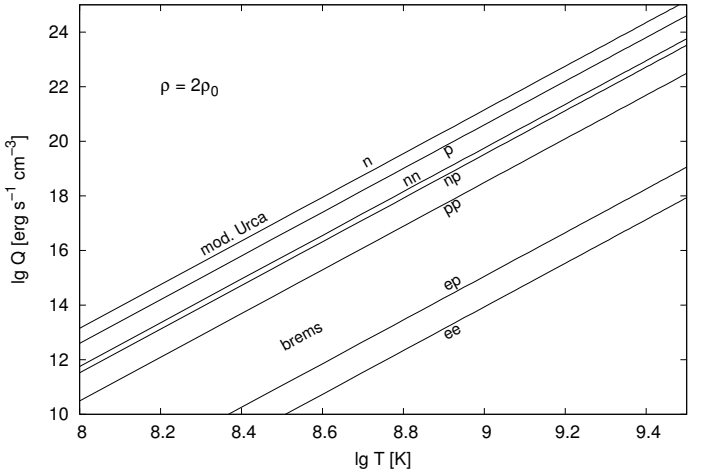

Figure 5.7: Log-log plot illustrating the temperature dependence of the neutrino emissivity associated with the different processes discussed in the text.

Appendix A

Derivation of the one-pion-exchange potential

Let us consider the process depicted in Fig. 3.2. The corresponding S-matrix element reads

$$\begin{aligned} S_{fi} &= (-ig)^2 \frac{m^2}{(E_1 E_2 E_{1'} E_{2'})^{1/2}} (2\pi)^4 \delta^{(4)}(p_1 + p_2 - p_{1'} - p_{2'}) \\ &\times \eta^\dagger_{1'} \boldsymbol{\tau} \eta_1 \; \bar{u}_{1'} i\gamma_5 u_1 \frac{i}{k^2 - m_\pi^2} \eta^\dagger_{2'} \boldsymbol{\tau} \eta_2 \; \bar{u}_{2'} i\gamma_5 u_2 \end{aligned} \tag{A.1}$$

where m_π is the pion mass, $k = p_2 - p_{2'}$ and η_i denotes the two-component Pauli spinor describing the isospin state of particle i. Equation (A.1) can be rewritten in the form

$$\begin{aligned} S_{fi} &= ig^2 \frac{m^2}{(E_1 E_2 E_{1'} E_{2'})^{1/2}} (2\pi)^4 \delta^{(4)}(p_1 + p_2 - p_{1'} - p_{2'}) \\ &\times \langle \boldsymbol{\tau}_1 \cdot \boldsymbol{\tau}_2 \rangle \; \bar{u}_{2'} \gamma_5 u_2 \bar{u}_{1'} \gamma_5 u_1 \frac{1}{k^2 - m_\pi^2} \,, \end{aligned} \tag{A.2}$$

with $\langle \boldsymbol{\tau}_1 \cdot \boldsymbol{\tau}_2 \rangle = \eta^\dagger_{2'} \boldsymbol{\tau} \eta_2 \; \eta^\dagger_{1'} \boldsymbol{\tau} \eta_1$.

Substituting the nonrelativistic limit

$$\begin{aligned} \bar{u}_{2'} \gamma_5 u_2 &= \frac{(E_{2'} + m)^{1/2} (E_2 + m)^{1/2}}{2m} \left[\chi^\dagger_{s'} \frac{\boldsymbol{\sigma} \cdot \mathbf{p}_2}{E_2 + m} \chi_s - \chi^\dagger_{s'} \frac{\boldsymbol{\sigma} \cdot \mathbf{p}_{2'}}{E_{2'} + m} \chi_s \right] \\ &\approx \chi^\dagger_{s'} \frac{\boldsymbol{\sigma}(\mathbf{p}_2 - \mathbf{p}_{2'})}{2m} \chi_s = \chi^\dagger_{s'} \frac{(\boldsymbol{\sigma} \cdot \mathbf{k})}{2m} \chi_s \end{aligned} \tag{A.3}$$

and the similar expression for $\bar{u}_{1'} \gamma_5 u_1$ in the definition of S_{fi} and replacing (use $E_i \approx E_{i'} \approx m_\pi$ and $k^2 = (E_i - E_{i'})^2 - |\mathbf{k}|^2 \approx -|\mathbf{k}|^2$)

$$\frac{1}{k^2 - m_\pi^2} \approx -\frac{1}{|\mathbf{k}|^2 + m_\pi^2} \tag{A.4}$$

we obtain

$$\begin{aligned} S_{fi} &\approx -i \frac{g^2}{4m^2} (2\pi)^4 \delta^{(4)}(p_1 + p_2 - p_{1'} - p_{2'}) \; \langle \boldsymbol{\tau}_1 \cdot \boldsymbol{\tau}_2 \rangle \\ &\times \chi^\dagger_{1'} \chi^\dagger_{2'} \frac{(\boldsymbol{\sigma}_1 \cdot \mathbf{k})(\boldsymbol{\sigma}_2 \cdot \mathbf{k})}{|\mathbf{k}|^2 + m_\pi^2} \chi_2 \chi_1 \end{aligned} \tag{A.5}$$

The corresponding potential in momentum space is

$$\begin{aligned} v^\pi(\mathbf{k}) &= -\frac{g^2}{4m^2}\frac{(\boldsymbol{\sigma}_1\cdot\mathbf{k})(\boldsymbol{\sigma}_2\cdot\mathbf{k})}{\mathbf{k}^2+m_\pi^2}\,\boldsymbol{\tau}_1\cdot\boldsymbol{\tau}_2 \\ &= \left(\frac{f_\pi}{m_\pi}\right)^2\frac{(\boldsymbol{\sigma}_1\cdot\mathbf{k})(\boldsymbol{\sigma}_2\cdot\mathbf{k})}{\mathbf{k}^2+m_\pi^2}\,\boldsymbol{\tau}_1\cdot\boldsymbol{\tau}_2 \end{aligned} \tag{A.6}$$

with $g^2/4\pi = 14$ and

$$f_\pi^2 = g^2\frac{m_\pi^2}{4m^2} \approx 4\pi\times 14\frac{(140)^2}{4\times(939)^2} \approx 4\pi\times 0.08 \approx 1 \tag{A.7}$$

The configuration space $v^\pi(\mathbf{r})$ is obtained from the Fourier transform:

$$\begin{aligned} v^\pi(\mathbf{r}) &= -\frac{f_\pi^2}{m_\pi^2}\int\frac{d^3k}{(2\pi)^3}\,\boldsymbol{\tau}_1\cdot\boldsymbol{\tau}_2\,\boldsymbol{\sigma}_1\cdot\mathbf{k}\,\boldsymbol{\sigma}_2\cdot\mathbf{k}\,\frac{1}{(|\mathbf{k}|^2+m_\pi^2)}\,e^{-i\mathbf{k}\cdot\mathbf{r}} \\ &= \frac{f_\pi^2}{m_\pi^2}\,\boldsymbol{\tau}_1\cdot\boldsymbol{\tau}_2\,\boldsymbol{\sigma}_1\cdot\nabla\,\boldsymbol{\sigma}_2\cdot\nabla\int\frac{d^3k}{(2\pi)^3}\frac{1}{(|\mathbf{k}|^2+m_\pi^2)}e^{-i\mathbf{k}\cdot\mathbf{r}} \\ &= \frac{1}{4\pi}\,\frac{f_\pi^2}{m_\pi^2}\,\boldsymbol{\tau}_1\cdot\boldsymbol{\tau}_2\,\boldsymbol{\sigma}_1\cdot\nabla\,\boldsymbol{\sigma}_2\cdot\nabla\,\frac{e^{-m_\pi r}}{r}. \end{aligned} \tag{A.8}$$

The Laplacian of the Yukawa function,

$$y_\pi(r) = \frac{e^{-m_\pi r}}{r} = 4\pi\int\frac{d^3k}{(2\pi)^3}\frac{1}{(|\mathbf{k}|^2+m_\pi^2)}e^{i\mathbf{k}\cdot\mathbf{r}}, \tag{A.9}$$

involves a δ-function singularity at the origin, as can be easily seen from

$$(-\nabla^2+m_\pi^2)\;y_\pi(r) = 4\pi\delta(\mathbf{r})\;. \tag{A.10}$$

Gradients in Eq. (A.8) have to be evaluated taking this singularity into account. For this purpose it is convenient to rewrite

$$\begin{aligned} \boldsymbol{\sigma}_1\cdot\nabla\,\boldsymbol{\sigma}_2\cdot\nabla y_\pi(r) &= \left(\boldsymbol{\sigma}_1\cdot\nabla\,\boldsymbol{\sigma}_2\cdot\nabla-\frac{1}{3}\boldsymbol{\sigma}_1\cdot\boldsymbol{\sigma}_2\,\nabla^2\right)y_\pi(r) \\ &+ \frac{1}{3}\boldsymbol{\sigma}_1\cdot\boldsymbol{\sigma}_2\,\nabla^2\,y_\pi(r)\,, \end{aligned} \tag{A.11}$$

as the δ-function contribution to $\nabla^2 y_\pi(r)$ does not appear in the first term, yielding

$$\begin{aligned} &\left(\boldsymbol{\sigma}_1\cdot\nabla\boldsymbol{\sigma}_2\cdot\nabla-\frac{1}{3}\,\boldsymbol{\sigma}_1\cdot\boldsymbol{\sigma}_2\nabla^2\right)y_\pi(r) \\ &\qquad=\left(\boldsymbol{\sigma}_1\cdot\hat{\mathbf{r}}\,\boldsymbol{\sigma}_2\cdot\hat{\mathbf{r}}-\frac{1}{3}\,\boldsymbol{\sigma}_1\cdot\boldsymbol{\sigma}_2\right)\left(m_\pi^2+\frac{3m_\pi}{r}+\frac{3}{r^2}\right)y_\pi(r), \end{aligned} \tag{A.12}$$

where $\hat{\mathbf{r}} = \mathbf{r}/|\mathbf{r}|$. The laplacian $\nabla^2 y_\pi(r)$ in the second term of Eq. (A.11) can be replaced with $m_\pi^2 y_\pi(r) - 4\pi\,\delta(r)$ using Eq. (A.10).

Carrying out the calculation of the derivatives in Eq. (A.8) in this way we find

$$v^{\pi}(\mathbf{r}) = \frac{1}{3}\frac{1}{4\pi} f_{\pi}^2 \, m_{\pi} \, \boldsymbol{\tau}_1 \cdot \boldsymbol{\tau}_2 \left[\, T_{\pi}(r) S_{12} + \left(Y_{\pi}(r) - \frac{4\pi}{m_{\pi}^3} \delta(\mathbf{r}) \right) \boldsymbol{\sigma}_1 \cdot \boldsymbol{\sigma}_2 \right] , \tag{A.13}$$

with

$$Y_{\pi}(r) = \frac{e^{-m_{\pi} r}}{m_{\pi} r} , \tag{A.14}$$

and

$$T_{\pi}(r) = \left(1 + \frac{3}{m_{\pi} r} + \frac{3}{m_{\pi}^2 r^2} \right) Y_{\pi}(r) , \tag{A.15}$$

i.e. Eqs. (3.39) and (3.40).

Appendix B

Neutron β-decay

Consider the reaction

$$n \longrightarrow p + e + \bar{\nu}\,, \tag{B.1}$$

illustrated by the Feynman diagram of Fig. B.1, where $p_n \equiv (E_n, \mathbf{p}_n)$, $p_p \equiv (E_p, \mathbf{p}_p)$, $p_e \equiv (E_e, \mathbf{p}_e)$ and $p_\nu \equiv (E_\nu, \mathbf{p}_\nu)$ denote the neutron, proton, electron and antineutrino four momenta, respectively.

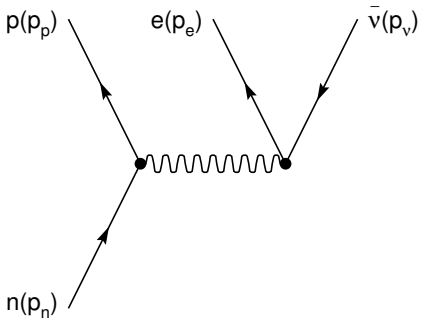

Figure B.1: Feynman diagram illustrating the neutron β-decay process (B.1)

The Fermi interaction hamiltonian, driving the decay process, is given by

$$H = \frac{G}{\sqrt{2}}\, j_\mu \ell^\mu\,, \tag{B.2}$$

with $G = G_F \cos\theta_C$, $G_F = 1.463\times10^{-49}$ erg cm^3 and $\theta_C \sim 13$ deg being the Fermi constant and Cabibbo's angle, respectively. The weak leptonic current ℓ^μ has the form

$$\ell^\mu = \bar{u}_{r'}(p_e)\gamma^\mu\left(1-\gamma^5\right) v_r(p_\nu)\,, \tag{B.3}$$

where $u_r(p)$ e $v_r(p)$ denote the four-spinors associated with the positive and negative energy solutions of the Dirac equation, describing a non interacting fermion of mass m with four-momentum p

and spin projection r. They are normalised is such a way as to satisfy the relations

$$\bar{u}_{r'}(p)u_r(p) = \bar{v}_{r'}(p)v_r(p) = 2m\,\delta_{rr'}\,. \tag{B.4}$$

In the non relativistic limit, fully justified in the present context, the hadronic weak current reduces to

$$j_\mu = \chi^\dagger_{s'}\left(\delta_{\mu 0}g_v + \delta_{\mu i}g_A\sigma_i\right)\chi_s\,, \tag{B.5}$$

where σ_i (i=1,2,3) are Pauli matrices, χ_s and $\chi_{s'}$ are Pauli spinors satisfying the relations $\chi^\dagger_{s'}\chi_s = \delta_{ss'}$ and the values of the vector and axial coupling constants are $g_v = 1$ and $g_A = 1.26$.

The transition rate from the initial state $|i\rangle$ to the set of accessible final states $|f\rangle$ can be obtained using Fermi's golden rule

$$dW_{i\to f} = 2\pi\,\delta(E_n - E_p - E_e - E_\nu)\sum_{spins}\left|H_{fi}\right|^2\frac{d\mathbf{p}_p}{(2\pi)^3}\frac{d\mathbf{p}_e}{(2\pi)^3}\frac{d\mathbf{p}_\nu}{(2\pi)^3}\,, \tag{B.6}$$

where

$$\sum_{spins}\left|H_{fi}\right|^2 = (2\pi)^3\frac{G^2}{2}\delta(\mathbf{p}_n - \mathbf{p}_p - \mathbf{p}_e - \mathbf{p}_\nu)\frac{1}{2E_e}\frac{1}{2E_\nu}J_{\lambda\mu}L^{\lambda\mu} \tag{B.7}$$

with

$$J_{\lambda\mu} = \sum_{spins} {j_\lambda}^\dagger j_\mu \tag{B.8}$$

and

$$L^{\lambda\mu} = \sum_{spins} {\ell^\lambda}^\dagger \ell^\mu\,. \tag{B.9}$$

Substituting the leptonic weak current in Eq. (B.9) and exploiting the completeness relations fulfilled by Dirac's spinors, we find

$$\begin{aligned} L^{\lambda\mu} &= \sum_{rr'}\bar{u}_{r'}(p_e)\gamma^\lambda(1-\gamma^5)v_r(p_\nu)\bar{v}_r(p_\nu)\gamma^\mu(1-\gamma^5)u_{r'}(p_e) \\ &= 8\left[p_e^\lambda p_\nu^\mu + p_e^\mu p_\mu^\lambda - g^{\lambda\mu}(p_e p_\nu) + i\epsilon^{\lambda\sigma\mu\rho}p_{e_\sigma}p_{\nu_\rho}\right]\,, \end{aligned} \tag{B.10}$$

where $g^{\lambda\mu} = \mathrm{diag}(1,-1,-1,-1)$ and $\epsilon^{\lambda\sigma\mu\rho}$ are the metric tensor and the fully antisymmetric unit tensor.

The explicit expression of $J_{\lambda\mu}$ is obtained using Eq. (B.5), implying

$$j^0 = \chi^\dagger_{s'}\chi_s = \delta_{ss'}\quad,\quad j^i = g_A\chi^\dagger_{s'}\sigma^i\chi_s\quad,\quad (i=1,2,3)\,. \tag{B.11}$$

Carrying out the spin sum we readily find that the the tensor $J_{\lambda\mu}$ is diagonal, and its non vanishing components are given by

$$J^{00} = 2,\;\; J^{11} = J^{22} = J^{33} = 2g_A^2\,. \tag{B.12}$$

Finally, substitution of Eqs. (B.10) and (B.12) in the expression of the differential decay rate leads to

$$\begin{aligned} dW_{i\to f} &= (2\pi)^4\delta(E_n - E_p - E_e - E_\nu)\delta(\mathbf{p}_n - \mathbf{p}_p - \mathbf{p}_e - \mathbf{p}_\nu) \\ &\times\; 2G^2\left[1 + \cos\theta + {g_A}^2(3-\cos\theta)\right]\frac{d\mathbf{p}_p}{(2\pi)^3}\frac{d\mathbf{p}_e}{(2\pi)^3}\frac{d\mathbf{p}_\nu}{(2\pi)^3}\,, \end{aligned} \tag{B.13}$$

where θ is the angle between the lepton momenta $\mathbf{p}_e$ and $\mathbf{p}_\nu$.

Neglecting the contribution of $\mathbf{p}_\nu$ in the argument of the δ-function expressing momentum conservation[1], we can perform the $\cos\theta$ integration, yielding the final result

$$\begin{aligned} dW_{i\to f} &= 2\pi\,\delta(E_n - E_p - E_e - E_\nu)\delta(\mathbf{p}_n - \mathbf{p}_p - \mathbf{p}_e) \\ &\times 2G^2\left(1+3{g_A}^2\right)4\pi E_\nu^2\,dE_\nu\frac{d\mathbf{p}_p}{(2\pi)^3}\frac{d\mathbf{p}_e}{(2\pi)^3}\,. \end{aligned} \tag{B.14}$$

[1]This approximation is fully justified for emission of antineutrinos of energy $E_\nu \sim T$, T being the temperature, in dense degenerate matter.

Appendix C

Basics of QCD thermodinamics

Lo studio delle diverse fasi della QCD a temperatura e potenziale chimico diversi da zero, richiede la conoscenza delle grandezze termodinamiche, definite a partire dalla funzione di partizione grancanonica $\mathcal{Z}$. Per un sistema a temperatura $T = \beta^{-1}$ la cui dinamica è descritta dall'hamiltoniana H

$$\mathcal{Z} = \mathrm{Tr}\exp[-\beta(H - \sum_i \mu_i N_i)]\,, \tag{C.1}$$

dove gli N_i sono gli operatori associati alle grandezze conservate (per esempio, nel caso della QED, la differenza tra il numero di elettroni e quello di positroni) e μ_i i potenziali chimici corrispondenti. Dalla (C.1) seguono immediatamente le relazioni

$$P = -T\,\frac{\partial \ln \mathcal{Z}}{\partial V}\,, \tag{C.2}$$

$$N_i = T\,\frac{\partial \ln \mathcal{Z}}{\partial \mu_i}\,, \tag{C.3}$$

$$S = \frac{\partial\; T\, \ln \mathcal{Z}}{\partial T}\,, \tag{C.4}$$

$$E = -PV + TS + \sum_i \mu_i N_i = T\,\frac{\partial \ln \mathcal{Z}}{\partial T} + T\,\sum_i \mu_i \frac{\partial \ln \mathcal{Z}}{\partial \mu_i}\,, \tag{C.5}$$

dove P, S ed E sono, rispettivamente, pressione, entropia ed energia del sistema.

Le equazioni (C.2)-(C.5) mostrano che è conveniente introdurre il potenziale termodinamico

$$\Omega = -T \ln \mathcal{Z} = -PV\,, \tag{C.6}$$

dal quale si ottengono in modo semplice le grandezze termodinamiche tramite derivate parziali.

In teoria quantistica dei campi, la traccia nella definizione di $\mathcal{Z}$, ovvero la somma sugli elementi diagonali della matrice densità, si effettua usando il formalismo degli integrali funzionali. Per esempio, nel caso semplice di un di campo scalare, la cui densità lagrangiana è

$$\mathscr{L} = \frac{1}{2}\,\partial^\mu \partial_\mu \phi - \frac{1}{2} m^2 \phi^2\,, \tag{C.7}$$

non ci sono cariche conservate e si ottiene [15, 17]

$$\mathcal{Z} = \mathcal{N} \int \mathcal{D}\phi \, \mathrm{e}^{S} \tag{C.8}$$

ovvero l'integrale esteso a tutti i cammini periodici, tali cioè che $\phi(\vec{x},0) = \phi(\vec{x},\tau)$, dell'esponenziale dell'integrale d'azione per tempi immaginari $\tau = it$

$$S = \int_0^\beta d\tau \int d^3x \, \mathcal{L}(\phi, \partial\phi/\partial\tau) = -\frac{1}{2}\int_0^\beta d\tau \int d^3x \left[\left(\frac{\partial\phi}{\partial\tau}\right)^2 + (\nabla)\phi)^2 + m^2\phi^2\right] . \tag{C.9}$$

Si noti che il fattore di normalizzazione $\mathcal{N}$ che compare nel secondo membro dalla (C.8) è irrilevante, poichè la presenza di un fattore moltiplicativo non cambia la termodinamica del sistema.

Il calcolo della funzione di partizione nel caso del campo di Dirac $\psi(x)$, discusso in dettaglio nella Sezione 4.2.2, da il risultato [15]

$$\mathcal{Z} = \int i\mathcal{D}\psi^\dagger \int \mathcal{D}\psi \exp \int_0^\beta d\tau \int d^3x \, \bar{\psi}\left(-\gamma^0\frac{\partial}{\partial\tau} + i\vec{\gamma}\cdot\vec{\nabla} - m_i + \mu_i\gamma^0\right)\psi \, , \tag{C.10}$$

dove $i\psi^\dagger$ e ψ vanno considerati come variabili dinamiche indipendenti e l'integrale è esteso a tutti i cammini che soddisfano alla condizione di antiperiodicità $\psi(\vec{x},0) = -\psi(\vec{x},\beta)$, come richiesto dalle regole di anticommutazione dei campi fermionici.

Appendix D

Phase-space decomposition

In the is Appendix, we describe the elements entering the calculation of neutrino emissivity associated with nucleonic Urca processes, carried out using the *phase-s[ace decomposition* method.

On account of the strong degeneracy of nucleons and electrons, the main contribution to the integral yielding the emissivity

$$Q^D = 2\int \frac{d\mathbf{p}_n}{(2\pi)^3}\, dW_{i\to f}\, f_n(1-f_p)(1-f_e)\,, \tag{D.1}$$

arises from quantum states with momenta within a thin shell around the Fermi surface. As a consequence, we can set $|\mathbf{p}_i| = p_{F_i}$ in the integrand. Moreover, the typical energy exchanged in the reactions is $\sim T$.

Because the energy carried by the neutrino is $E_\nu \sim T$, the corresponding momentum, being of the same order, is much smaller than the momenta of the degenerate fermions involved in the process. Hence, it can be safely neglected in the argument of the momentum-conserving δ-function. The resulting expression is

$$\begin{aligned} dW_{i\to f}\,\frac{d\mathbf{P}_n}{(2\pi)^3} = \frac{(2\pi)^4}{(2\pi)^{12}}\,\delta(E_n - E_p - E_e - E_\nu)\,\delta(\mathbf{p}_n - \mathbf{p}_p - \mathbf{p}_e) \\ \times |M_{fi}|^2\, 4\pi E_\nu^2 dE_\nu \prod_{j=1}^{3} p_{Fj} m_j^* dE_j d\Omega_j\,. \end{aligned} \tag{D.2}$$

We now transform to the new variables

$$x_\nu = \frac{E_\nu}{T} \quad , \quad x_j = \frac{E_j - \mu_j}{T} \quad (j = n,\ p,\ e)\,,$$

and replace $x_j \to -x_j$ for $j = p,\ e$, to exploit the property of the Fermi distribution $1 - f(x_j) = f(-x_j)$. In addition, we introduce the quantity

$$A = 4\pi \int d\Omega_1 d\Omega_2 d\Omega_3\, \delta(\mathbf{p}_n - \mathbf{p}_p - \mathbf{p}_e)\,. \tag{D.3}$$

Using the above definitions, Eq.(D.1) can be rewritten in the form

$$Q^D = \frac{2}{(2\pi)^8}|M_{fi}|^2 A\left[T^7\int_0^\infty dx_\nu x_\nu^3\left(\int_{-\frac{\mu_1}{T}}^\infty\int_{-\infty}^{\frac{\mu_2}{T}}\int_{-\infty}^{\frac{\mu_3}{T}} dx_j f_j\right)\right.$$
$$\left.\times\frac{1}{T}\delta(x_1+x_2+x_3-x_\nu)\right]\prod_{j=1}^3 p_{Fj}m_j^*\,. \tag{D.4}$$

As the system is strongly degenerate, we can replace $\mu_j/T\to\infty$, the associated error being exponentially small. Thus, we finally obtain

$$Q^D = \frac{2}{(2\pi)^8}|M_{fi}|^2\,T^6 AI\prod_{j=1}^3 p_{Fj}m_j^*\,, \tag{D.5}$$

where

$$I=\int_0^\infty dx_\nu x_\nu^3\left[\prod_{j=1}^3\int_{-\infty}^\infty dx_j f_j\right]\delta(x_1+x_2+x_3-x_\nu)\,. \tag{D.6}$$

D.1 Calculation of A

Let us start rewriting the momentum conserving δ-function in spherical coordinates. To do this, we exploit the fundamental property of Dirac's δ

$$\int\delta(\mathbf{a}-\mathbf{b})\,d\mathbf{a}=\int\delta(a_x-b_x)\,da_x\int\delta(a_y-b_y)\,da_y\int\delta(a_z-b_z)\,da_z=1\,.$$

The requirement that the above relation still hold true in spherical coordinates, i.e. that

$$\int\delta_s(\mathbf{a}-\mathbf{b})\,d\mathbf{a}=\int\delta_s(\mathbf{a}-\mathbf{b})\,a^2\,da\,d\Omega_a=1\,,$$

implies

$$\delta_s(\mathbf{a}-\mathbf{b})=\delta(a-b)\,\frac{\delta(\Omega_a-\Omega_b)}{a^2}\,.$$

In the case under consideration the above expression becomes

$$A=4\pi\int d\Omega_1 d\Omega_2 d\Omega_3\,\delta(p_n-|\mathbf{p}_p+\mathbf{p}_e|)\,\frac{\delta(\Omega_1-\Omega_{2+3})}{p_n^2}$$
$$=4\pi\int d\Omega_2 d\Omega_3\,\frac{\delta(p_n-|\mathbf{p}_p+\mathbf{p}_e|)}{p_n^2}\,. \tag{D.7}$$

The radial δ-function can be transformed into a δ-function for one of the angular variables. We first rewrite the δ-function in the form

$$\delta(f(\cos\theta_2))=\delta[p_n-(p_p^2+p_e^2+2p_pp_e\cos\theta_2)^{\frac{1}{2}}]\,,$$

with the z-axis chosen along the direction electron momentum $\mathbf{p}_e$. The root of the function $f(\cos\theta_2)$ is

$$\cos\theta_2=\frac{p_n^2-p_p^2-p_e^2}{2p_pp_e}=a\,,$$

and

$$|f'(a)| = \frac{p_p p_e}{p_n} .$$

It follows that

$$\frac{\delta(p_n - |\mathbf{p}_p + \mathbf{p}_e|)}{p_n^2} = \frac{1}{p_n^2}\frac{1}{|f'(a)|}\delta(\cos\theta_2 - a) = \frac{1}{p_n p_p p_e}\delta(\cos\theta_2 - a) ,$$

and replacing in (D.7) we obtain

$$A = \frac{32\pi^3}{p_{Fn} p_{Fp} p_{Fe}}\Theta_{npe} , \tag{D.8}$$

where the function Θ_{npe} takes into account the triangular condition on the Fermi momenta of the degenerate fermions.

D.2 Calculation of I

Le us rewrite I in the form

$$I = \int_0^\infty dx_\nu x_\nu^3 J(x_\nu) , \tag{D.9}$$

with

$$J(x_\nu) = \int_{-\infty}^{\infty}\prod_{j=1}^{3} dx_j (1+e^{x_j})^{-1}\,\delta\left(\sum_{j=1}^{3} x_j - x_\nu\right) , \tag{D.10}$$

and start with the calculation of J.
Using the definition of the δ-function in terms of its Fourier transform

$$\delta(x) = \frac{1}{2\pi}\int_{-\infty}^{\infty} e^{izx} ,$$

we find

$$\begin{aligned} J(x_\nu) &= \frac{1}{2\pi}\int_{-\infty}^{\infty} dz \int_{-\infty}^{\infty}\prod_{j=1}^{3} dx_j (1+e^{x_j})^{-1} e^{iz(x_j - x_\nu)} \\ &= \frac{1}{2\pi}\int_{-\infty}^{\infty} dz\, e^{-izx_\nu}\left(\int_{-\infty}^{\infty} dx\,(1+e^{x})^{-1} e^{izx}\right)^3 \\ &= \frac{1}{2\pi}\int_{-\infty}^{\infty} dz\, e^{-izx_\nu}\left[f(z)\right]^3 , \end{aligned} \tag{D.11}$$

where

$$f(z) = \int_{-\infty}^{\infty} dx\,(1+e^{x})^{-1} e^{izx} . \tag{D.12}$$

To obtain the expression of $f(z)$, consider the integral

$$K = \oint dx\,(1+e^{x})^{-1} e^{izx} , \tag{D.13}$$

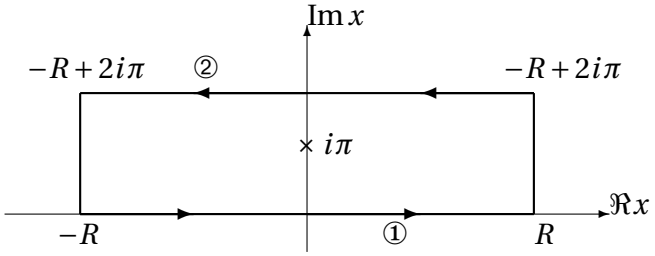

Figure D.1: Integration contour employed for the evaluation of K (see Eq.(D.13)).

to be evaluated using Cahchy's theorem, with the contour shown in Fig. D.1.

As $R\to\infty$ the contributions of the vertical sides become negligible. Along the real axis, ①, $K = f(z)$, whereas along the path marked with ②

$$K=\int_{-\infty}^{\infty} dx\,(1+e^{\Re x+2i\pi})^{-1}e^{iz(\Re x+2i\pi)} = e^{-2\pi z}f(z)\,.$$

It follows that

$$K = f(z)-e^{-2\pi z}f(z) = (1-e^{-2\pi z})f(z)\,.$$

The value of K can be obtained using the mot hod of residues. From

$$\begin{aligned}\operatorname{Res}K(z) &= \lim_{x\to i\pi}(x-i\pi)\frac{e^{izx}}{1+e^{x}} = \lim_{x\to i\pi}(x-i\pi)\frac{e^{izx}}{1-\sum_{n=0}^{\infty}\frac{1}{n!}(x-i\pi)^{n}}\\ &= \lim_{x\to i\pi}-\frac{e^{izx}}{\sum_{n=1}^{\infty}\frac{1}{n!}(x-i\pi)^{(n-1)}} = -e^{-\pi z}\,,\end{aligned}$$

it follows that

$$K(z) = (1-e^{-2\pi z})\,f(z) = -2i\pi e^{-\pi z}\,,$$

. and using the above result we find

$$f(z)=\frac{\pi}{i\sinh\pi z}\,. \tag{D.14}$$

Using the above results, we can write J in the form

$$J(x_v) = -\frac{1}{2i\pi}\int_{-\infty-i\epsilon}^{\infty-i\epsilon} dz\,e^{-izx_v}\left(\frac{\pi}{\sinh\pi z}\right)^3\,, \tag{D.15}$$

where the quantity $-i\epsilon$, with $\epsilon = 0^+$ takes into account the presence of a pole of third order in the itegrand. To determine a suitable integration contour, we carry out the transformation $z = z' - i$, leading to

$$J(x_v) = \frac{e^{-x_v}}{2i\pi}\int_{-\infty-i\epsilon+i}^{\infty-i\epsilon+i} dz\,e^{-izx_v}\left(\frac{\pi}{\sinh\pi z}\right)^3\,. \tag{D.16}$$

Summing Eqs. (D.15) and (D.16) we obtain an integration along the contour shown in Fig. D.2

$$\begin{aligned}(1+e^{x_v})\,J(x_v) &= -\frac{1}{2i\pi}\left[\int_{-\infty-i\epsilon}^{\infty-i\epsilon}+\int_{-\infty-i\epsilon+i}^{\infty-i\epsilon+i}\right]dz\,e^{-izx_v}\left(\frac{\pi}{\sinh\pi z}\right)^3\\ &= -\frac{1}{2i\pi}\oint dz\,e^{-izx_v}\left(\frac{\pi}{\sinh\pi z}\right)^3\,.\end{aligned} \tag{D.17}$$

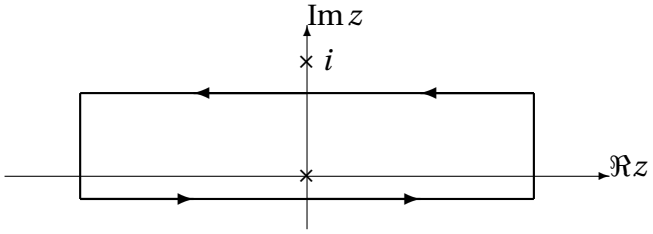

Figure D.2: Integration contour employed for the evaluation the integral of Eq.(D.17).

From Eq. (D.17) it follows that

$$\begin{aligned}(1+e^{x_v})\,J &= -\mathrm{Res}\left[e^{-izx_v}\left(\frac{\pi}{\sinh\pi z}\right)^3\right]_{z=0}\\ &= -\lim_{z\to 0}\frac{1}{2}\frac{d^2}{dz^2}\left[z^3 e^{-izx_v}\left(\frac{\pi}{\sinh\pi z}\right)^3\right]\\ &= -\lim_{z\to 0}\frac{1}{2}\left\{-x_v^2 e^{-izx_v}\left(\frac{\pi}{\sinh\pi z}\right)^3 + 6ix_v e^{-izx_v}\left(\frac{\pi}{\sinh\pi z}\right)^3\left(\pi z^3\frac{\cosh\pi z}{\sinh\pi z}-z^2\right)\right.\\ &\quad\left.+\left[6z-18\pi z^2\frac{\cosh\pi z}{\sinh\pi z}+3\pi^2 z^3\frac{1}{(\sinh\pi z)^2}+9\pi^2 z^3\left(\frac{\cosh\pi z}{\sinh\pi z}\right)^2\right]\frac{\pi^3 e^{-izx_v}}{(\sinh\pi z)^3}\right\}.\end{aligned}$$

Let us consider the first line of the above result. In the $z\to 0$ limit, the second contribution vanishes, as can be easily seen substituting the first order expansion

$$\frac{\cosh\pi z}{\sinh\pi z}\approx\frac{1}{\pi z},$$

while the first contribuito reduces to $-x_v^2$. The second line must be expanded up to the zero-th order term. The resulting contributions are

1. $\dfrac{6\pi^3 z}{(\pi z)^3\left[1+\frac{(\pi z)^2}{2}\right]}\approx\dfrac{6}{z^2}\left(1-\dfrac{1}{2}\pi^2 z^2\right)=\dfrac{6}{z^2}-3\pi^2;$

2. $\dfrac{3\pi^5 z^3}{(\pi z)^5\left[1+\frac{5(\pi z)^2}{6}\right]}\approx\dfrac{3}{z^2}-\dfrac{5}{2}\pi^2;$

3. $\dfrac{9\pi^5 z^3}{(\pi z)^5\left[1+\frac{5(\pi z)^2}{6}\right]}(1+\pi^2 z^2)\approx\dfrac{9}{z^2}+\dfrac{3}{2}\pi^2;$

4. $-\dfrac{18\pi^4 z^2}{(\pi z)^4\left[1+\frac{2(\pi z)^2}{3}\right]}\left(1+\dfrac{1}{2}\pi^2 z^2\right)\approx-\dfrac{18}{z^2}+3\pi^2$.

and their sum is $-\pi^2$. Hence

$$(1+e^{x_v})\,J(x_v)=\frac{x_v^2+\pi^2}{2},$$

implying

$$J(x_\nu) = \frac{\pi^2 + x_\nu^2}{2(1+e^{x_\nu})}\,. \tag{D.18}$$

Finally, the integral

$$I = \int_0^\infty dx_\nu x_\nu^3 J(x_\nu)\,,$$

that can be found in Ref. [24], Eq. (3.411), is given by

$$\int_0^\infty \frac{x^{2n-1}}{e^{px}+1} dx = (1-2^{1-2n})\left(\frac{2\pi}{p}\right)^{2n} \frac{|B_{2n}|}{4n}\,,$$

where B_n is a Bernoulli number. In the case under consideration, correponding to $p = 1$ e $n = 2,\ 3$, we use $B_4 = -\frac{1}{30}$ e $B_6 = \frac{1}{42}$, to find

$$I = \frac{457\pi^6}{5040}\,. \tag{D.19}$$

Substitution of the above results in Eq. (5.7), yields the expression of the neutrino emissivity of Eq. (5.12).

Bibliography

[1] W. Baade and F. Zwicky, Phys. Rev. **45** (1934) 138.

[2] S.L. Shapiro e S.A. Teukolsky, *Black Holes, White Dwarfs and Neutron Stars*, Wiley Interscience, New York, NY, 1983.

[3] N.K. Glendenning, *Compact Stars*, Springer, New York, NY, 2000.

[4] F. Weber *Pulsars as Astrophysical Laboratories for Nuclear and Particle Physics*, Institute of Physics Publishing, Philadelphia, PA, 1999.

[5] Y.C. Leung, *Physics of Dense Matter*, World Scientific, Singapore, 1984

[6] L.D. Landau e E.M. Lifshitz *Statistical Physics*, Addison-Wesley, Reading, MA, 1958

[7] S. Chandrasekhar, Astrophysical Journal, **74** (1931) 81.

[8] J.R. Oppenheimer and G.M. Volkoff, Phys. Rev. **55** (1939) 374.

[9] R.C. Tolman, Phys. Rev. **55** (1939) 364.

[10] J.W. Negele and D. Vautherin, Phys. Rev. C **5**, (1972) 1472.

[11] L. Kadanoff and G. Baym, *Quantum Statistical Mechanics* (Benjamin, Reading MA, 1976)

[12] Ya. B. Zel'dovich, Sov. Phys. JETP **14** (1962) 1143.

[13] E. Laermann e O. Philipsen, Ann. Rev. Nucl. Part. Sci **53** 163 (2003).

[14] F. Karsch e E. Lärmann, hep-lat/0305025.

[15] J. I. Kapusta, *Finite-Temperature Field Theory* (Cambridge University Press, Cambridge, 1989).

[16] T.D. Lee *Particle Physics and introduction to field theory* (Harwood, London, 1988).

[17] M. Le Bellac, *Thermal field theory*, (Cambridge University Press, Cambridge, 1996).

[18] T. De Grand, R.L. Jaffe, K. Johnsson and J. Kiskis, Phys. Rev. D **12**, 2060 (1975).

[19] J. Boguta, Phys. Lett. B **106**, 255 (1981).

[20] J.M. Lattimer, C.J. Pethick, M. Prakash, and P. Haensel, Phys. Rev. Lett. **66**, 2701 (1991).

[21] A. Akmal, V.R. Pandharipande, and D.G. Ravenhall, Phys. Rev. C **58**, 1804 (1998).

[22] B.L. Friman and O.V. Maxwell, ApJ **232**, 541 (1979).

[23] D.G. Yakovlev and K.P. Levenfish, ApJ **297**, 717 (1995).

[24] I.S. Gradshteyn and I.M. Ryzhik. *Table of Integrals, Series, and Products. 7th Edition.* (Academic Press, New York, 2007).